Project CUNIT-2-112Y6580

Qualitative Evaluation of Inclusions In Moderna, AstraZeneca and Pfizer Covid-19 vaccines.

by

UNIT

Executive Summary

UNIT was commissioned by EbMCsquared CiC under project UNITC-112980 to investigate the contents of four injection vials (Moderna 01, Moderna 02, AstraZeneca, Pfizer) for any undeclared ingredients that may cause bodily harm.

This report is the submission of initial findings that confirm the presence of graphene compounds in each of the injection vials. Though a quantitative estimate has not be established for the concentration of graphene in the samples, its occurrence is on a high frequency range on an average 2cm transect when counts were conducted on a higher magnification (40x).

TABLE OF CONTENTS

1. Introduction

The following report is a product of a joint cooperation between EbMCsquared CiC and UNIT in an attempt to identify the undeclared contents of the current vaccines that are being administered to the UK public causing high numbers of adverse reactions and deaths.

1.1. Background

UNIT was commissioned by EbMCsquared under UNITC-112980 to 91 to analyse contents of four vaccine vials and identify if any of the following components were present in these vials – graphene, graphene oxide, parasites, biological filaments.

The four vaccines that form the subject of this first investigation by UNIT belonged to Moderna, Pfizer, and AstraZeneca.

The entire process of collection and delivery is reported in ANNEXE 1A.

1.2. Descriptions of Vials

1.2.1. Moderna 01 Labelling

The manufacturing label had the following information on the vial:

COVID-19 Vaccine Moderna. 020mg/mL Dispersion for injection. COVID-19 mRNA Vaccine (nucleoside modified) Multidose vial doses of .5mL.

Lot-3004737 Exp. 24/01/2022.

The liquid contained in the Moderna bottle was cloudy to naked eye against the sunlight.

1.2.2. Moderna 02 Labelling

The manufacturing label had the following information on the vial:

COVID-19 Vaccine Moderna. 020mg/mL Dispersion for injection. COVID-19 mRNA Vaccine (nucleoside modified) Multidose vial doses of .5mL.

Lot- Lot-3004737 Exp. 24/01/2022.

The bottle weight prior to breaking of the seal was 18.842gm.

The liquid contained in the Moderna bottle was cloudy to naked eye against the sunlight.

1.2.3. AstraZeneca Labelling

The manufacturing label had the following information on the vial:

Covid-19 Vaccine 4 ml, Astrazeneca Injection. Covid-19 Vaccine: (ChAd0x1-S (recombinant)), Intramuscular use. Multidose vial (8x0.5ml doses). 108439/2 Lot-PW40167 Expiry- 01-22. (Figure 2.1)

The bottle weight prior to the breaking of the seal was 12.184g and after the breaking of the seal was 11.803g.

The liquid contained in the AstraZeneca bottle was transparent to naked eye.

1.2.4. Pfizer Labelling

The manufacturing label had the following information on the vial as in figure 1.1:

Figure 1.1. Pfizer vaccine vial

Lot-FC9001 Exp. 09/01/2022.

The liquid contained in the Pfizer bottle was cloudy to naked eye against the sunlight

1.2.5.

1.3. Aims and Objectives of the study

The aim of the study was to identify any solid inclusions in the vials as were undeclared by the manufacturers.

The study was to verify the findings of graphene related compounds such as graphene oxide, graphene hydroxide by Campara (2021) and report any other biological inclusions that may be interpreted as toxic to human body.

1.4. Report Structure and Outline

The vials went through evaluation of contents at four different laboratory sites that are identified in ANNEXE 1B on request and the methodology adopted is presented in Chapter two.

The report presents an in depth analysis of the findings of this project and is divided into five chapters. Chapter one is the introduction, the second chapter is a description and analysis of the methods used for the evaluation. Chapter three presents the results of the analysis, Chapter four is the interpretation, discussions and conclusions of the study. The Bibliography forms the last chapter of the report.

The entire project involved the inputs of experts in individual fields and their names, affiliations and expertise are identified for reference purposes in Annex 2.

2. Methodology

2.1. Vial Descriptions

The secured vials were made of glass and the vaccines contained within the vials were in a liquid form. The different parts of the vial are shown in figure 2.1. Each of these vials were stored at 4°C in the sample storage rooms until the evaluation of their contents took place. Each of the four vials undertook the same process for evaluation.

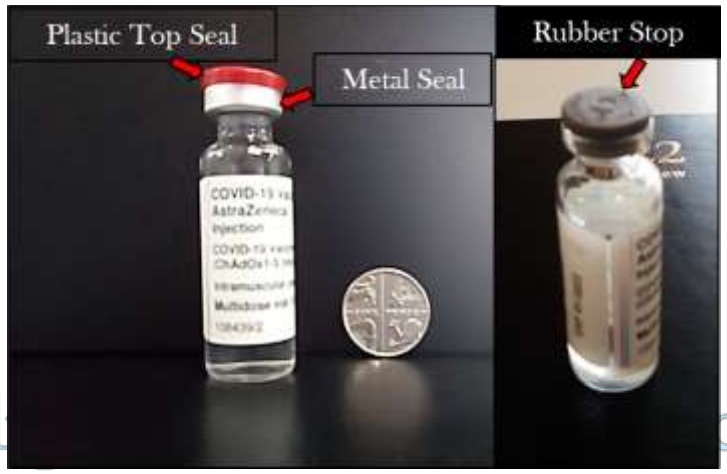

Figure 2-1 Different parts of the sealing process of the vial. The vial shown here is the AstraZeneca vial. The same three seal components were present for the Moderna and Pfizer vials.

2.2. Process of Sampling and Slide Preparation

Stage 1 - Opening of the vial

Stage 1 involved the opening of the vial while the process was recorded on the camera for posterity. Each of the vials were sealed with a plastic seal on the top (figure 2.1). This seal had to be broken off before one could access the rubber top of the injection vial. The rubber top was held securely in place with a metal ring.

There were two options of accessing the liquids from within the vials. One, was to use an injection syringe and draw out the required amount of liquid. However, knowing that the objective of the study was to identify and report any nano graphene particles within the vials, this method of sample acquisition was not thought to be appropriate. The reasoning being, that during the penetration of the vial, the syringe would carry nanoscopic amounts of rubber seal material, which is a carbon product, each time, it would access the liquid. Therefore, the second option of material access was adopted, which meant, breaking off the metal ring and simply removing the rubber seal on top each time the sample material was required.

Stage 2 – Subsampling for evaluation of experimental steps required

Stage 2 had the simple purpose of the first evaluation of the sample. As there was no prior study available at hand to determine the chemistry and the physical properties of the material at hand, a small subsample was used from the vial to be evaluated under a polarising microscope to identify the gross composition of the material of the vaccine and to have a brief understanding of any inclusions if they were present.

Each of the vaccine's active ingredients seemed to have been preserved in a sucrose-salt rich medium. The optical and physical properties of the preserving medium posed a challenge to the identification of the actual inclusions. In addition to being of nearly the same refractive index as the medium, the micro and nano crystalline nature of the expected inclusions rendered an additional impediment to the task of their isolation.

During, wet microscopic evaluation at the dry laboratories, it was noted from the onset, that the denser material settled at the bottom of the slide and got impregnated and encrusted with the medium solution, while the slide was still in the process of wet examination. Additionally, the deposition of the inclusions occurred at different depths within the medium.

Cummulatively, such characteristics, posed a grave challenge to the central objective of the study, in that, isolation of the objects of interest was deemed impossible. The medium masked all signatures of the inclusions by impregnation and encrustation in a manner that the inclusions were completely camouflaged into the background.

These challenges were attempted to be overridden by vacuum filteration. The first attempt at vacuum filteration failed due to equipment failure. This resulted in the loss of the test material. As, at the time of this experiment, the material at hand was quite limited, any further attempts for both vacuum filteration processes were paused.

(It should be noted, that the ongoing continuation of this project will be using checmical filteration to isolate the inclusions from the onset as the current project has given a clear insight into the chemistry of the product.)

Stage 3- Partitioning of sample for clean slide preparation

This stage included the partitioning of sample into two. The clean portions of the sample were stored in a pyrex glass vial which was cleaned using hydrogen per oxide, hydrochloric baths, then rinsed with distilled water. The vials were then sterilised in the sterilisation chamber prior to the transfer of the sample into them.

0.0125ml of sample was then transferred onto clean slides within fume cupboard and left there to air dry at 20°C under a glass chamber.

The dried slides were mounted using glass coverslips and used for microscopic evaluation. It should be noted that none of the prepared clean slides dried out completely even after a few days.

Stage 3- Optical and Petrological Microscopy

Prepped slides were examined under a reflection and transmission light microscope for organic content and petrological microscope for mineral contents.

Microscopic stage involved preparation of several test slides to identify the typical nature of the content.

On representative slides, counts were done along a specific transect. These were then represented on psimpol to get density options on a typical 0.006ml of sample.

Stage 4 – Raman sampling and preparation

Subsamples from original vials were obtained for Raman spectroscopy. These were transferred onto standard slides using sterilised glass pipettes. The slides were left to dry under glass chambers inside a fan heating oven before being taken for examination to the Raman Laboratories.

2.3. Raman Spectroscopy

As most of the observed inclusions belonged categorically to carbon compounds, Raman Spectroscopy was the chosen method for initial identification of the inclusions. All Raman spectra were recorded in air and at room temperature in back scattering geometry using Renishaw in Via Raman spectrometer. A tunable Ar ion laser was used as an excitation source of 488 nm. The laser beam was tightly focused on the sample surface through a Leica 50x LWD microscope objective with a numerical aperture equal to .5, leading to a laser beam diameter of about 2µm. Spectral resolution was about $2cm^{-1}$.

3.Results

3.1. Description of Inclusions

The analysis of all four vial contents identified objects that are similar. For ease of nomenclature and related descriptions per vaccine, these inclusions are illustrated and defined individually below-

The identified inclusions were-

1. Graphene nano ribbons coated with Polyethylene Glycol
2. Graphene Composite Form 1
3. Graphene Composite Form 2
4. Microcrystalline Calcite with Carbonaceous inclusions
5. Graphene Nano Forms with and without fluorescence
    a. Graphene nano objects
    b. Graphene nano scrolls

3.1.1. Graphene Composites in the form of Nano Ribbons

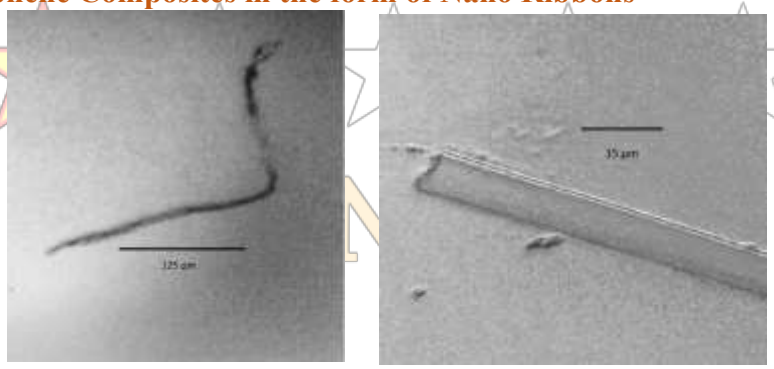

Figure. 3.1. Carbon Composite Ribbon Forms from a sample in Moderna 01. The first picture is of a wet sample and at a low magnification. The second picture is that of the same sample when it is dry and embedded in solution at a high magnification.

This micro inclusion form appears dark grey in wet slides, resembling filamentous ribbons. As the material dries, the form becomes nearly transparent. On high magnifications of 40x, lamellar structures can be identified as sheets. Raman spectrum on these sheets shows a carbon oxygen bond with added polyethylene glycol imprints (figure 3.9). A longer range of the Raman requires to be shot for a better grasp on the distribution of defects and other characteristics of this form.

3.1.2. Graphene Composite form 1

GC1 appears in a translucent folded form of about 10-15microns across. The form is transparent to translucent in transmitted light and shows light structure within it.

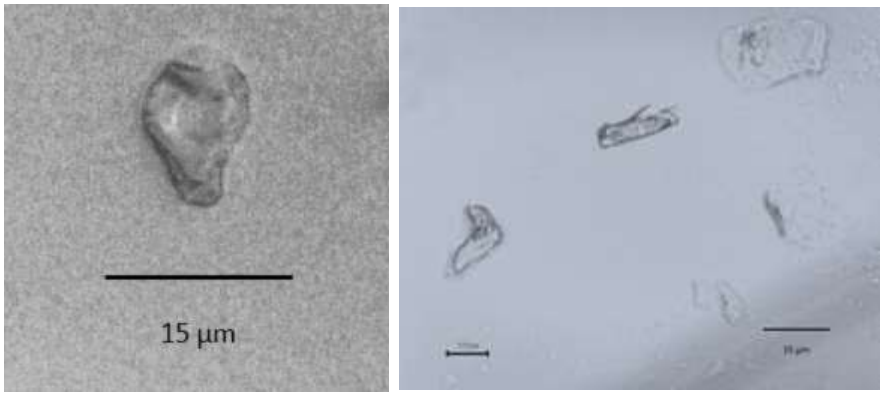

Figure 3.2. An assemblage of different forms with some embedded in the solution appearing translucent and those on the top show a good relief.

GC1 is isotropic under crossed polars. Raman spectroscopic results for this form shows dominant dual peaks of calcite at 1100 cm^{-1} and of some form of iron oxide nearly 500 cm^{-1} . The spectrum beyond 1300 cm^{-1} is quite noisy due to the presence of some fluorescence.

3.1.3. Graphene Composite Form 2

These forms are visibly more intricate and give a rather complex Raman signature. The deciphered components were graphene with iron oxide and calcite. The forms are quite distinct in their lamellar, structure.

The signature for carbon-carbon bond is quite distinct at 1600 cm^{-1} , 1100 cm^{-1} fpeak is picked up for calcite.

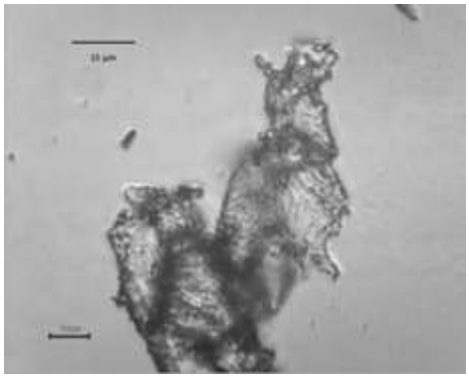

Figure 3.3. Carbon composite Form 2

3.1.4. Calcite

Figure 3.4. Microcrystalline Calcite with graphene inclusions.

Microcrystalline Calcite is another inclusion which is present in the samples. The form can be described as lumpy with inclusions of graphene nano forms. The form gives a very clear Raman signal for Calcite. Calcite is also present in GC1 and GC2 as identified through Raman spectra.

3.1.5. Graphene Nano Forms

Nano forms of graphene were identified in all the samples that were evaluated (figure 3.5). Upon shooting of the Raman when focused on some of these nano objects (in different vaccines), the obtained signals were found to be markedly masked with fluorescence.

Identification of Graphene nano forms was therefore conducted on the basis of microscopic morphological correlation with the forms where, the signal was clear and undebatable (figure 3.24).

Nano forms of Graphene dominated the counts in all the samples. They were found to be present both in roundish shapes and long spiculate shapes. The rounded forms were almost entirely found in association with nano particles.

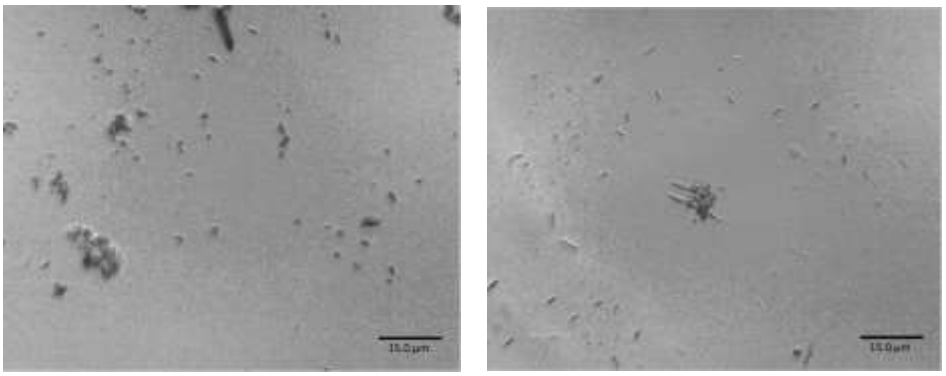

Figure 3.5. (a) Nano forms of Graphene. (b) Nano scrolls.

Quite conspicuously the spiculate forms were noticeably strewn in random orientations at the bottom of all the samples that were examined (figure 3.5).

These nano Graphene spicules were impossible to be evaluated by Raman, as their radius was measurably smaller than the resolution of the laser.

Given, the sheer number of the Graphene scrolls that were noted to be present in the samples, a separate project with the central focus on these scrolls is underway, where, high resolution Raman and invasive FTIR investigations are being undertaken to establish the structures of these scrolls and to get a quantitative estimate of their concentrations.

3.1.6. Crystalised forms of the solution

All the four vaccines are sugar based, and on the edges of the coverslip, as the material dried it crystallised into sugar crystals form in varied shapes. Figure 3.6. shows some varied forms of these crystals under polarised light.

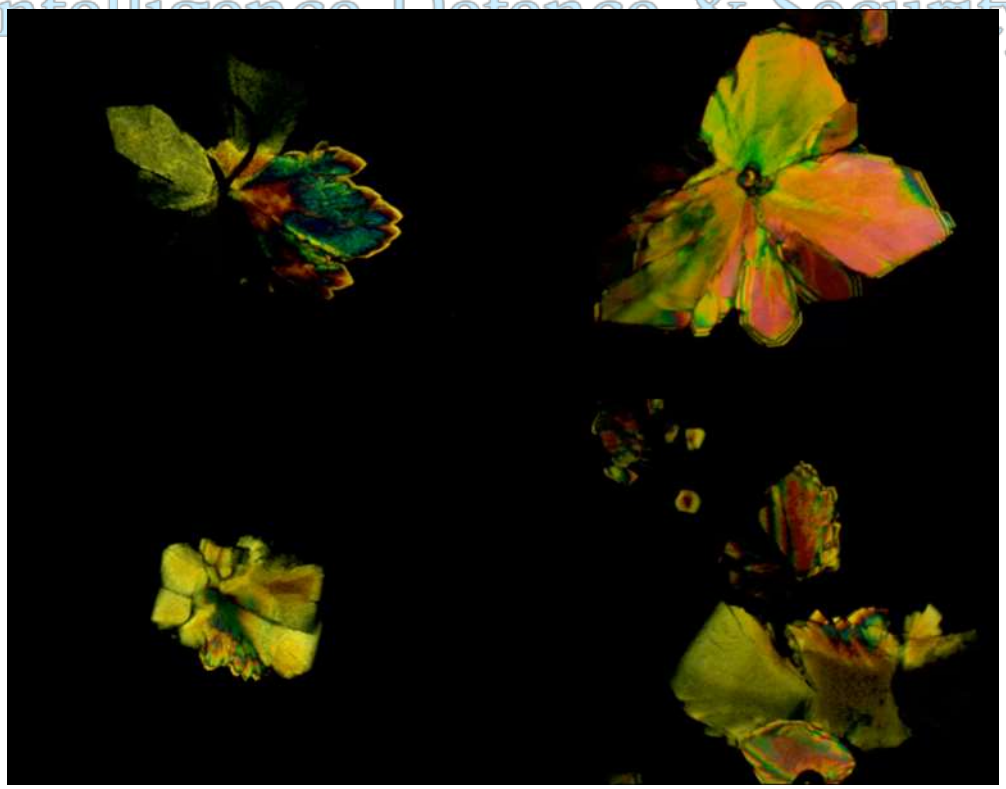

Figure 3.6. Four different forms of sugar base crystals identified in a dried Moderna slide. The crystals display third order interference colours under polarised light with an angular extinction in most cases. The crystals stem from distinctive nucleii.

3.2. Moderna 01

3.2.1. Microscopy

Moderna 01 was the first sample that was evaluated. Under wet microscopy, the sample showed several filamentous forms (figure 3.7). These forms seemed to shed off some of their filaments in form of small flakes (figure 3.7).

As the slide dried, these filamentous forms became incorporated in the solution medium and were optically difficult to distinguish from the background (figure 3.8).

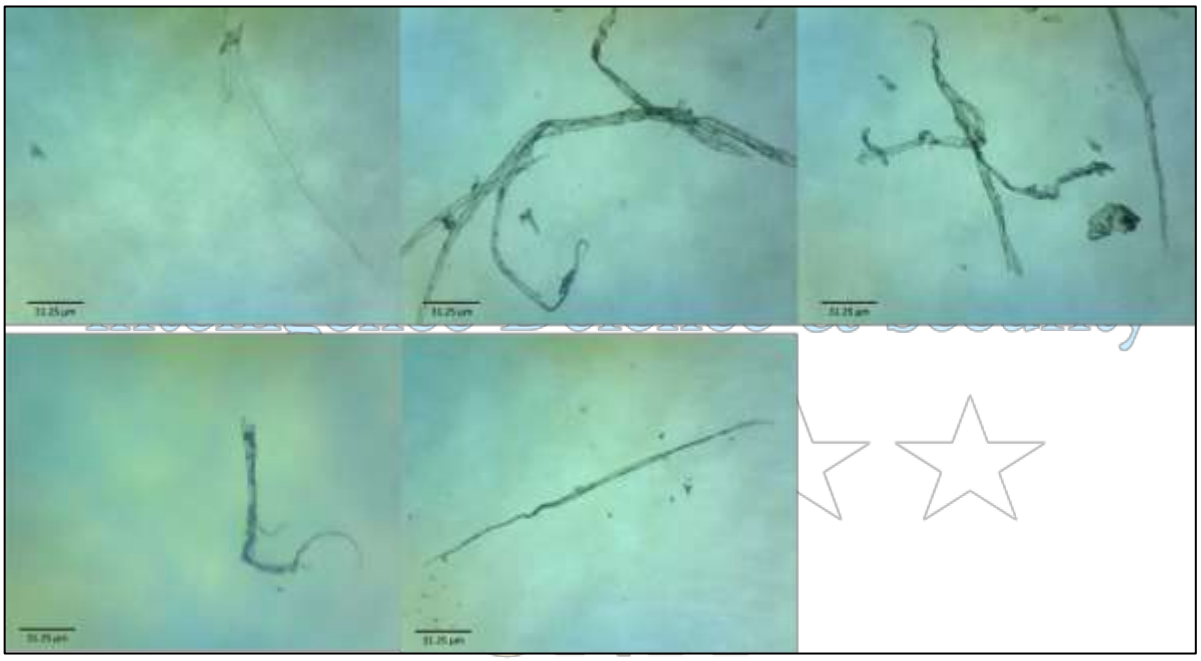

Figure 3.7. Filament forms as observed under wet microscopy.

In the dried state, various forms of particulate inclusions were identified. The settlement of these inclusions took place at multiple levels within the solidified medium. Lighter material came to rest and settle on top and denser material was found at the bottom of the slide.

The crystalised solution seemed to be quite viscous, and it solidified in a thick multi-layered pattern which is quite obvious in form of large sheets with perforations (figure 3.9). On the edges of the slide, the material crystallised into pleochroic crystals stemming from a seed nucleus (figure 3.6). The optical properties of these structures displayed third order interference colours along with the distinct presence of growth nucleus clearly identifying these crystals to be formed of the host solution which includes sucrose.

The ribbon like structures were seen in two states of deposition. One, where partial structure of the inclusion was visible above the solidified medium and part of it was almost transparent and embedded into the medium and the other state was, where the ribbon was incorporated in the medium and was barely distinguishable. The embedded portions seemed to create a quadrilateral geometry with a faint visual signal that seemed like a folded ribbon (figure *3.6*).

Figure 3.8. Ribbon shaped forms half embedded in the medium. Square and quadrilateral crystals in the background.

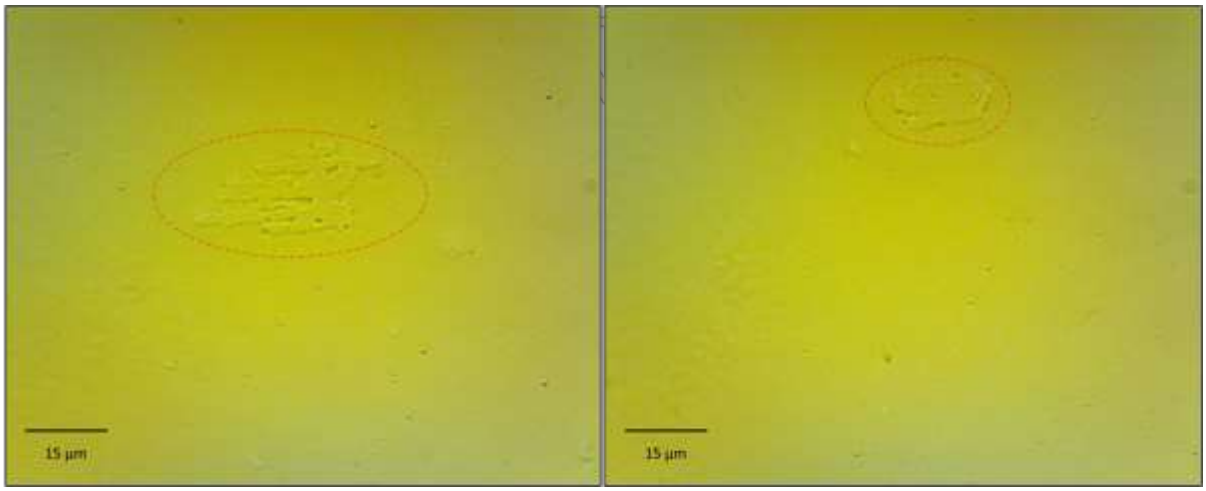

Figure 3.9. Flat, perforated several layered settlements of the medium.

Figure 3.10 exhibits various representative forms that were found in the vaccine. These forms ranged from transparent or translucent sheet like forms, to dark almost opaque amorphous carbon like materials of different sizes (figure 3.10j,k).

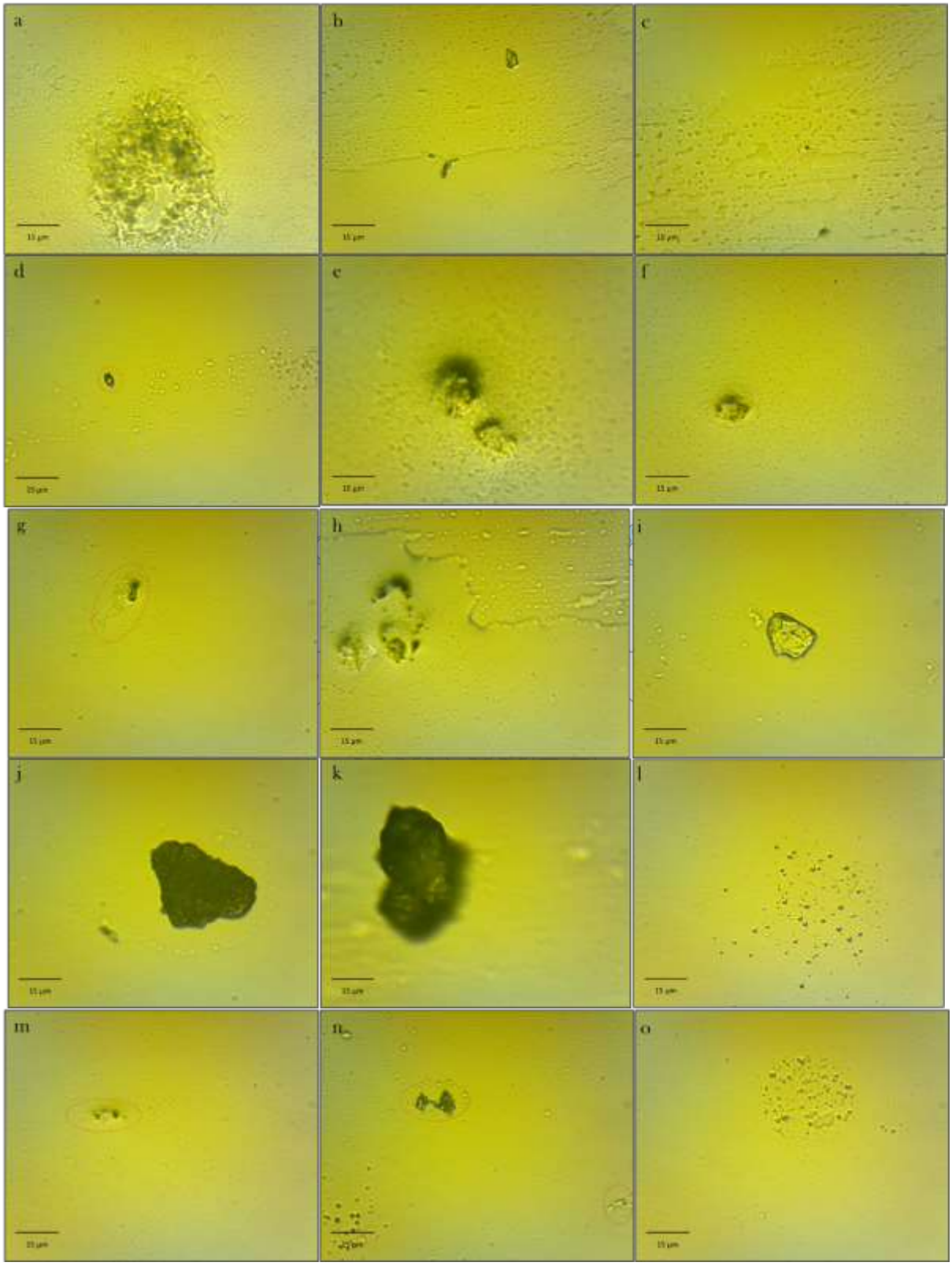

Figure 3.10. Various inclusions found within Moderna 01.

3.2.2. Raman Spectroscopic Investigation

Representative inclusions from Moderna 01 were examined by Raman spectroscopy. The investigation clearly showed that all the inclusions have a strong carbon signal with confirmed graphene compositions of some representative forms.

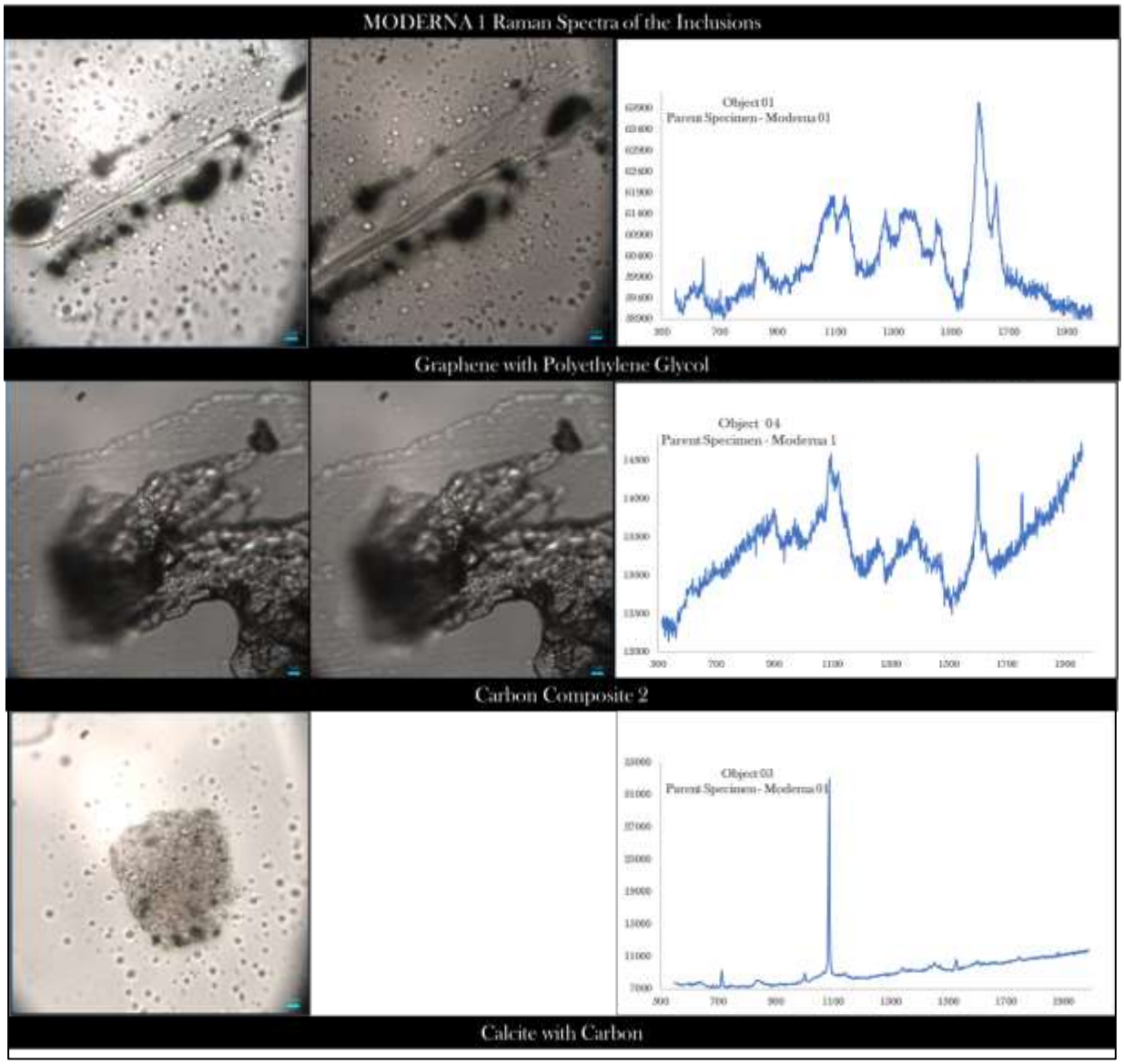

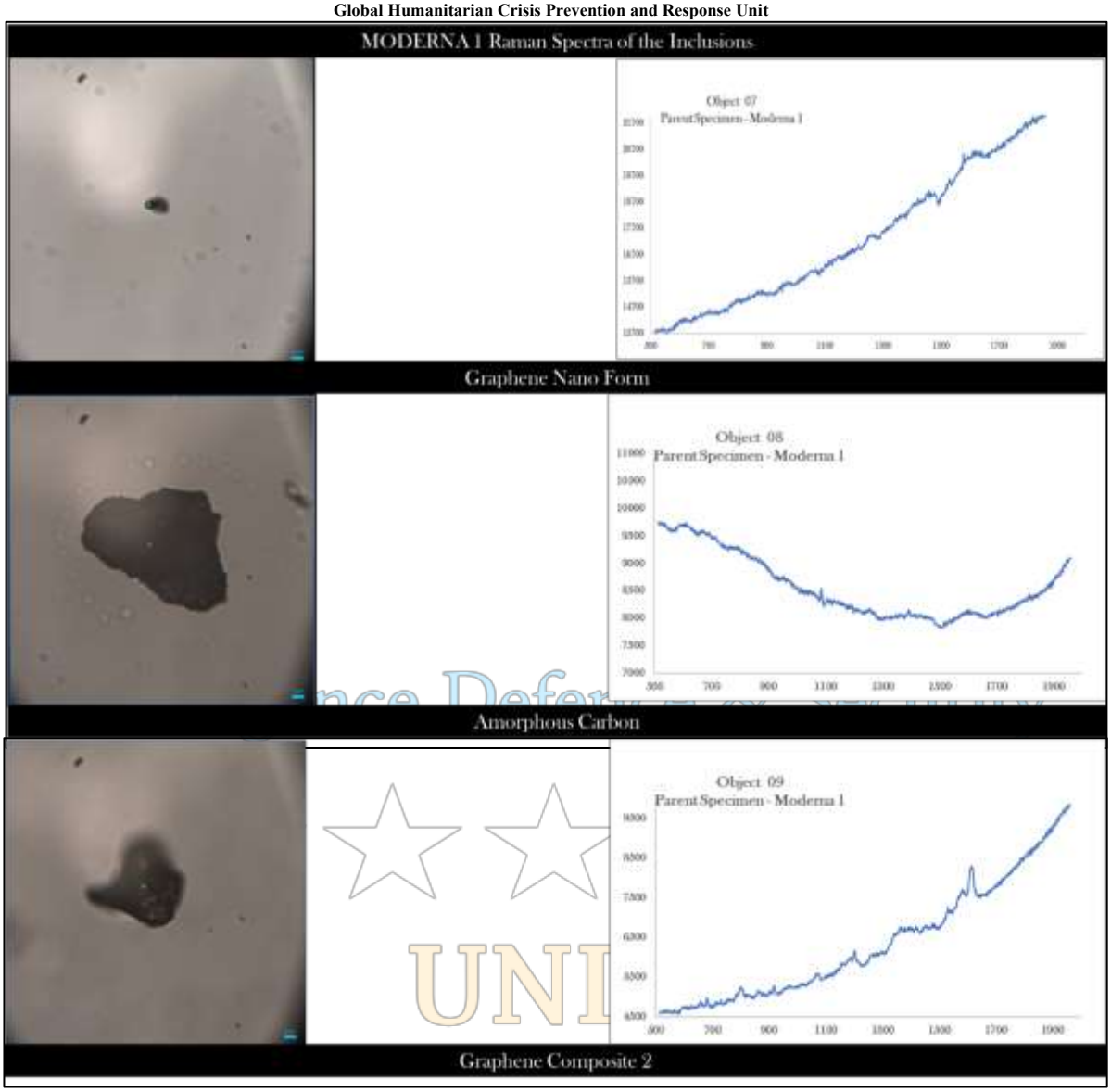

Figure 3.11. Raman spectrum of representative inclusions in Moderna01.

The two clear Raman signals were obtained from two objects. The flat ribbon like inclusions exhibited clear graphene spectra integrated with the spectrum of polyethylene glycol and other minor compounds. The other clear signal was obtained from a calcite microcrystalline form with a distinct strong peak at 1100cm^{-1}.

The carbon composite forms had a highly complicated signal with clear graphene peak at 1600cm^{-1}, but other peaks at 1100 cm^{-1} making the signal quite difficult to separate. Further analysis is currently underway to isolate these signals and identify the other components of this form of carbon. Some nano amorphous carbon forms showed a clear Graphene signal however, these forms also exhibited fluorescence which masked the Graphene peak.

These same forms were identified in other vaccine vials as well allowing for the establishment of their composition consistency across the spectrum of various samples with confidence.

The compositional identities derived of the inclusions through Raman spectroscopy was used to quantify the comparative occurrence of these inclusions along a 2D track. This abundance is presented as counts in the next section.

3.2.3. Counts

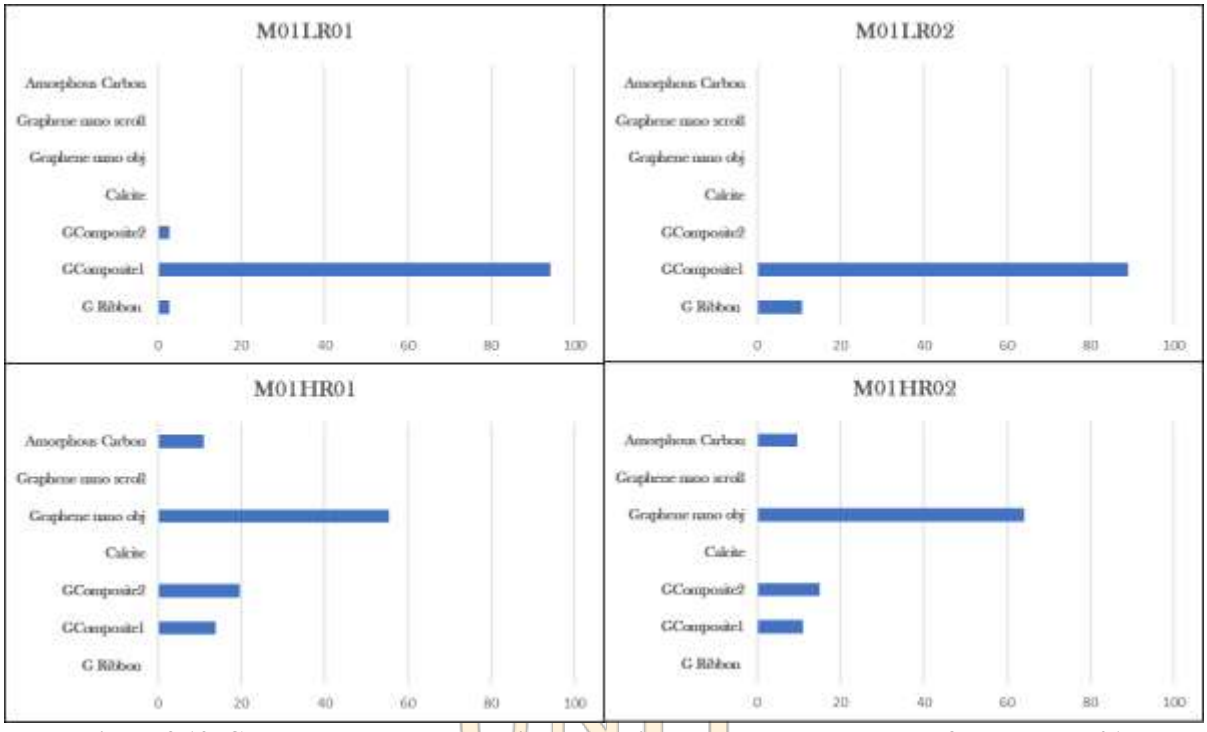

Figure 3.12. Count sheets at low and high resolutions along two tracks each for Moderna 01.

The inclusions were counted along two transects. Each transect was 2cm long. The counts were performed at both: low and high magnifications.

The count distribution is dominated at the low resolution by GComposite 01. At low resolution, GComposite 2 is present in very low quantities, but the abundance reverses at higher magnifications. The counts are overall dominated by Graphene nano objects (figure 3.11).

It should be noted, that Graphene nano scrolls were omitted in the counts. This step was necessary because though, these nano scrolls form a significant percentage of the total counts, a confirmation of their composition could not be attained within the limitations of this project. As mentioned above in Section 3.1.5, thorough investigation of these forms now constitutes the subject of enhanced second investigation project following this report.

3.3. Moderna 02

3.3.1. Microscopy

The sample material from Moderna 2, was translucent on slide with granular particulate material in suspension. On observation of the slide material under wet microscopy, several floating bits of transparent sheet like objects were observed (figure 3.12). Heavier material sank below as traction bedload and salted across the slide while the medium evaporated under the microscopic lamp light.

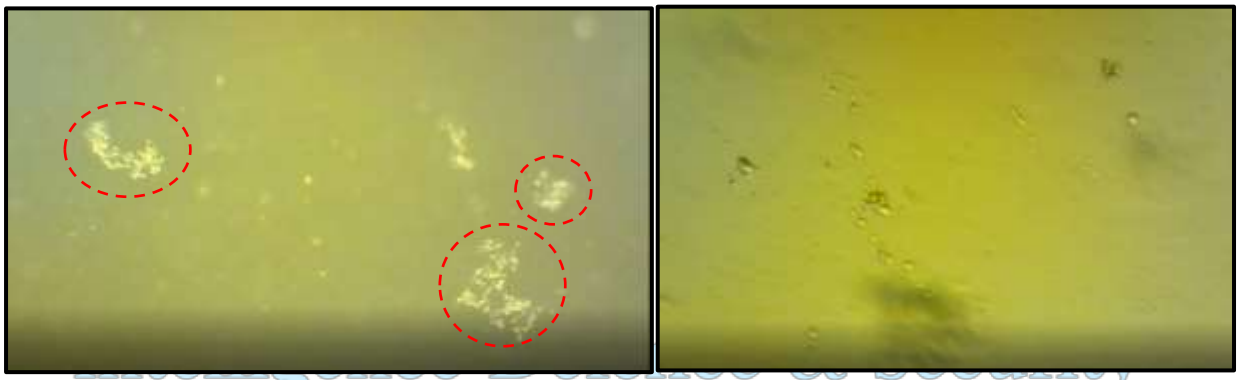

Figure 3.13. Floating sheets of translucent material in a wet sample as observed under an optical microscope. (b) The settled detrital material at the bottom of the slide. The shadows of the lighter floating material can be seen as dark hazy figures.

In regions where the solution column was of a significant thickness, bubbles were observed as flowing with the convection undercurrent towards the edge of the extent of the material. The locus of these particles was clearly striking, even under the lowest magnification.

The graphs obtained by tracking the movement for these particles were typical of self-assemblage systems composed of particles coming together under the influence of various intermolecular forces (figure 3.14).

An interpretation is here drawn in light of the knowledge, that these particles carry the required m-RNA load and under the designated conditions, exhibit the self assemblage characteristics using a combination of non-covalent intermolecular interactions such as electrostatic, hydrophobism, vander Waals and pi effects (figure 3.15).

The self assembly processes seem to be driven by a constantly changing competitive environment which is driven by the kinematic and thermodynamically driven cursours following a typical LaMer model. The seeding of the process seems to be around the nucleic acid form of molecules and Graphene nano objects. According to Kulkarni et al. (2018), the growth of the particle relies on the pH neutralisation and migration of neutral, unbound

ionisable lipid towards the LNP core regardless of the payload (mRNA, minicircular DNA or pDNA).

These particles were observed in ubiquity across the sample preparations and each of these structures began with the formation of a small seed like particle to which the surrounding particles aggregated, based on hydrophobic interactions.

What seems to be obvious through observation is that hydrophobic interactions appear to be the dominant driving force of the LNP growth and electrostatic interactions guide the seed formation and stability of the final assembly.

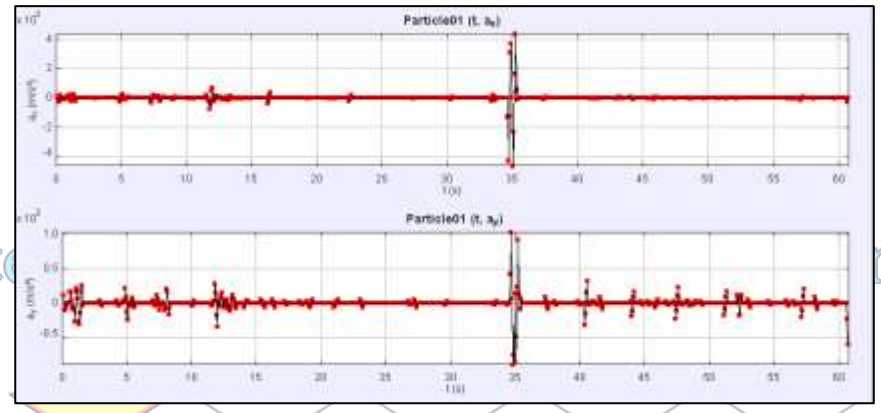

Figure 3.14. Motion graph of a characteristic self-assemblage particle. Accelerations in both X and Y directions show typical staggered forms that typify hydrophobic/philic jumps and movements.

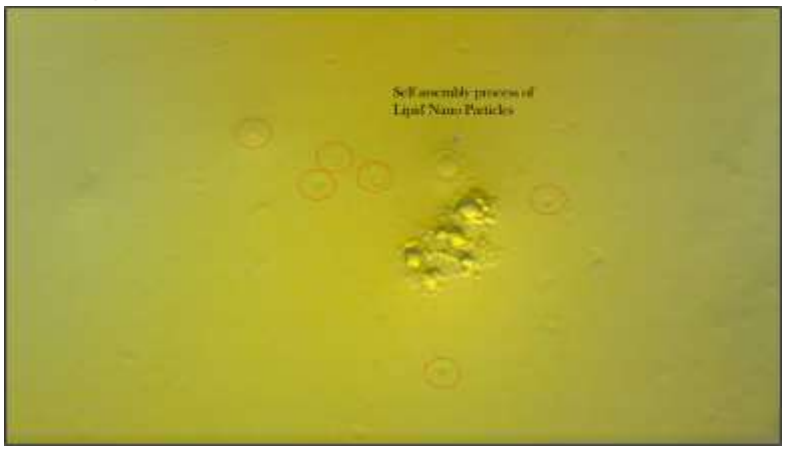

Figure 3.15. Self-Assembled Nano Particles with Payload of mRNA.

On drying of the sample, the solution settled into a thick layer, which retained some form of moisture. The relatively denser material settled to the bottom, while, the lighter material was on the top of the solidified solution with an additional detrital layer in the middle of the medium.

General overview of the dried slide at low resolution exhibited a translucent medium with forms akin to fibres and transparent sheets on the top surface (figure 3.16).

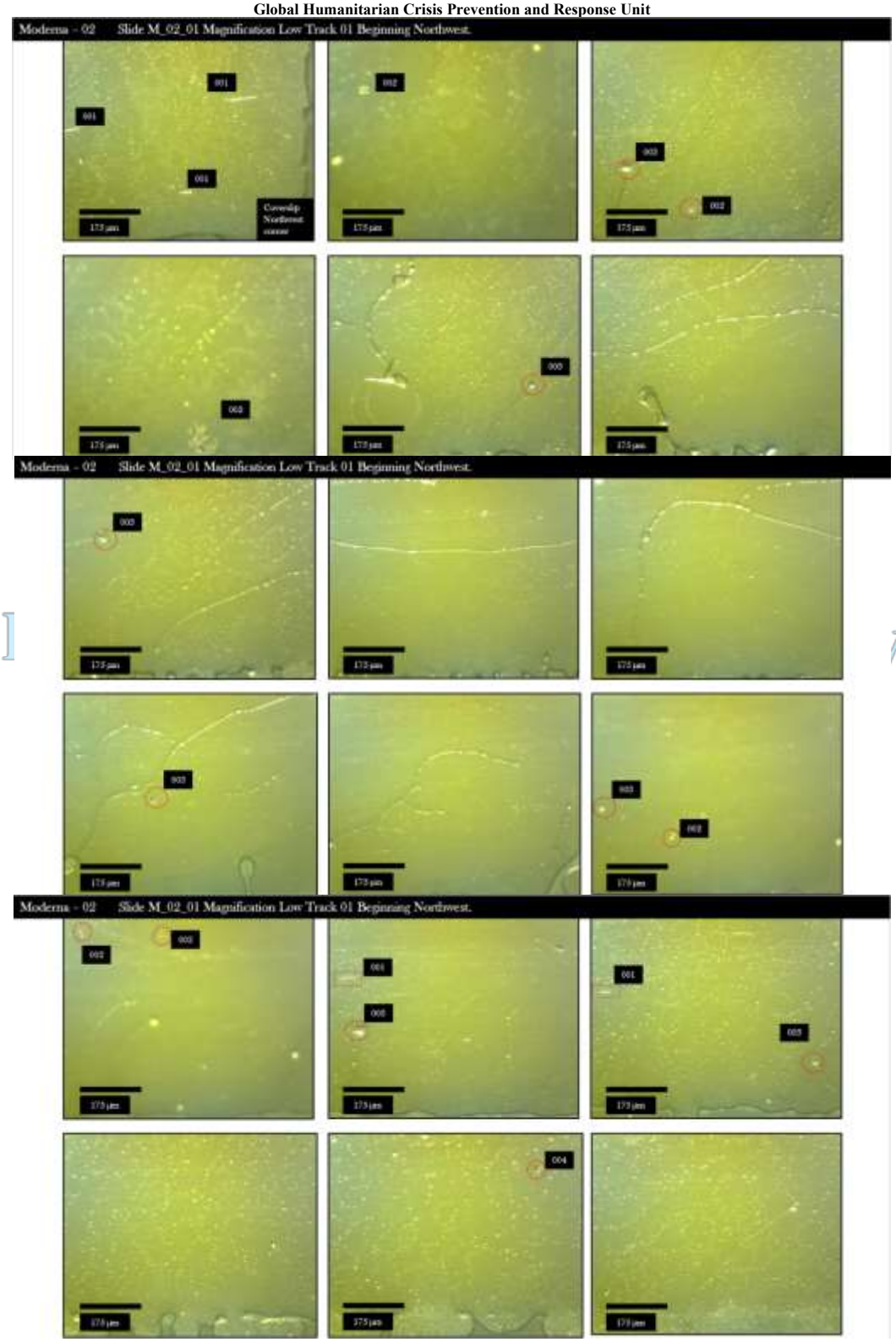

Figure 3.16. Moderna 02 Low Magnification overview of the slide.

On higher magnification, the slide material seemed to abound in carbon-related forms. Figure 3.17 shows different shapes and forms that were noted along various transects across the slide. It is noteworthy, that the noted deposits are on three separate planes, with a significant difference in the depth of focus.

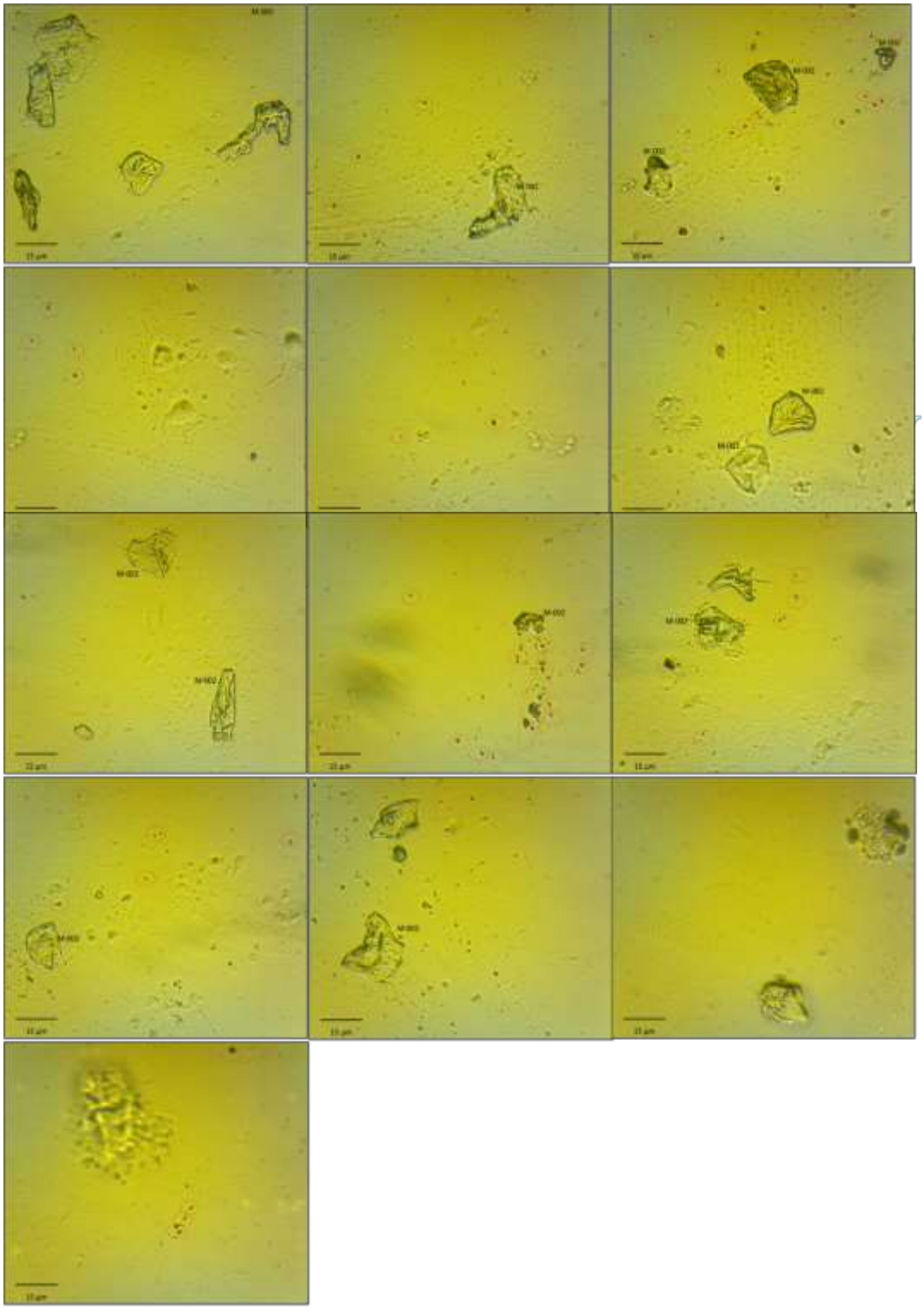

Figure 3.17. Representative inclusions across Moderna 02 at high magnification.

3.3.2. Raman Spectroscopic Investigation

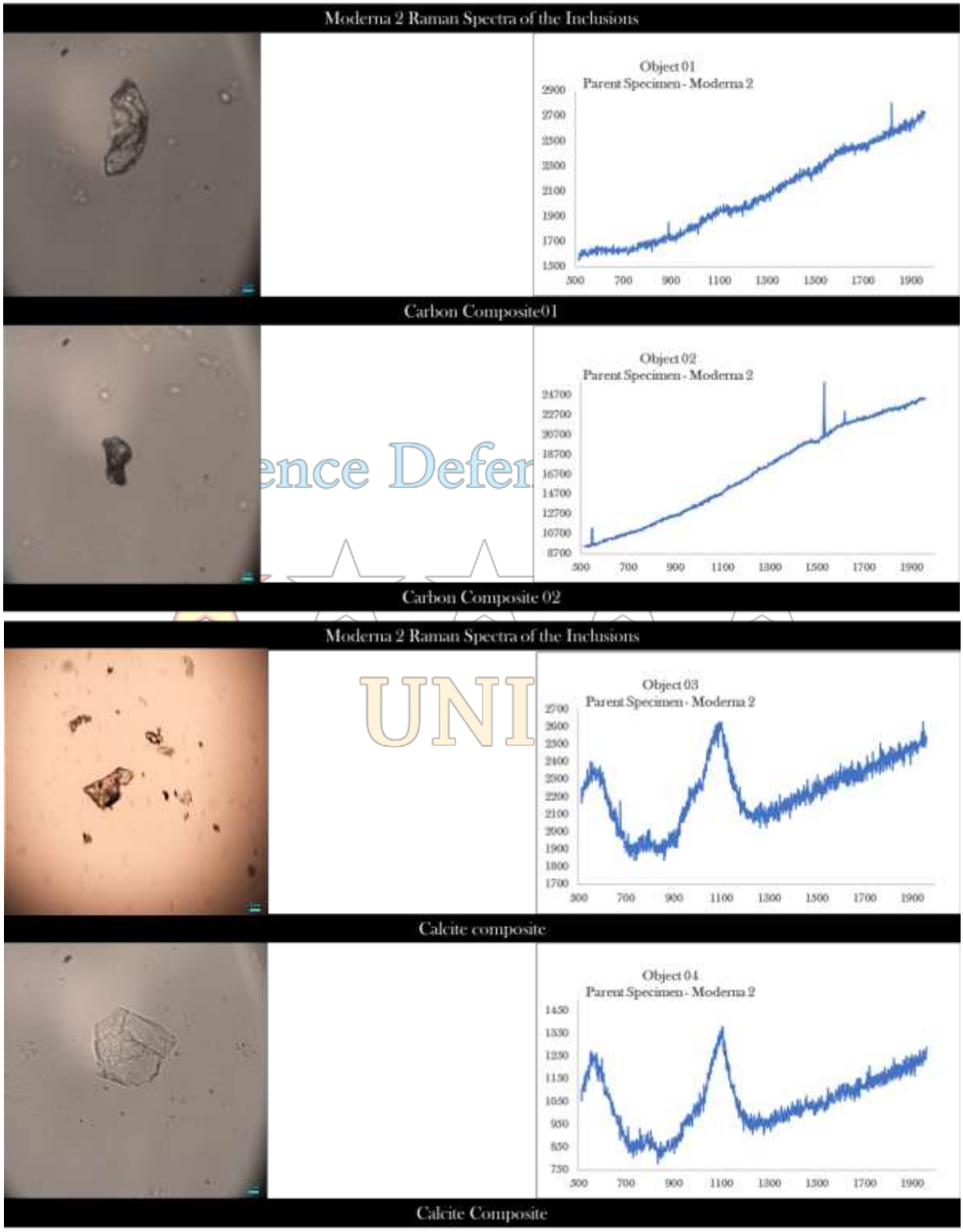

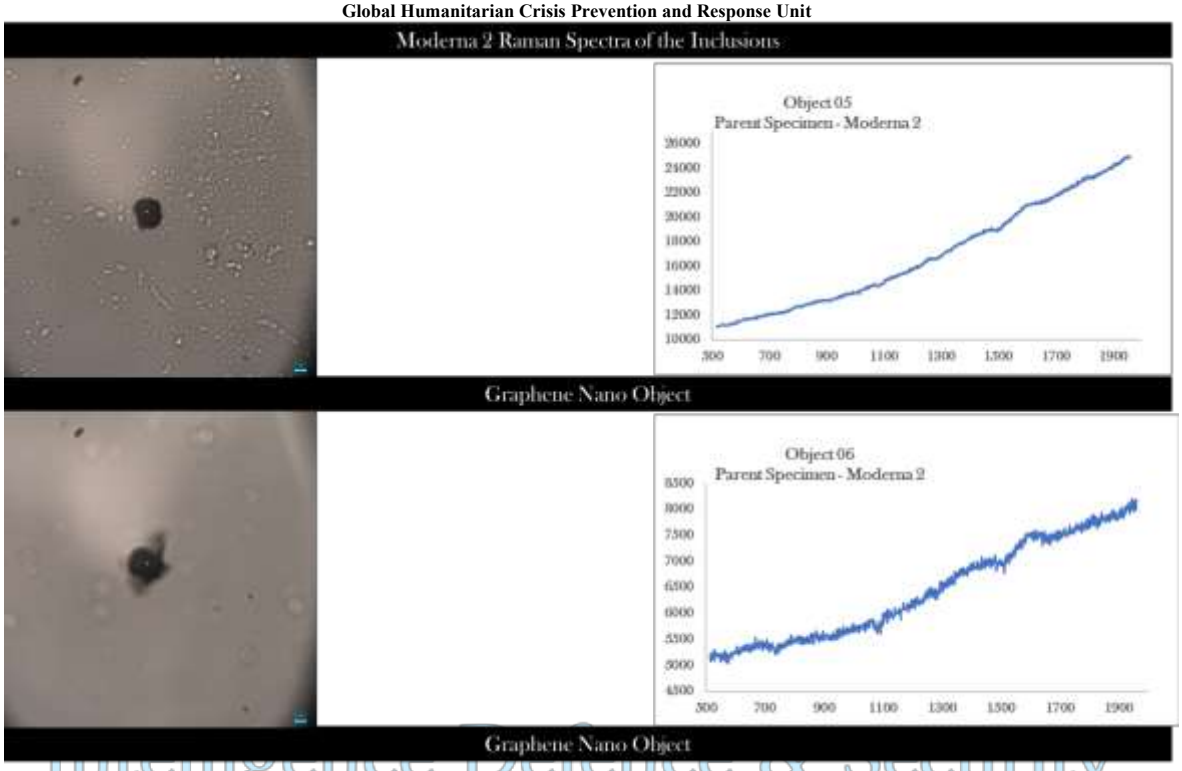

Figure 3.18. Raman spectra of various inclusions in Moderna 02.

Raman spectroscopy was used on the inclusions of Moderna 2 to identify the main representations of the sample (figure 3.18). With the exception of calcite composite samples, the rest showed a highly interfered spectrum. The carbon peaks at around 1600 cm^{-1} and 1350 cm^{-1} were only vaguely discernable in the Graphene nano objects. With the fluorescent background, it was extremely difficult to interpret the spectrum for any other component except carbon.

A reshooting and further processing of the data is highly recommended for these Moderna inclusions to be reasonably identified with some confidence.

In the absence of confident Raman signtures, for analysis of these inclusions, a comparative similarity was used in the presence of the known chemistries of the other inclusions. These chemistries were used to do the counts which are present in figure.

3.2.3. Counts

Counting of inclusions along four tracks of two at low and two at high magnifications showed results similar to Moderna 01 (figure 3.19). Graphene Composite 01 were prominently present

at lower resolution and at higher resolutions, Graphene Nano objects are present in great abundance.

It is clear from the counts, that the nanoscopic structures far exceed the density counts than microscopic structures.

It should be noted, that Graphene nano scrolls were omitted in the counts. This step was necessary because though, these nano scrolls form a significant percentage of the total counts, a confirmation of their composition could not be attained within the limitations of this project. As mentioned above in Section 3.1.5, thorough investigation of these forms now constitutes the subject of enhanced second investigation project following this report.

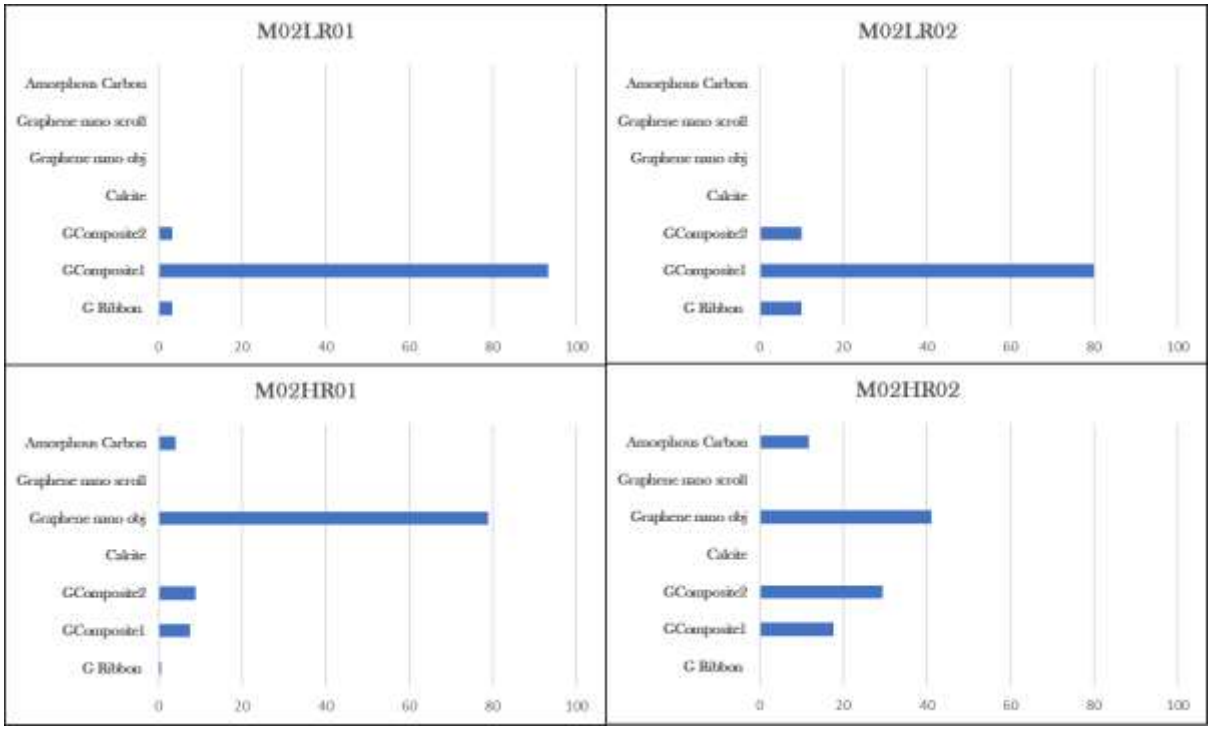

Figure 3.18. Count sheets at low and high resolutions along two tracks each for Moderna 02.

3.4. AstraZeneca

3.4.1. Microscopy

AstraZeneca was the third vaccine that was evaluated for its inclusions. Several fresh runs of the wet samples were seen under the microscope. The AstraZeneca vaccine is almost transparent when seen through the microscope, making the spotting of any inclusions with inherent colours slightly easier.

The wet microscopic observation was that the fresh solution exhibited instantaneous movement of nanoscopic particulate material (figure 3.20) which when observed closely, evolved from being driven by the convection current, to being quite random. As the solution dried up, the particles exhibited traction movement.

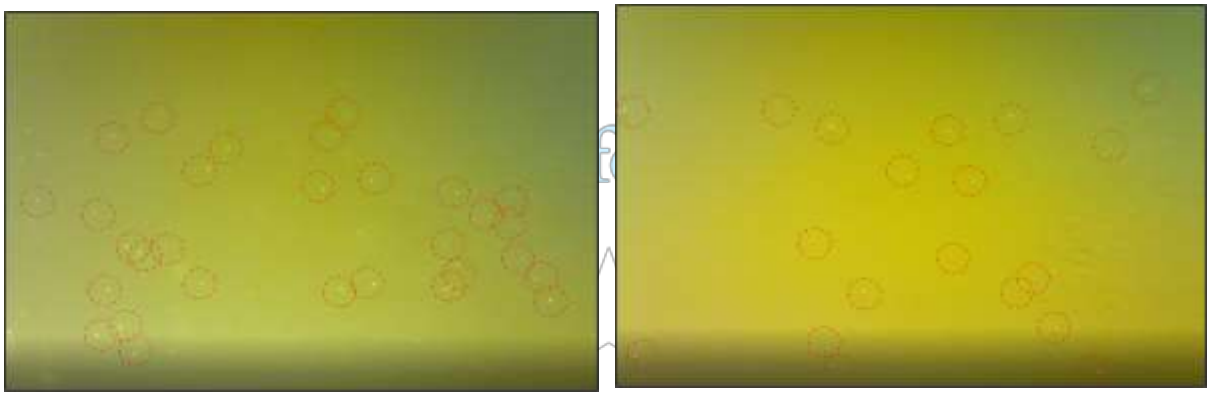

Figure 3.20. Nano Particles in motion when depth of the solution is greater than the height of the particle. The particles coalesce to form bigger particles and the dominating influence on the direction of the movement is through the currents within the solution.

These nanoscopic particles were quite noticeable as white specs in the beginning, as moving in a swarm like motion in the same general direction. With time, these evolved into bigger droplets with more random vectors following the principles of self assembly.

As the solution dried, from the heat of the lamp of the microscope from the top, the sedimentation process began with sheet like forms being deposited on the top of the medium which begins to crystallise early while the liquid below is still able to flow partially. This difference in the crystallisation or solidification pace was clearly discernible from a few slide shots off a video, as are presented in figure 3.21. In the figure, the microscopic form is clearly visible as it is lying on top of the solid film while the nanoparticles are still in motion in the background as can be seen by the shifting position of the shadow. A clear output of this mechanism was that as the medium solidified, it becames more difficult for the nanoparticles to navigate through the viscous material. The core of the nanoparticles was seeded with carbon nanotubes and carbon nano objects: formed of some form of detrital carbon particles. These were dragged along with the eddie currents at the bottom of the medium and as the material

settled, the flute casts were left behind which were identified easily in the dry microscopic sections.

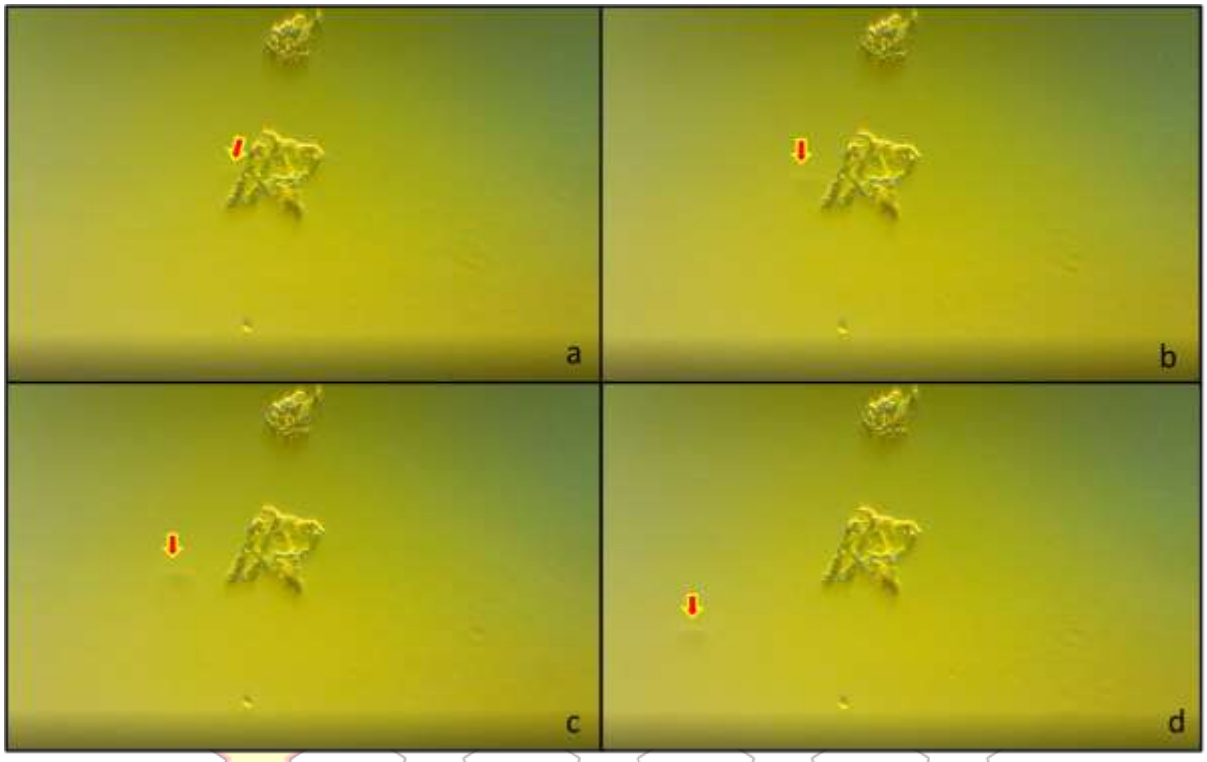

Figure 3.21. Lamellar convection columns with solidified top resulting in deposition of the flaky particle. The arrow points to the position of the nanoparticle in the deeper column of cooler material.

Even, in a wet slide under the microscope, several forms of inclusions were observed. These are described in detail below.

Nano particle movement and self assembly process was noted in AstraZeneca, similar to what was noted in the Moderna vaccines. Here too, the nano particles self assembled through typical signatory movements attributed to the inter-particle forces. While the solution dried up, the heavier carbon material that had sunk to the bottom of the slide was released from the nucleus of the nanoparticles and these now began to exhibit traction movement. Figure 3.22, shows the relative movement vectors of some of these solid materials. When these inclusions settled down, they sank to the lower strata. A later, high resolution examination of the lower strata shows a dump of graphene nano objects (figure 3.23) including graphene nano scrolls (figure 3.24).

Figure 3.22. Distance covered by the object through combined movement vectors

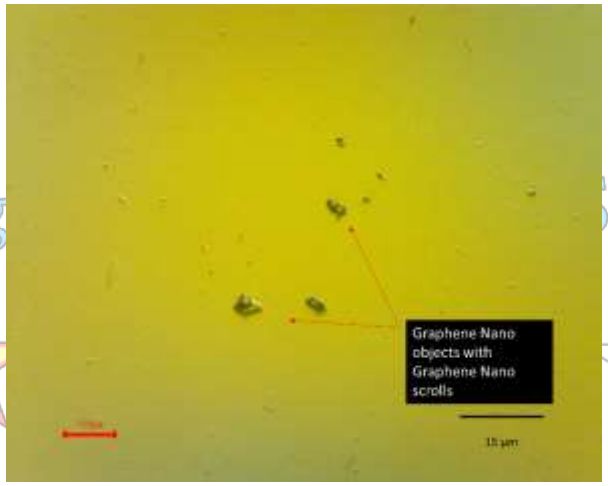

Figure 3.23. Graphene based structures settled down on drying. These structures demonstrated self-movement against the growing viscosity of the drying solution. When the solution dried, they were found to have settled at the bottom of the slide.

Figure 3.24. Graphene scrolls or spicules dumped at the bottom of the slide.

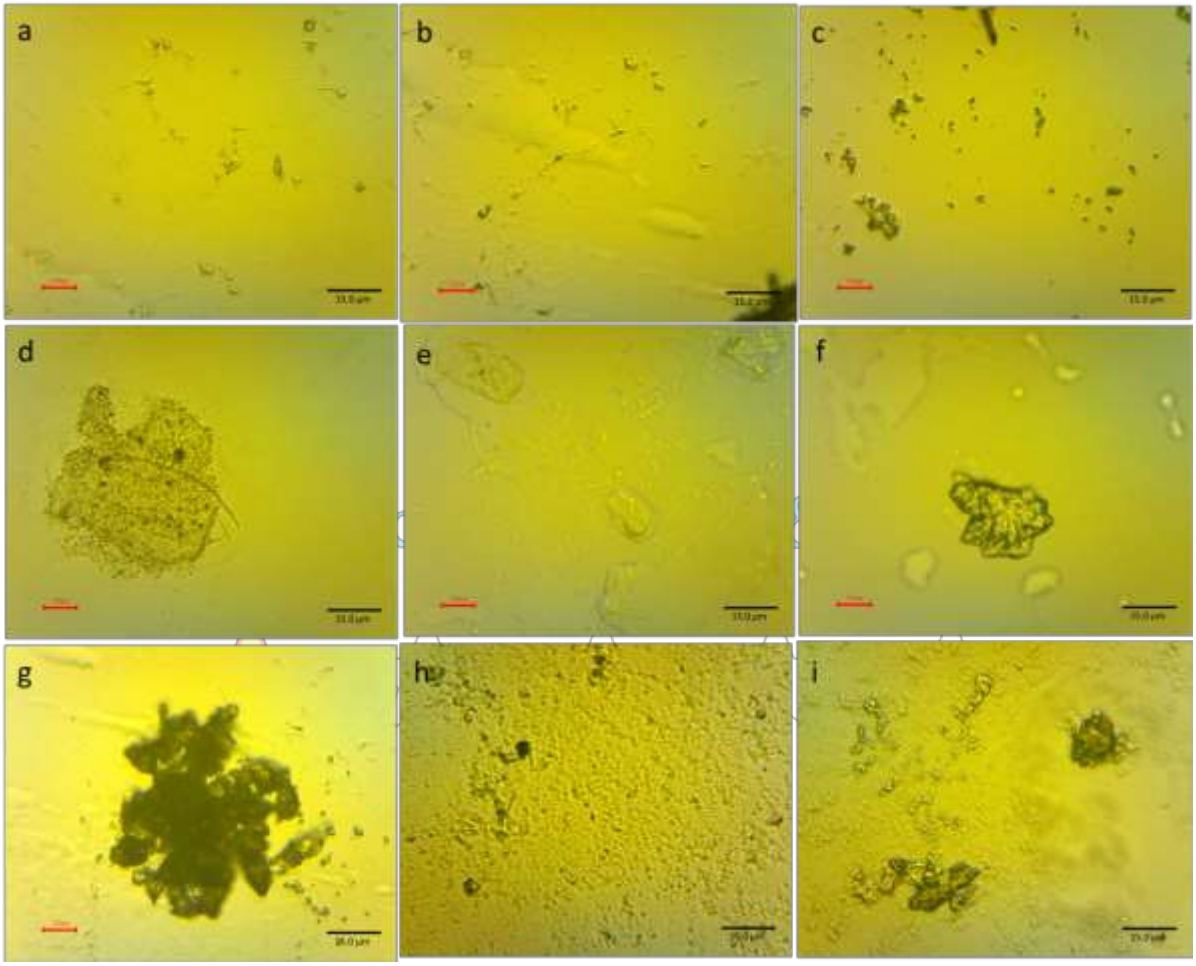

Figure 3.25. Representative inclusions found within AstraZeneca vaccine.

The inclusions identified within AstraZeneca were of the same category as described in section 3.1. These included Graphene composites of two variations, Graphene ribbons impregnated with polyethylene glycol, Graphene Nano Objects including a vast number of nano scrolls and a high count of amorphous carbon. Calcite was also distinctly present in the vaccine in a microcrystalline carbon composite form.

The type inclusions were targeted for Raman identification.

3.4.2. Raman Spectroscopic Investigation

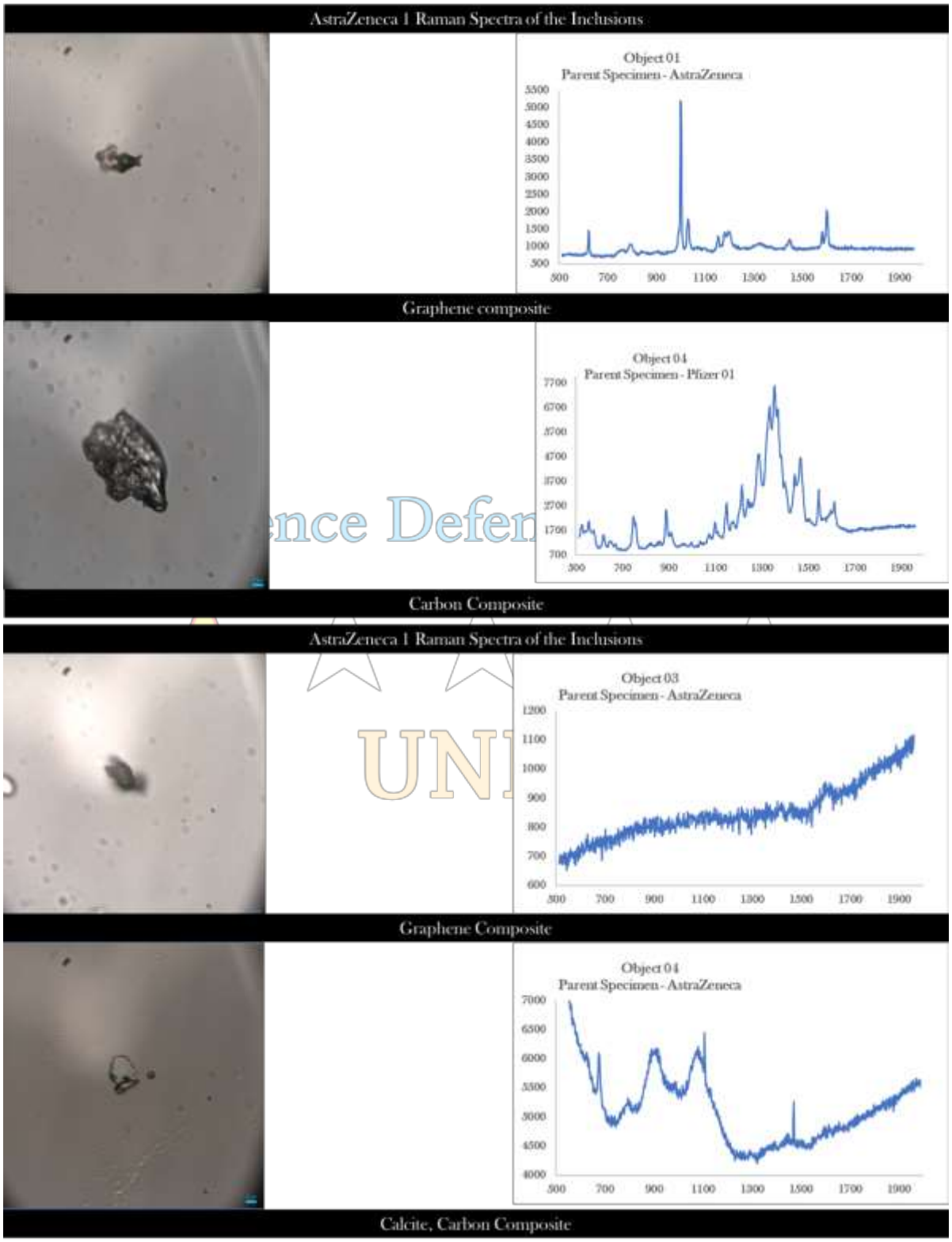

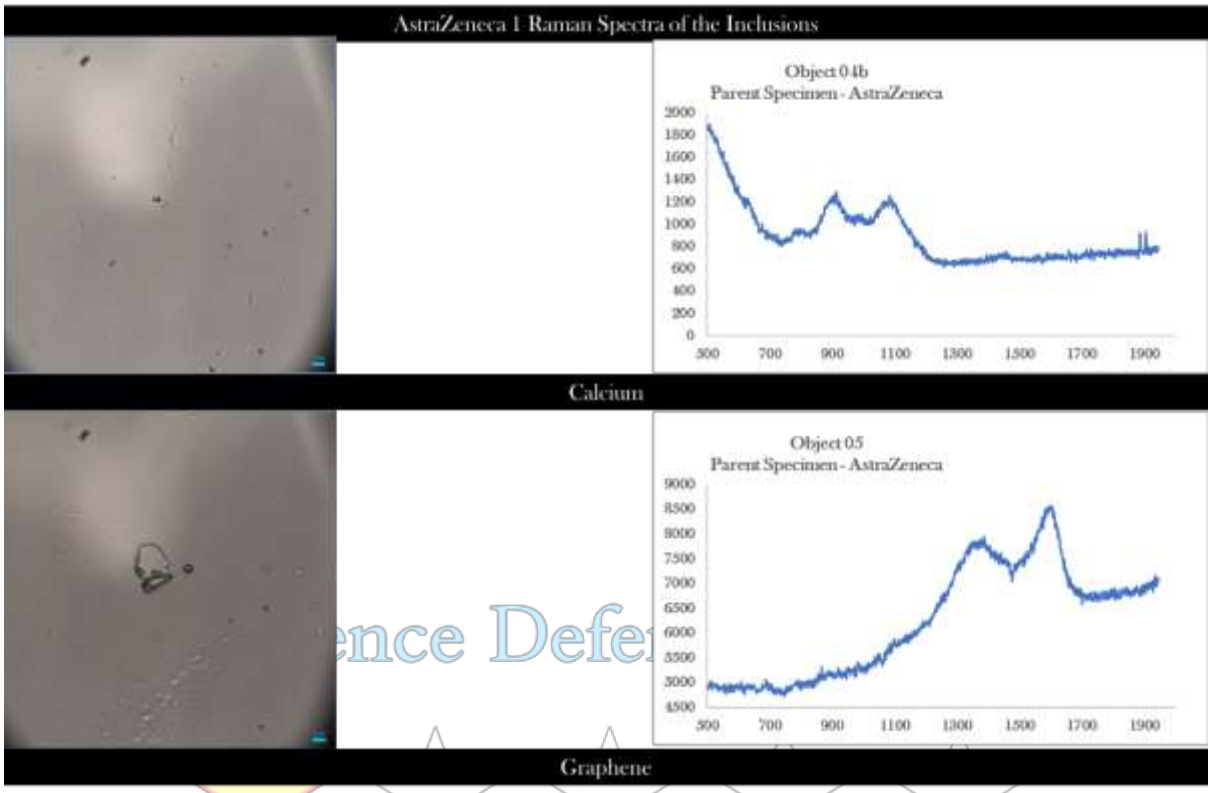

Figure 3.26. Raman spectra of various inclusions in AstraZeneca.

Raman spectroscopy results on inclusions within AstraZeneca yielded direct confirmation of the presence of Graphene in all the identified representative forms.

The carbon composites are of two forms as they are in the Moderna vaccines. These two forms showed distinct graphene signatures through the characteristic Graphene peaks at 1600 cm^{-1} and 1350 cm^{-1}. Besides Graphene, the spectrum is dominated by iron oxide and some other forms of carbon associations.

Further work is ongoing to isolate the signals and help to identify individual compounds. With the exception of one sample of graphene composite, the effect of fluorescence was found to be minimal in AstraZeneca's selected inclusions.

Calcium composites with carbon also showed the same signature as the ones present in the two Moderna vaccines.

The inclusions in the calcite composites contained pristine graphene nano particles. These particles were evaluated to show a clear signal for graphene. Though, the Graphene nano objects were present in clear association with the Graphene nano scrolls, Raman investigations were not carried out on scrolls due to the limitation of the laser size and the microscope's

magnification. In any future work on AstraZeneca, shooting Raman on the scrolls would be one of the main targets in quantifying the concentration of Graphene.

The identification of the inclusions assisted in accurate counting process in the following stage.

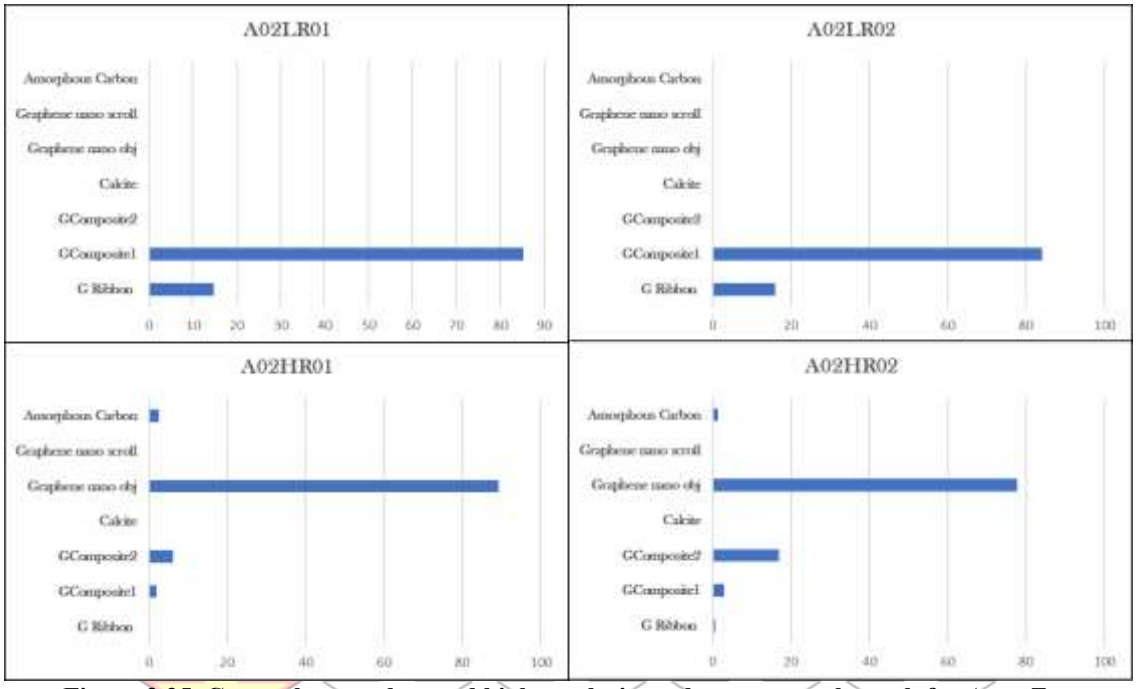

Figure 3.25. Count sheets at low and high resolutions along two tracks each for AstraZeneca.

3.4.3. Counts

AstraZeneca counts do not pick up Graphene composite 2 in the lower magnifications however these are present in significant numbers at higher magnifications. It is clear from the graph that graphene nano objects dominate the count at higher resolutions.

It should be noted, that Graphene nano scrolls were omitted in the counts. This step was necessary because though, these nano scrolls form a significant percentage of the total counts, a confirmation of their composition could not be attained within the limitations of this project. As mentioned above in Section 3.1.5, thorough investigation of these forms now constitutes the subject of enhanced second investigation project following this report.

3.5. Pfizer

3.5.1. Microscopy

Pfizer was the fourth vaccine vial that was evaluated for its inclusions. The vaccine was noted to be of the same offwhite colour as Moderna. 0.006 µL of the sample was transferred on the slide for wet evaluation and an equal amount was left in a slightly inclined pippette to allow for examination in a closed environment in 3dimensions.

The pippete specimen showed some extremely interesting inclusions which were not found when the slide dried. As the material was sucked into the pipette, distinct translucent to transparent sheets were seen floating about (figure 3.28). These were recognized from previous observations in AstraZeneca and Moderna to be the Graphene Composite 1.

Active sedimentation of the denser material on the bottom curve of the cylinder was noted immediately afterwards (figure 3.29).

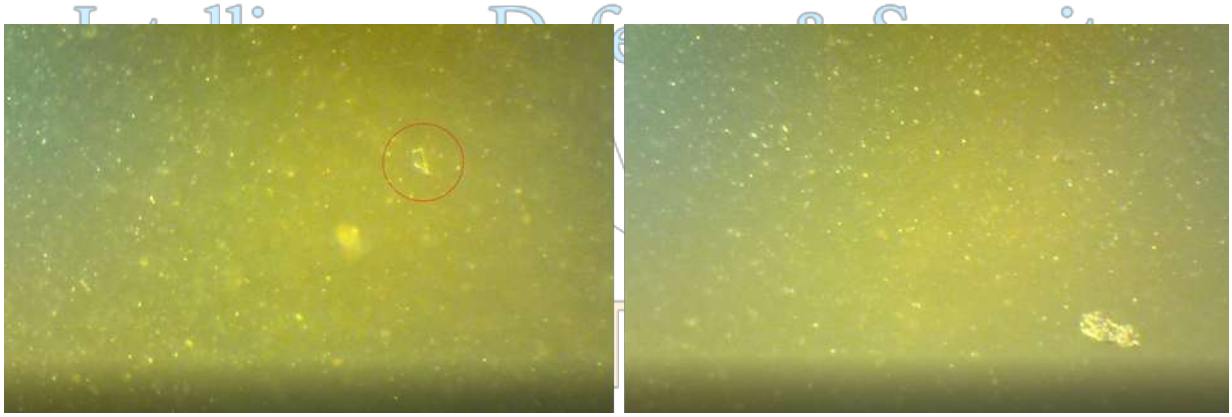

Figure 3.28. Floating lighter material. In the background, the golden sparkly particles are the future self-assembly nano particles that will encapsulate the mRNA.

The two objects of interest that were clearly noted to be floating about but could not be located once the slide had dried, were: (1) an extremely pointy transparent spicule like object (figure 3.30) and the other was a thin translucent perforated sheet (figure 3.31).

Where, both the objects are of interest to this study, the nature of the spicule remains vital for future work to identify.

As the solution was poured onto a slide for observation, the mixture exhibited the same nanoparticulate self assembly mechanism as was observed in both Moderna and AstraZeneca vaccines. As the material dried out, the inclusions settled at various depths depending upon their relative densities.

Figure 3.32 shows an assembly of various forms of inclusion that were identified within Pfizer. These fall in the same category as mentioned in section 3.1.

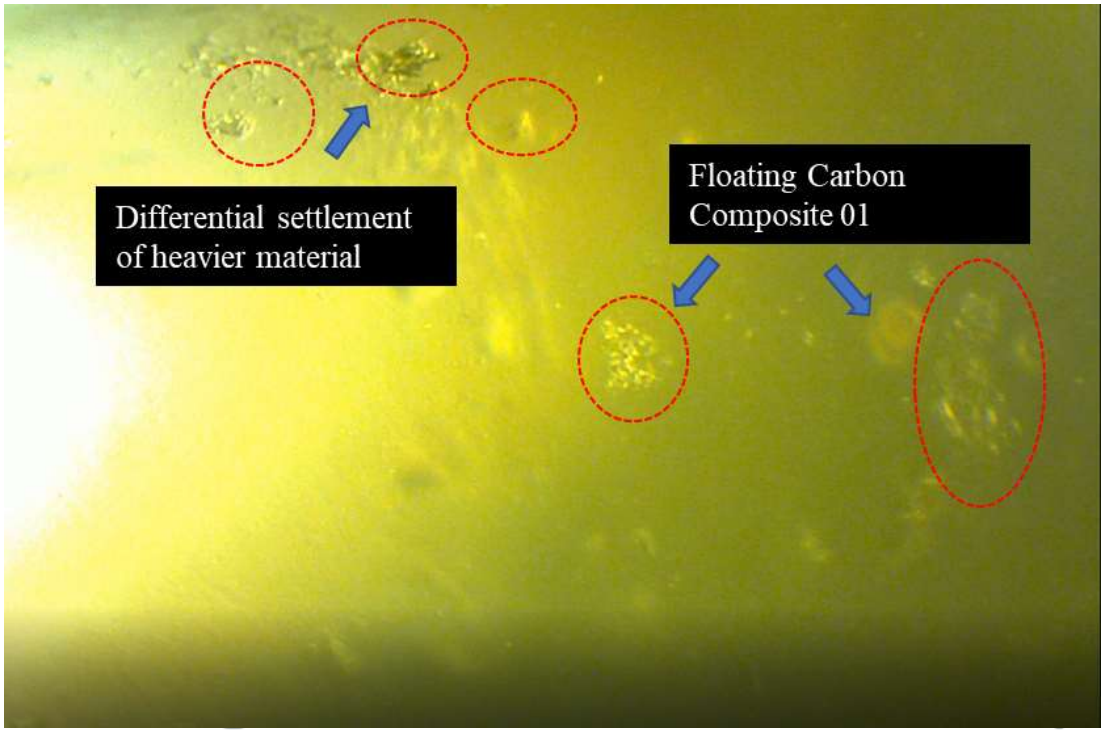

Figure 3.29. Sedimentation of the heavier load on the curved bottom of the pipette and the floating transparent composite 01.

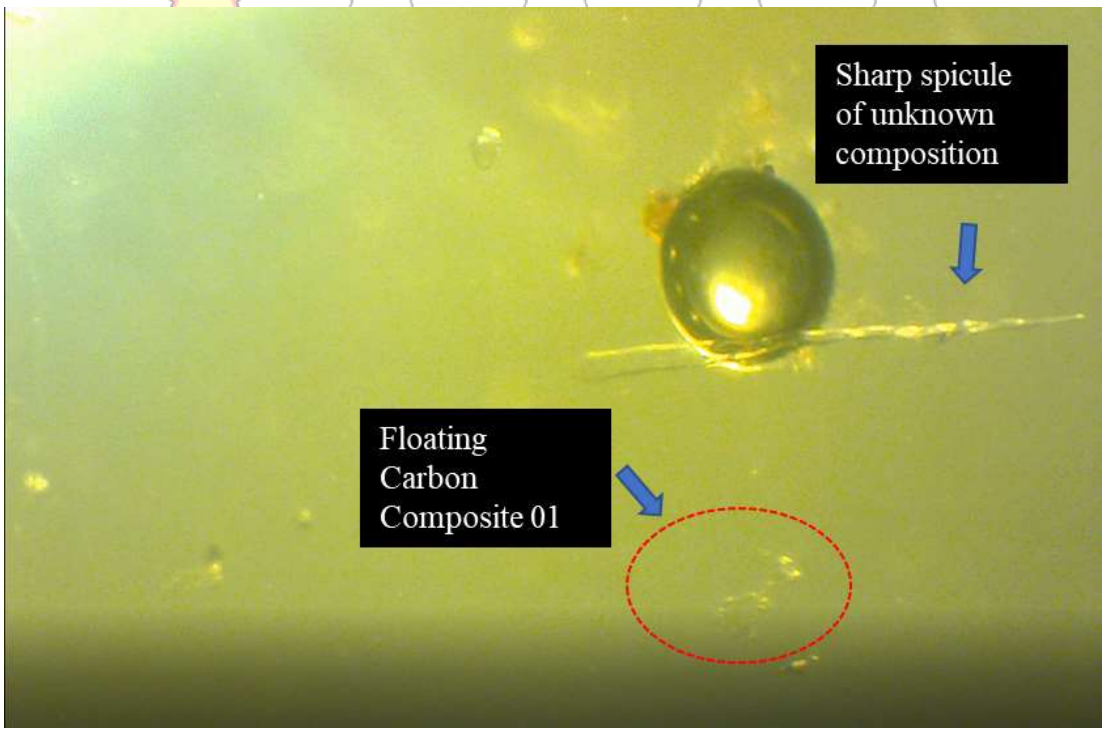

Figure 3.30. Sharp transparent spicule floating in the liquid.

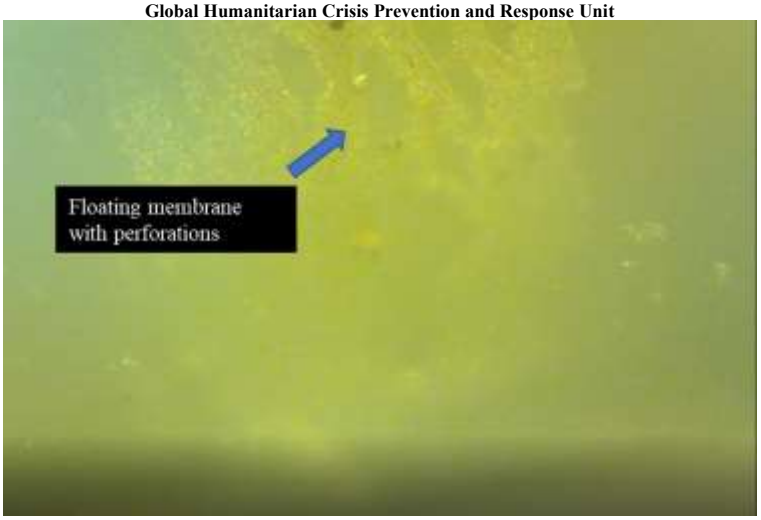

Figure 3.31. Floating perforated membrane.

Ribbon forms of nearly transparent microforms are found in fair number in the slide. These are often half embedded in the solution with one end projecting outside the material.

The carbon composites of both form 1 and 2 also are present in great numbers. Form 1 settles on top of the material while form 2 is found at mid levels of the solidified medium.

Graphene nano forms are present in fair numbers within the slide material along with some scrolls.

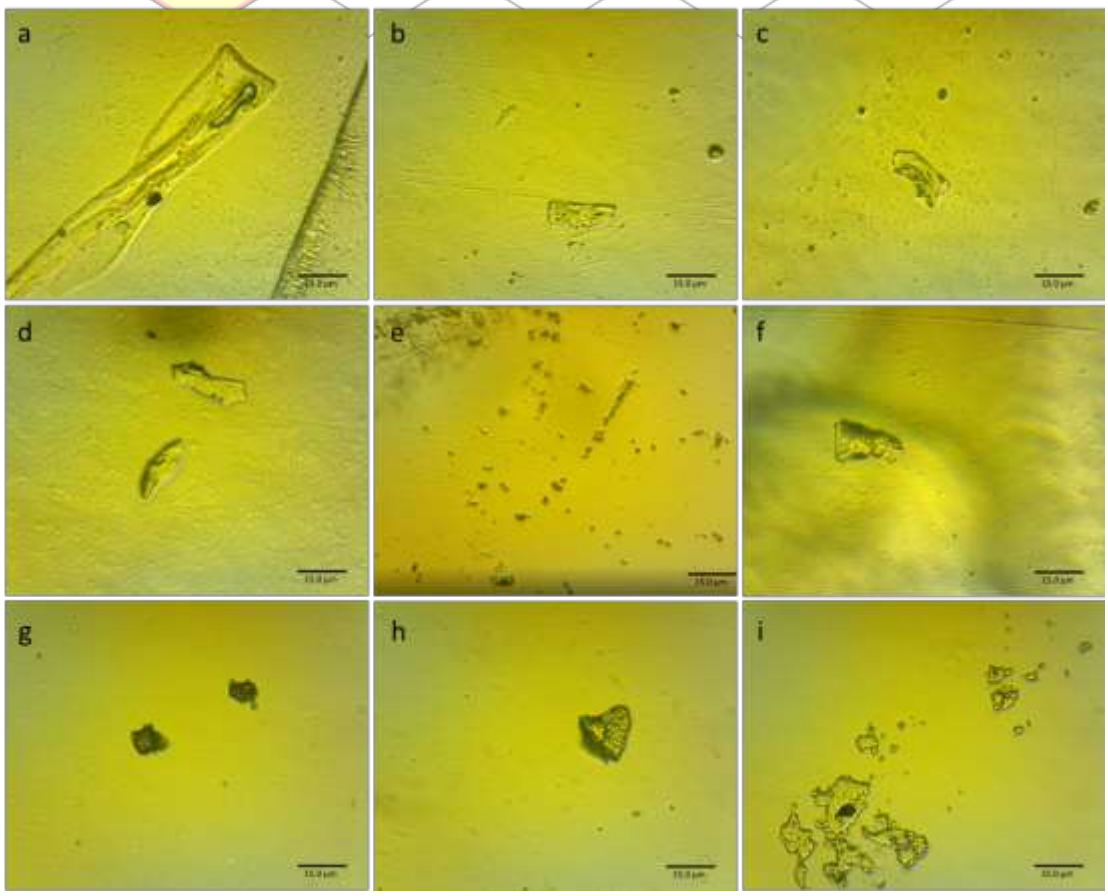

Figure 3.32. Representative inclusions found within Pfizer vaccine.

3.5.2. Raman Spectroscopic Investigation

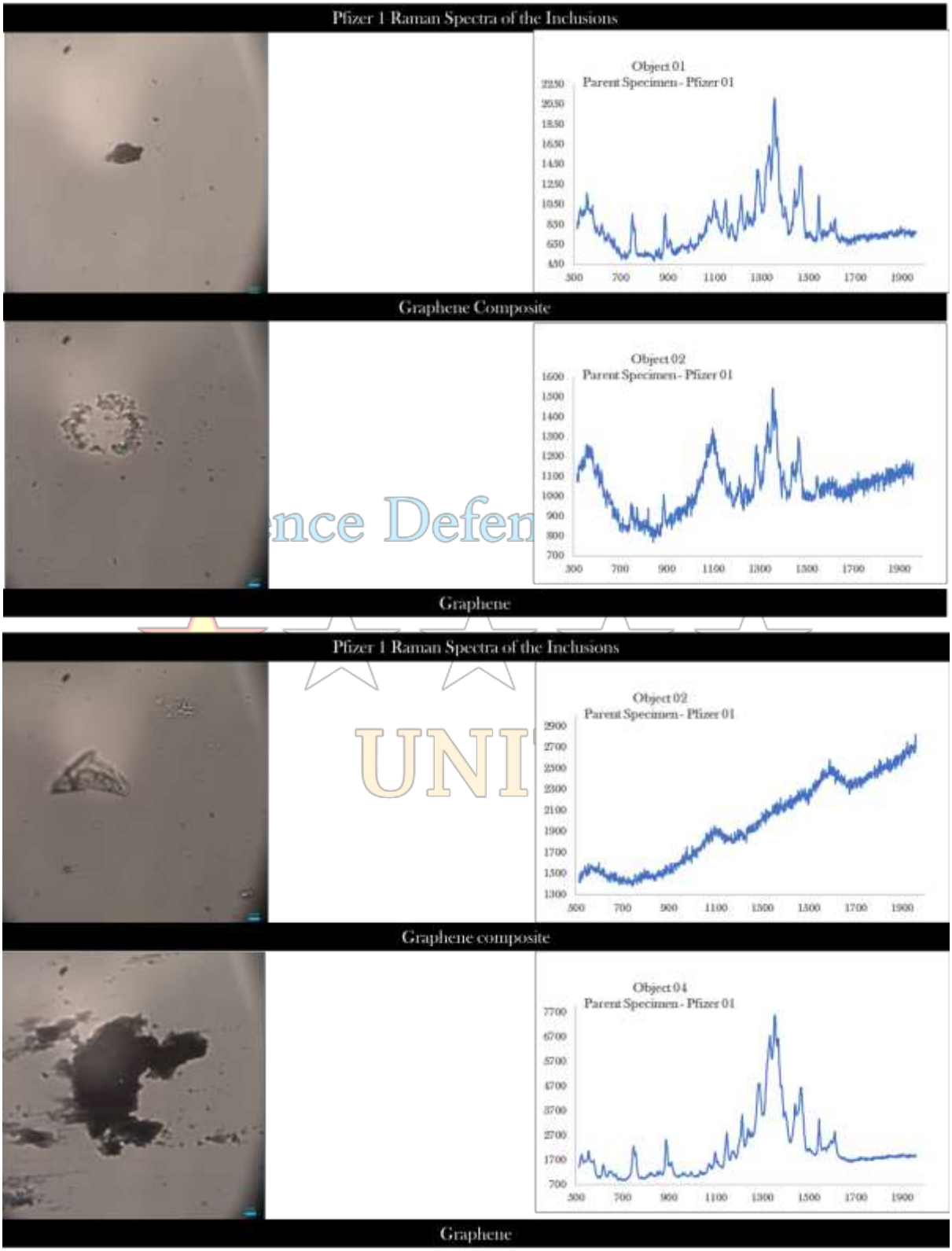

Figure 3.33. Raman spectra of various inclusions in AstraZeneca.

Raman spectroscopy was conducted on four selected representative samples for Pfizer (figure 3.32). Three of these samples showed carbon composite signatures with possible graphene in

them. The signals of amorphous carbon like materials were extremely complex with carbon along with iron oxide and several other compounds in them. The graphene complex 1 is graphene with polyethylene glycol signal forming the bulk of the spectrum. Though, for initial assessments, this study can confirm the presence of graphene in Pfizer, however, the complex with which it is associated still requires to be established through further work.

One of the sample that was shot, displayed a fair influence of fluorescence. Reshooting this sample at longer exposures is important to separate the signal from the article of interest with the signal of the background.

In summary, Raman helped identify the inclusions within Pfizer and these identifications were classed in the counts.

3.5.3. Counts

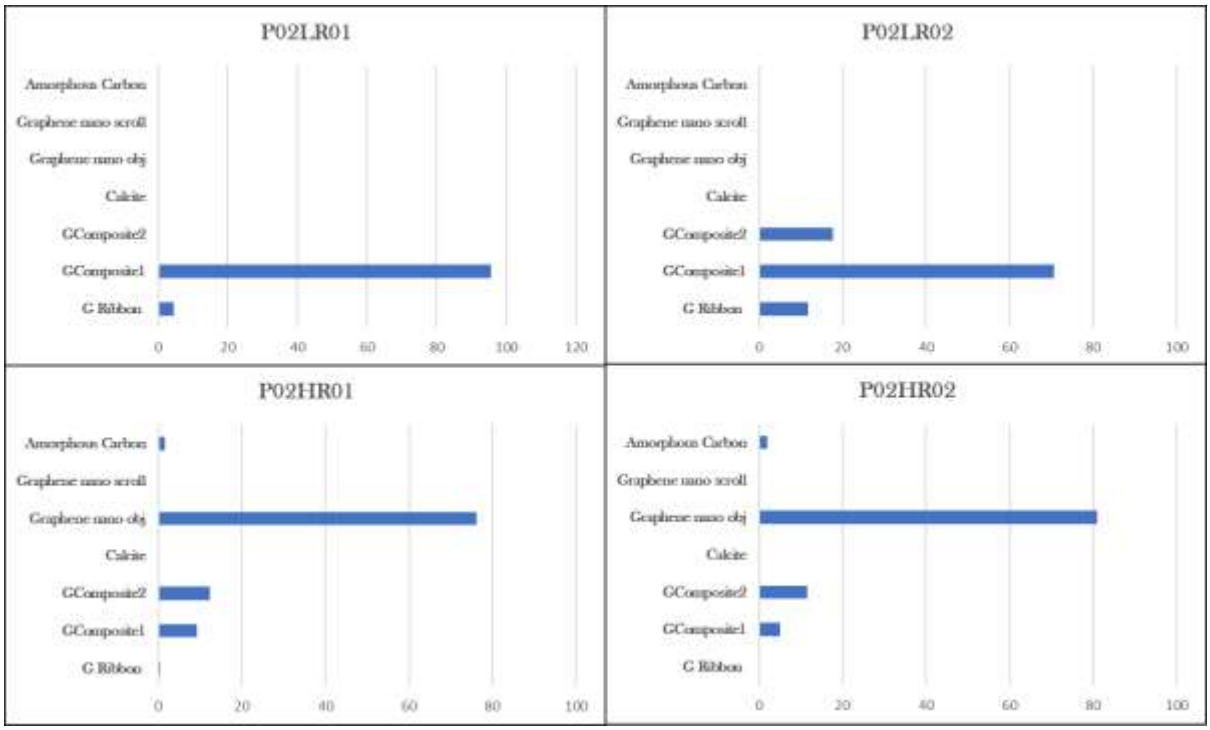

Figure 3.34. Count sheets at low and high resolutions along two tracks each for AstraZeneca.

The counts for Pfizer were conducted along four tracks of two each for Low and High magnifications (figure 3.34). The relative numbers of carbon composite 2 is quite high in one of the tracks whereas it is completely absent in the first track. At higher magnifications the counts are dominated by the sheer number of nano graphene objects.

It should be noted, that Graphene nano scrolls were omitted in the counts. This step was necessary because though, these nano scrolls form a significant percentage of the total counts, a confirmation of their composition could not be attained within the limitations of this project. As mentioned above in Section 3.1.5, thorough investigation of these forms now constitutes the subject of enhanced second investigation project following this report.

4. Interpretation, Discussions and Conclusion

Table 1
List of declared ingredients for the vaccines.

Moderna

Active Ingredients
- mRNA

Vehicles
- SM102
- Polyethylene Glycol
- 2000 dimyristoyl glycerol (DMG)
- Cholesterol
- 1,2-distearoyl-sn-glycero-3phosphocholine (DSPC)

Inactive Ingredients
- Tromethmine
- Tromethamine hydrochloride
- Acetic Acid
- Sodium Acetate
- Sucrose

AstraZeneca

Active Ingredients
- Adenovirus

Vehicles
- L-histidine
- L-histidine hydrochloride monohydrate

Inactive Ingredients
- Magnesium Chloride Hexahydrate
- Polysorbate 80
- Ethanol
- Sucrose
- Sodium Chloride
- Disodium edetate dihydrate (EDTA)
- Water

Pfizer

Active Ingredients
- mRNA

Vehicles
- 4-hydroxybutyl azanediyl bis hexane -6.1-diyl bis 2 hexyldecanoate
- Polyethylene Glycol
- N,N di tetra decylacetamide
- 1,2 di stearoyl sn glycerol 3phosphocholine
- Cholesterol

Inactive Ingredients
- Potassium Chloride
- Monobasic Potassium Phosphate
- Sodium Chloride
- Dibasic sodium, phosphate dehydrate
- Sucrose.

The study subjects were four vaccine samples (2 of Moderna, 1 of AstraZeneca and 1 of Pfizer). The objective of this study was to examine these four vaccine vials and document any undeclared ingredients in the composition of the vaccines, with special focus on graphene and related products as well as any biological forms.

It should be noted, that all three vaccines have very different chemical ingredients as declared by the manufacturers (Table 1). Despite, this genetic difference between them, upon examination, the results reveal common undeclared inclusions in the four vials.

These inclusions are primarily with a focus on graphene and carbon related nano structures in form of carbon or graphene composites, graphene in association with polyethylene glycol, graphene oxide, iron oxide compounds, and calcite. The variation in shapes of the logged inclusions, points to their varied purposes in the wider arena of drug delivery and biosensory fields.

The shapes identified during the course of this project can be classified into five different categories-

1. Ribbon Forms (G-PEG)
2. Sheet forms (GC-1)
3. Tubular forms (GC-2)
4. Nano Dots
5. Nano Scrolls

Where, the roles of the Ribbons and sheets remain unclear due to their microscopic sizes, the tubular forms along with nano dots and scrolls seem to be aimed at enhancing cell acceptance for the drug.

All three vaccines commonly employ the self-assembling lipid nano particles as drug delivery mechanisms. Where, the central find of this project has been the confirmation of the presence of graphene in all four samples, it is important to evaluate this find in the context of the subject itself.

As mentioned above, self-assembly processes are the core delivery mechanisms for the three types of vaccines. As has been reported under observations in the Chapter 3, the process in itself, is primarily dependent on weak intermolecular interactions (Mendes et al. 2013) which, in the case of lipid nanoparticles is driven and determined by the kinetics and the thermodynamic environment. However, based on the observations within this study, to kickstart the nucleation or seeding of these particles in the first state, Graphene nanoparticles

seem to play an important role. This interpretation is drawn from the observation that each of the nanoparticles seem to have a graphene core made of nano particles that float in the beginning and then saltate prior to settling down. This process creates a defect in the solution medium thereby, facilitating the formation of the nano particle seed. Given, the high concentration of graphene nano objects in all four vaccines, as the nanoparticles move through the medium, they must be incorporating not only graphene nanodots, but also nano scrolls, thereby increasing their binding efficiency and their ability to carry their pay load.

As is already well known, the structure of the lipid nano particle plays a crucial role in determining its efficiency to carry the nucleic acid payload. However, it is the payload's structure that defines the geometry of the lipid nanoparticles (Hajj et al. 2019, Kulkarni et al. 2018).

Though, these structures can be varied, depending upon the payload itself, the core responsibilities of the nano lipid particles are the same; viz (1) protection of nucleic acids from nucleases, (2) controlled release of nucleic acid, (3) cell and tissue selectivity, (4) high delivery yield, (5) minimal toxicity, and (6) stability especially in long-term storage. These required characteristics for a vector can been enhanced significantly by use of carbon nanotubes, graphene and graphene oxide. This process was observed in action, when the experiments were being conducted during the course of this study and as reported in detail within in Chapter 3.

Nano tubes, both single and multiwalled, along with graphene forms are increasingly, paving their way into targeted drug delivery (Sattari et al. 2021, Wu et al. 2018, Wierzbicki 2017, Eatemadi et al. 2014). The samples evaluated during the course of this project have identified graphene and other carbon composites as forming a striking percent portion of the ingredients of these vaccines. Given the context of the increasing use of graphene in drug delivery, the findings of this project seem to fit in the reference frame of attempts towards enhanced and tailored drug delivery.

The work carried out so far has been essentially a qualitative assessment of the contents. There are several forms within these vaccines that require quantitative assessment and determination. A major hurdle in achieving a good quantitative result was the failure to isolate the solid faction. The method used in this project was the traditional method of slide preparation. It is

hoped, that if similar work were to be performed on additional samples, vacuum filtering would be adopted as a mechanism of attaining cleaner samples for both Raman and SEM imaging.

Further, it is quite important to mention, that the source of fluorescence within the samples was unknown while Raman investigations were underway. Due to extremely tight timescales, it was not possible to complete the Raman re-runs where the effects of fluorescence would have been removed through targeted emittance and processing of the data. Despite this, the signals were interpreted using similar data from various catalogues. It is hoped that further work will continue on the Raman spectroscopic investigations to attain cleaner spectra and to isolate the individual spectrums of the current specimens.

In conclusion, it can be stated that the four samples of vaccines (Moderna 1, Modern 2, AstraZeneca, Pfizer) all contain significant amount of carbon composites, graphene compounds and iron oxide. These ingredients were undeclared by the manufacturers and are absent from the list of ingredients for the vaccines.

5. Bibliography

- Bonneville, S., Delpomdor, F., Preat, A., Chevaller,C., Arkaki, T., Kazemlan, M., Steele, A., Schrelber, A., Wirth, R., Benning, L.G. (2020). Molecular identification of fungi microfossils in a Neoproterozoic shale rock. Palentology, 6, 1-11.
- Buzgar, N. and Apopei, A. (2009). The Raman study of certain carbonates. Analele stiintifice ale univesrsitatii, al. i. cuza iasi. Geologie. Tomul LV, 2.
- Brennan, T.V., Lin, L., Huang, X. and Yang, Y. (2018). Generation of Luciferase-expressing Tumor Cell Lines. Bioprotocol, 8(8), 1-1
- Childres, I., Jauregui, L.A., Park, W., Cao, H. and Chen, Y.P. Raman spectroscopy of Graphene and related materials. Chapter 19.
- Crystal, R.G. (2014). Adenovirus: The First Effective In Vivo Gene Delivery Vector. Human Gene Therapy 25,3-11.
- Das, A., Chakraborty, B. and Sood, A.K. (2008). Raman Spectroscopy of graphene on different subsrates and influence of defects. Bulletin of Material Sciences, 31, 3, 579-584.
- Doerfler, W. (2021). Adenoviral Vector DNA- and SARS-CoV-2 mRNA-Based Covid-19 Vaccines: Possible Integration into the Human Genome – Are Adenoviral Genes Expressed in Vector -based Vaccines.
- Dychalska, A., Popielarski, P., Frankow, W., Fabisiak, K., Paprocki, K. and Szybowicz. (2015). Study of CVD diamond layers with amorphous carbon admixture by Raman scattering spectroscopy. Materials Science-Poland.
- Ghosh, S., Calizo, I., Teweldebrhan, D., Pokatilov, E.P., Nika, D.L., Balandin, A.A., Bao, W., Miao, F. and Lau, C.N. (2008). Extremely high thermal conductivity of graphene: Prospects for thermal management applications in nanoelectronic circuits. Applied Physics Letters, 92, 151911-1-3.
- Griffith, W.P. (1969). Raman spectroscopy of Minerals. Nature, 244, 264-266.
- Guo, W., Chen, Z., Feng, X., Shen, G., Huang, H., Liang, Y., Zhao, B., Lo, G. and Hu, Y. (2021). Graphene oxide (GO)- based nanosheets with combined chemo/photothermal/photodynamic therapy to overcome gastric cancer (GC) paclitaxel resistance by reducing mitochondria-derived adenonsine-triphosphate (ATP).
- Haskin, L.A., Wang, A., Rockow, K.M., Jolliff, B.L., Korotev, R.L. and Viskupic, K.M. (1997). Raman spectroscopy for mineral identification and quantification for insitu

planetary surface analysis: A point count method. Journal of Geophysical Research, 102, 8. 19293-19306.

- Hajj, A., Ball, R.L., Deluty, S.B., Singh, S.R., Strelkova, D., Knapp, C.M., Whitehead, K. (2019) Branched-tail lipid nanoparticles potently deliver mRNA in vivo due to enhanced ionization at endosomal pH. Small, 15,1–7.
- Jiao, L., Zhang, L., Wang, X., Diankov, G. and Dai, H. (2009). Narrow graphene nanoribbons from carbon nanotubes. Nature Letter, 458, 877-880.
- Jiang, W., Liang, F., Wang, J., Su, L., Wu, Y and Wang, L. (2014). Enhanced electrochemical performances of FeO – graphene nanocomposite as anode materials for alakaline nickel-iron batteries. **RSC Adv.**, 2014,**4**, 15394-15399.
- Kato, M., Guan, S. and Zhao, X. (2021). In-situ observation of graphene using an optical microscope. Applied Surface Science Advances, 6,
- Kim, J., Eygeris, Y., Gupta, M. and Sahay, G. (2021). Self-assembled mRNA vaccines. Advanced Drug Delviery Review, 170, 83-112.
- Kulkarni, A., Darjuan, M.M., Mercer, J.E., Chen, S., van der Meel, R., Thewalt, J.L., Tam, Y.Y.C., and Cullis, P.R. (2018). On the formation and morphology of lipid nanoparticles containing ionizable cationic lipids and siRNA. ACS Nano, 12, 4787–4795.
- Kuzmin, V.V., Novikov, V.S., Ustynyuk, L.Y., Prokhorov, K.A., Sagitova, E.A. and Nikolaeva, G.Y. (2020). Raman Spectra of polyethylene glycols: Comparative experimental and DFT study. Journal of Molecular Structure, 1217, 5,
- Liu, J., Cui, L. and Losic, D. (2013). Graphene and Graphene oxide as new nanocarriers for drug delivery applications. Acta Biomaterialia, 9(22).
- Malard, L.M., Pimenta, M.A., Desselhaus, G., Dresselhaus, M.S. (2009). Raman spectroscopy in graphene. Physics Reports, 473, 51-87.
- Mendes, A.C., Baran, E.T., Reis, R.L. and Azevedo, H.S. (2013). Self-assembly in nature: Using the principles of nature to create complex nanobiomaterials. Wiley Interdiscip Rev. Nanomed. Nanobiotechnol 5, 582-612.
- Osvath, Z., Zambo, D., Sulyok, A., Palinkas, A. and Deak, A. 2021. Tuning the nanoparticle rippling of graphene with PEGylated gold nanoparticles and ion radiation. Carbon Trends, 5, 1-5.
- Paillard, V. (2001). On the origin of the 1100cm^{-1} Raman band in amorphous and nanocrystalline sp^3 carbon. Europhysics Letters, 54(2), 194-198.

- Pierna, J.A.F., Abbas, O., Dardenne,P. and Baeten, V. (2011). Discrimination of Corsican honey by FT-Raman spectroscopy and chemometrics. Biotechnological Agron. Society Environment, 15,1, 75-84.
- Pop, E., Varshney, V., Roy, A. (2012). Thermal properties of graphene: Fundamentals and applications. MRS Bulletin 37, 1273-1281
- Prawer,S and Nemanich, R.J. (2004). Raman Spectroscopy of diamond and doped diamond. Philosophical Transactions of the Royal Society of London. Series A. Mathematical, Physical and Engineering Sciences. 362, 2537- 2565.
- Romann, J., Valmalette, J.C., Chevallier, V. and Merlen, A. (2010). Surface interactions between moleules and nanocrystals in copper oxalate nanostructures. Journal of Physical Chemistry, C. 114, 10677-19682.
- Roy, S. and Jaiswal, A. (2017). Graphene-based nanomaterials for theranostic applications. Reports in Advances of Physical Sciences, 1,4, 53pp.
- Sagitova, E.A., Prokhorov, K.A., Nikolaeva, G.Y., Baimova, A.V., Pashinin, P.P., Yarysheva, A.Y. and Mendeleev, D.I. (2018). Raman analysis of polyethylene glycols and polyethylene oxides. Journal of Physics Conference Series. 999 012002, 1-10.
- Sharma, S.K., Misra, A.K., Ismail, S. and Singh,U.N. (2006). Remote Raman Specroscopy of Various Mixed and Composite Mineral Phases at 7.2m Distance. https://www.researchgate.net/publication/252521525.
- Tallant, D.R., Friedmann, T.A., Missert, N.A., Siegal, M.P. and Sullivan, J.P. (1998). Raman spectroscopy of amorphous carbon. Material Research Society Symposium Proceedings, 498, 37-47.
- Zhao, X., Liu, L., Li, X., Zeng, J., Jia, X. and Liu P. (2014). Biocompatible graphene oxide nanoparticle-based drug delivery platform for tumor microenvironment-responsive triggered release of doxorubicin. Langmuir, 30(34),
- Wierzbicki, M., Jaworski, S., Kutwin, M., Grodzik, M., Strojny, B., Kurantowicz, N., Zdunek, K., Chodun, R., Chwalibog, A., Sawosz, E. (2017). Diamond, graphite and graphene oxide nanoparticles decrease migration and invasiveness in glioblastoma celllines by impairing extracellular adhesion. International Journal of Nanomedicine, 12, 7241-7254.
- Wu, J., Phillips, J.A., Liu, H. and Tan, Y.W.(2008). Carbon nanotubes protect DNA strnds during cellular delivery. ACS Nano.2 (2008) 2023-2028.

- Xie, W., Xu, G. and Feng, X. (2012). Self-assembly of lipid nano particles in aqueous solution; Self-consistent field simulations. Theoretical and Applied Mechanics Letters, 2, 014004, 1-5.
- Yong Tai, M.J., Perumal, V., Gopinath, S.C.B., Raja, P.B., Ibrahimm M.N.M., Jantan, I.N., Suhaimi, N.S.H. and Liu, W.W. (2021). Laser-scribed graphene nanofiber decorated with oil palm lignin capped silver nanoparticles: a green biosensor. Scientific Reports, 11,5475.

Ou et al. Particle and Fibre Toxicology (2016) 13:57
DOI 10.1186/s12989-016-0168-y

Particle and Fibre Toxicology

REVIEW Open Access

Toxicity of graphene-family nanoparticles: a general review of the origins and mechanisms

Lingling Ou[2], Bin Song[1], Huimin Liang[1], Jia Liu[1], Xiaoli Feng[1], Bin Deng[3], Ting Sun[2] and Longquan Shao[1*]

Abstract

Due to their unique physicochemical properties, graphene-family nanomaterials (GFNs) are widely used in many fields, especially in biomedical applications. Currently, many studies have investigated the biocompatibility and toxicity of GFNs in vivo and in intro. Generally, GFNs may exert different degrees of toxicity in animals or cell models by following with different administration routes and penetrating through physiological barriers, subsequently being distributed in tissues or located in cells, eventually being excreted out of the bodies. This review collects studies on the toxic effects of GFNs in several organs and cell models. We also point out that various factors determine the toxicity of GFNs including the lateral size, surface structure, functionalization, charge, impurities, aggregations, and corona effect ect. In addition, several typical mechanisms underlying GFN toxicity have been revealed, for instance, physical destruction, oxidative stress, DNA damage, inflammatory response, apoptosis, autophagy, and necrosis. In these mechanisms, (toll-like receptors-) TLR-, transforming growth factor β- (TGF-β-) and tumor necrosis factor-alpha (TNF-α) dependent-pathways are involved in the signalling pathway network, and oxidative stress plays a crucial role in these pathways. In this review, we summarize the available information on regulating factors and the mechanisms of GFNs toxicity, and propose some challenges and suggestions for further investigations of GFNs, with the aim of completing the toxicology mechanisms, and providing suggestions to improve the biological safety of GFNs and facilitate their wide application.

Keywords: Graphene-family nanomaterials, Toxicity, Toxicokinetics, Mechanisms, Physicochemical properties, Future prospects

Background

Graphene, which is isolated from crystalline graphite, is a flat monolayer composed of single-atom-thick, two-dimensional sheets of a hexagonally arranged honeycomb lattice [1]. Because of its unique structural, specific surface area and mechanical characteristics, the functions and applications of graphene have gained considerable attention since the discovery of the material in 2004 [2, 3]. Graphene and its derivatives include monolayer graphene, few-layer graphene (FLG), graphene oxide (GO), reduced graphene oxide (rGO), graphene nanosheets (GNS), and graphene nanoribbons, etc. [4–7]. GO is one of the most vital chemical graphene derivatives of the graphene-family nanomaterials (GFNs), which attracts increasing attention for its potential biomedical applications. Graphene-based materials usually have sizes ranging from several to hundreds of nanometer and are 1-10 nm thick [8, 9], which is also the definition of 'nanoparticles' or 'nanomaterials'. Due to their exceptional physical and chemical properties, graphene materials have been widely used in various fields, including energy storage; nanoelectronic devices; batteries [10–12]; and biomedical applications, such as antibacterials [13, 14], biosensors [15–18], cell imaging [19, 20], drug delivery [8, 21, 22], and tissue engineering [23–25].

Along with the application and production of GFNs increasing, the risk of unintentional occupational or environmental exposure to GFNs is increasing [26]. And recently, there are some investigation on GFNs exposure in occupational settings and published data showed that

* Correspondence: shaolongquan@smu.edu.cn
[1]Nanfang Hospital, Southern Medical University, Guangzhou 510515, China
Full list of author information is available at the end of the article

the occupational exposure of GFNs had potential toxicity to the workers and researchers [27–29]. GFNs can be delivered into bodies by intratracheal instillation [30], oral administration [31], intravenous injection [32], intraperitoneal injection [33] and subcutaneous injection [34]. GFNs can induce acute and chronic injuries in tissues by penetrating through the blood-air barrier, blood-testis barrier, blood-brain barrier, and blood-placenta barrier etc. and accumulating in the lung, liver, and spleen etc. For example, some graphene nanomaterials aerosols can be inhaled and substantial deposition in the respiratory tract, and they can easily penetrate through the tracheobronchial airways and then transit down to the lower lung airways, resulting in the subsequent formation of granulomas, lung fibrosis and adverse health effects to exposed persons [2, 29]. Several reviews have outlined the unique properties [35, 36] and summarized the latest potential biological applications of GFNs for drug delivery, gene delivery, biosensors, tissue engineering, and neurosurgery [37–39]; assessed the biocompatibility of GFNs in cells (bacterial, mammalian and plant) [7, 40, 41] and animals (mice and zebrafish) [42]; collected information on the influence of GFNs in the soil and water environments [43]. Although these reviews discussed the related safety profiles and nanotoxicology of GFNs, the specific conclusions and detailed mechanisms of toxicity were insufficient, and the mechanisms of toxicity were not summarized completely. The toxicological mechanisms of GFNs demonstrated in recent studies mainly contain inflammatory response, DNA damage, apoptosis, autophagy and necrosis etc., and those mechanisms can be collected to further explore the complex signalling pathways network regulating the toxicity of GFNs. It needs to point out that there are several factors which largely influence the toxicity of GFNs, such as the concentration, lateral dimension, surface structure and functionalization etc. Herein, this review presents a comprehensive summary of the available information on the mechanisms and regulating factors of GFNs toxicity in vitro and in vivo via different experimental methods, with the goals of providing suggestions for further studies of GFNs and completing the toxicology mechanisms to improve the biological safety of GFNs and facilitate their wide application.

Toxicity of GFNs (in vivo and in vitro)

GFNs penetrate through the physiological barriers or cellular structures by different exposure ways or administration routes and entry the body or cells, eventually resulting in toxicity in vivo and in vitro. The varying administration routes and entry paths, different tissue distribution and excretion, even the various cell uptake patterns and locations, may determine the degree of the toxicity of GFNs [44–46]. So to make them clear may be helpful to better understand the laws of the occurrence and development of GFNs toxicity.

Administration route

The common administration routes in animal models include airway exposure (intranasal insufflation, intratracheal instillation, and inhalation), oral administration, intravenous injection, intraperitoneal injection and subcutaneous injection. The major exposure route for GFNs in the working environment is airway exposure, thus inhalation and intratracheal instillation are used mostly in mice to simulate human exposure to GFNs. Though the inhalation method provides the most realistic simulation to real life exposure, instillation is more effective and time-saving method, and GFNs was found that causing longer inflammation period using instillation (intratracheal instillation, intrapleural installation and pharyngeal aspiration) than inhalation [24, 30, 47, 48]. GFNs were investigated to deposit in the lungs and accumulate to a high level, which retained for more than 3 months in the lungs with slow clearing after intratracheal instillation [49]. Intravenous injection is also widely used to assess the toxicity of graphene nanomaterials, and graphene circulates through the body of mice in 30 min, accumulating at a working concentration in the liver and bladder [32, 50–52]. However, GO derivatives had rather finite intestinal adsorption and were rapidly excreted in adult mice via oral administration [31, 53]. Nano-sized GO (350 nm) caused less mononuclear cells to infiltrate subcutaneous adipose tissue after subcutaneous injection in the neck region compared to micron-sized GO (2 μm) [34]. GO agglomerated near the injection site after intraperitoneal injection, and numerous smaller aggregates settled in the proximity of the liver and spleen serosa [31, 33]. Experiments on skin contact with or skin permeation of GFNs were not found in the papers reviewed here, and there is insufficient evidence available to conclude that graphene can penetrate intact skin or skin lesions. The route of nasal drops, which has been widely used to test the neurotoxicity or brain injury potential of other nanomaterials, was not mentioned in the papers reviewed here.

GFNs entry paths

GFNs reach various locations through blood circulation or biological barriers after entering the body, which results in varying degrees of retention in different organs. Due to their nanosize, GFNs can reach deeper organs by passing through the normal physiological barriers, such as the blood-air barrier, blood-testis barrier, blood-brain barrier and blood-placental barrier.

Blood-air barrier

The lungs are a potential entrance for graphene nanoparticles into the human body through airway. The inhaled GO nanosheets can destroy the ultrastructure and biophysical properties of pulmonary surfactant (PS) film, which is the first line of host defense, and emerge their potential toxicity [54]. The agglomerated or dispersed particles deposit on the inner alveolar surface within the alveoli and then be engulfed by alveolar macrophages (AMs) [55]. Clearance in the lungs is facilitated by the mucociliary escalator, AMs, or epithelial layer [56–58]. However, some small, inhaled nanoparticles infiltrate the intact lung epithelial barrier and can then transiently enter the alveolar epithelium or the interstitium [59, 60]. Intratracheally instilled graphene can redistribute to the liver and spleen by passing through the air-blood barrier [61]. The study of blood-air barrier may draw an intensive attention, since the researchers and workers occupational exposure of GFNs usually through inhalation. To make clear how the blood-air barrier plays a role in the toxicity of GFNs may become a research hot topic.

Blood-brain barrier

The intricate arrangement of the blood-brain barrier, consisting of numbers of membrane receptors and highly selective carriers, only exerts subtle influence on blood circulation and the brain microenvironment compared to the peripheral vascular endothelium [62]. The research on the mechanism of blood-brain barrier had made some progress involved in diseases and nanotoxicity. Matrix-assisted laser desorption/ionization (MALDI) mass spectrometry imaging (MSI) revealed that rGO, with an average diameter of 342 ± 23.5 nm, permeated through the paracellular pathway into the inter-endothelial cleft in a time-dependent manner by decreasing the blood-brain barrier paracellular tightness [63]. In addition, graphene quantum dots (GQDs), with a small size of less than 100 nm, can cross through the blood-brain barrier [64]. Studies on how graphene materials pass through the blood-brain barrier and cause neurotoxicity are very rare, and more data are needed to draw a conclusion.

Blood-testis barrier

The blood-testis and blood-epididymis barriers are well known for being some of the tightest blood-tissue barriers in the mammalian body [65]. GO particles with diameters of 54.9 ± 23.1 nm had difficulty penetrating the blood-testis and blood-epididymis barriers after intra-abdominal injection, and the sperm quality of the mice was not obviously affected even at 300 mg/kg dosage [66].

Blood-placenta barrier

The placental barrier is indispensable in maintaining pregnancy, as it mediates the exchange of nutrients and metabolic waste products, exerts vital metabolic functions and secretes hormones [67]. A recent review suggested that the placenta does not provide a tight barrier against the transfer of nanoparticles to foetuses, specifically against the distribution of carbonaceous nanoparticles to and in the foetus [42]. It was suggested that rGO and gold particles (diameter of 13 nm) are barely present or are absent in the placenta and foetus in late gestation after intravenous injection [44, 68]. However, other reports showed that transplacental transfer does occur in late gestational stages [69, 70]. Much attention had been paid to the developmental toxicity of nanomaterials, and reports showed that many nanoparticles did cross the placental barrier and strongly influenced the development of embryos [71–75]. But studies of the exposure to graphene materials through the placenta barrier are deficient, and how these particles transfer to embryos should be evaluated in detail in the future.

These four barriers were the most frequently mentioned barriers in the literature, and other barriers have not been evaluated in recent studies, such as skin barriers, which have not been mentioned in any of the hundreds of GFNs toxicity studies searched. Moreover, the mechanism by which GFNs pass through these barriers is not well understood, and more systematic investigations are urgently needed.

Distribution and excretion of GFNs in tissue

The absorption, distribution, and excretion of graphene nanoparticles may be affected by various factors including the administration routes, physicochemical properties, particle agglomeration and surface coating of GFNs.

The different administration routes influence the distribution of GFNs, for example, intratracheally instilled FLG passing through the air-blood barrier mainly accumulated and was retained in the lungs, with 47 % remaining after 4 weeks [61]. Intravenously administered GO entered the body through blood circulation and was highly retained in the lung, liver, spleen and bone marrow, and inflammatory cell infiltration, granuloma formation and pulmonary edema were observed in the lungs of mice after intravenous injection of 10 mg kg/body weight GO [49]. Similarly, high accumulation of PEGylated GO derivatives was observed in the reticulo-endothelial (RES) system including liver and spleen after intraperitoneal injection. In contrast, GO-PEG and FLG did not show detectable gastrointestinal tract absorption or tissue uptake via oral administration [31].

The different properties of GFNs, such as their size, dose and functional groups, always lead to inconsistent

results in the distribution profiles of graphene. For instance, Zhang et al. found that GO was mainly entrapped in mouse lungs [49]; however, Li et al. observed that GO accumulated in mouse liver [76]. Notably, small GO sheets, with diameters of 10–30 nm, were mainly distributed in the liver and spleen, whereas larger GO sheets (10–800 nm) mainly accumulated in the lungs [49, 52, 77]. If the size of GO is larger than the size of the vessels, GO usually becomes stuck in the arteries and capillaries in the proximity of the injection site. The accumulation of GO in the lungs was shown to increase with an increase in the injected dose and size, but that in the liver significantly decreased [78]. Coating biocompatible polymers onto GO also affects the biodistribution, for instance, the intravenous injection of GO-PEG and GO-dextran (GO-DEX) accumulate in the reticuloendothelial system (RES), including the liver and spleen, without short-term toxicity [31, 79]. Moreover, the charge of plasma proteins and adsorption of GO by plasma proteins also affects the biodistribution [34].

The excretion and clearance of GFNs vary in different organs. In the lungs, observations indicated that NGO is drawn into and cleared by AMs, which might be eliminated from the sputum through mucociliary clearance or other ways [57], and 46.2 % of the intratracheally instilled FLG was excreted through the faeces 28 d after exposure [61]. In the liver, nanoparticles can be eliminated thorough the hepato-biliary pathway following the biliary duct into the duodenum [80]. In addition, PEGylated GNS that mainly accumulates in the liver and spleen can be gradually cleared, likely by both renal and faecal excretion. As recently reviewed, GO sheets larger than 200 nm are trapped by splenic physical filtration, but small sizes (approximately 8 nm) can penetrate the renal tubules into the urine and be rapidly removed without obvious toxicity [81]. The excretion paths of GFNs have not yet been clearly explained, but renal and faecal routes appear to be the main elimination routes for graphene.

Recently, the distribution and excretion/toxicity strategy has become an important part of nano-toxicological studies. To date, several controversial results regarding the distribution and excretion of graphene in vivo have been reported in several papers, and a systematic evaluation of the toxicokinetics of GFNs is still needed. The metabolism and excretion of nanomaterials are long-period processes, however, the recent studies of GFNs had been limited to short-term toxicological assessments, and the long-term accumulation and toxicity of GFNs on different tissues remain unknown. Therefore, long-term studies on the deposition and excretion of GFNs need to be performed using different cells and animals to ensure the materials' biosafety before utilization in human biomedical applications.

Uptake and location of GFNs in cells

The uptake and location of GFNs have also been observed to exert different effects in different cell lines. Graphene is taken up into cells via various routes [82, 83]. Basically, the physicochemical parameters such as the size, shape, coating, charge, hydrodynamic diameter, isoelectric point, and pH gradient are important to allow GO to pass through the cell membrane [84]. As stated previously, nanoparticles with diameters <100 nm can enter cells, and those with diameters <40 nm can enter the nucleus [85]. For example, GQDs possibly penetrate cell membranes directly, rather than through energy-dependent pathways [86, 87]. Larger protein-coated graphene oxide nanoparticles (PCGO) (~1 μm) enter cells mainly through phagocytosis, and smaller PCGO nanoparticles (~500 nm) enter cells primarily through clathrin-mediated endocytosis [88]. GO sheets could adhere and wrap around the cell membrane, insert in the lipid bilayer or be internalized into the cell as a consequence of interactions with cells [89]. Similarly, PEGylated reduced graphene oxide (PrGO) and rGO were shown to adhere onto the lipid bilayer cell membrane prominently due to the interaction of hydrophobic, unmodified graphitic domains with the cell membrane [90, 91]. Consequently, it was suggested that prolonged exposure to or a high concentration of graphene induces physical or biological damage to the cell membrane, along with destabilization of actin filaments and the cytoskeleton [92].

Current data demonstrates that GO sheets interact with the plasma membrane and are phagocytosed by macrophages. Three major receptors on macrophages take part in the phagocytosis of GNS: the Fcg receptor (FcgR), mannose receptor (MR), and complement receptor (CR). Furthermore, FcgR is a key receptor in the mediated phagocytic pathway [90, 93, 94]. The protein corona of GO promotes the recognition by macrophage receptors, especially the IgG contained within the protein corona. Macrophages were observed to undergo prodigious morphological changes upon contact with GO [34]. After internalization, graphene accumulated in the cell cytoplasm, perinuclear space, and nucleus, which induced cytotoxicity in murine macrophages by increasing intracellular ROS through depletion of the mitochondrial membrane potential and by triggering apoptosis through activation of the mitochondrial pathway [83]. The possible interactions and accumulation sites of GFNs are summarized in Fig. 1.

Toxicity of GFNs in organs

The toxicity and biocompatibility of GFNs has been observed and assessed through theoretical and animal model studies. At present, there are a mass of data demonstrating the toxicity of GFNs in different organs or systems in animals, so that it is hard to list all the data

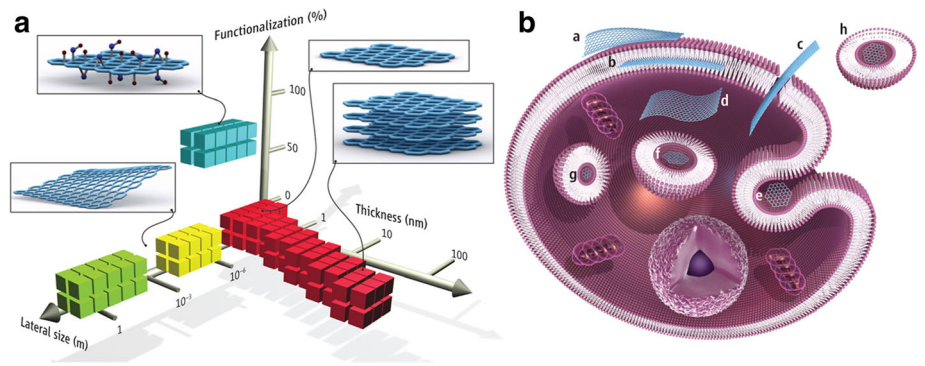

Fig. 1 Graphene materials and their biological interactions. (**A**) A parameter space for the most widely used graphene materials can be described by the dimensions and surface functionalization of the material, the latter defined as the percentage of the carbon atoms in sp3 hybridization. Green squares represent epitaxially grown graphene; *yellow*, mechanically exfoliated graphene; *red*, chemically exfoliated graphene; *blue*, graphene oxide. Note that a number of other graphene-related materials (such as graphene quantum dots and graphene nanoribbons) are also being used in experiments. (**B**) Possible interactions between graphene-related materials with cells (the graphene flakes are not to scale). (*a*) Adhesion onto the outer surface of the cell membrane. (*b*) Incorporation in between the monolayers of the plasma membrane lipid bilayer. (*c*) Translocation of membrane. (*d*) Cytoplasmic internalization. (*e*) Clathrin-mediated endocytosis. (*f*) Endosomal or phagosomal internalization. (*g*) Lysosomal or other perinuclear compartment localization. (*h*) Exosomal localization. The biological outcomes from such interactions can be considered to be either adverse or beneficial, depending on the context of the particular biomedical application. Different graphene-related materials will have different preferential mechanisms of interaction with cells and tissues that largely await discovery. [90] Copyright (2014), with permission from American Association for Advancement of Science

in this review. Thus we summarized a certain number literature and chose some in vivo toxicological studies of GFNs listed in Table 1.

Toxicity in internal organs

GO can result in acute inflammation response and chronic injury by interfering with the normal physiological functions of important organs [32, 81]. Oral gavage experiments did not show detectable absorption of GO through the gastrointestinal tract [95]. Interesting, a low dose of GO caused serious damage to the gastrointestinal tract after maternal mice drank a GO suspension rather than a high-dose of GO because a low dose of GO without agglomeration can easily attach to the gastrointestinal surface and cause destruction through its abundant sharp edges [53]. GFNs caused inflammation and remained in the lung on day 90 after a single intratracheal instillation, and even translocated to lung lymph nodes by a nose-only inhalation [96, 97]. A high dose of GO that forms aggregations can block pulmonary blood vessels and result in dyspnea [50, 98], and platelet thrombi were observed at high concentrations of 1 and 2 mg/kg body weight via intravenous injection [89]. GO reportedly disrupted the alveolar-capillary barrier, allowing inflammatory cells to infiltrate into the lungs and stimulate the release of pro-inflammatory cytokines [99]. Fibrosis and inflammation could be verified by the increased levels of the protein markers collagen1, Gr1, CD68 and CD11b in the lungs. The use of Tween 80 to disperse FLG or a pluronic surfactant to disperse graphene was suggested to reduce the likelihood of lung fibrosis formation in cells or mice, whereas lung fibrosis was observed when graphene was suspended with bovine serum albumin (BSA) [100]. In addition, radioactive isotopes can be delivered into the lungs, accompanied by a depth distribution of ^{125}I-NGO in the lungs, and the isotopes might deposit there and result in mutations and cancers [30]. However, recent publications claimed no obvious pathological changes in mice exposed to low dosages of GO and functionalized graphene by intravenous injection, including aminated GO (GO-NH2), poly(acrylamide)-functionalized GO (GO-PAM), poly(acrylic acid)-functionalized GO (GO-PAA) and GO-PEG; only GO-PEG and GO-PAA induced less toxicity than pristine GO in vivo [31, 79, 89]. So the functional groups of GFNs and the working concentration or aggregate state largely influence the toxicity of GFNs. Recently, the ways to modify the functional group of GFNs, decrease the working concentration or change the aggregate condition are usually used to decrease the toxicity of GFNs.

Toxicity in the central nervous system

Graphene has largely benefited neurosurgery with the application of drug/gene delivery for brain tumour treatment, intracranial and spinal biocompatible devices, biosensing and bioimaging techniques. Studies regarding the potentialities or risks of graphene in the brain have emerged. In the chicken embryo model, pristine graphene flakes decreased the ribonucleic acid level and the rate of deoxyribonucleic acid synthesis, leading to

Table 1 Toxicity of GFNs in organs

Graphene family nanomaterials	Physiochemial properties and functionalization	Animals	Dose and time incubation	Effects	Reference
Nanoscale graphene oxide (NGO)	No information	C57BL/6 mice	0, 1, 5, 10 mg/kg, intratracheal instillation 0 h, 24 h, 48 h, 72 h and 1 week	Result in acute lung injury (ALI) and chronic pulmonary fibrosis	[30]
Few layer graphene (FLG)	No information	ICR mice	0.1, or 1 mg/mL, oral gavage or intratracheal instillation 3 or 28 days	Intratracheally instilled FLG resulted in acute lung injury and pulmonary edema, FLG didn't show detectable absorption through the gastrointestinal tract by oral gavage.	[61]
Graphene platelets (GPs)	No information	Mice	inhalation exposure, 1 day-6 weeks	GP caused acute inflammation in lung at 1 day, and alleviated inflammation in lung after 6 weeks	[48]
Graphene nanoplatelets (GPs)	Thickness of 10 nm Size of 5–30 μm	Female C57BL/6 strain mice	50 μg per mouse, pharyngeal aspiration or intrapleural installation, 24 h- 7 days	Large GP were inflammogenic in both the lung and the pleural space	[24]
GO	Thickness of 0.93 nm Size of 150–250 nm	Sprague-Dawley rats	0.5 or 4 mg/m3, inhalation exposure, single 6 h	The single inhalation exposure to GO induce minimal toxic responses in rat lungs	[235]
GO	Thickness of 0.9 nm size of l-GO: 1–5 μm size of s-GO:100–500 nm	Male ICR mice	1.0 mg/kg, intravenous injected, 24 h	Accumulated mainly in the liver and lungs	[78]
GO	Thickness of < 4 nm size of l-GO:237.9 ± 79.3 nm; size of s-GO: 54.9 ± 23.1 nm	Male and female ICR-strain mice	24 mg/kg, tail vein injected, 5 days	Didn't effect pup numbers, sex ratio, weights, pup survival rates or pup growth, low toxicity for male reproduction	[66]
GO	Thickness of ~1.0 nm sizes of 10–800 nm	Kun Ming mice	1,10 mg/ kg, intravenous injection 14 days	Led to high accumulation, long-time retention, pulmonary edema and granuloma formation	[49]
NGO-PEG	Thickness of 1 nm size of 10–800 nm	Male Kunming mice	5 mg/kg, tail intravenous injection 10 min-24 h	NGO-PEG alleviated acute tissue injuries, decreased the early weight loss	[81]
GO GO-PEG RGO-PEG nRGO-PEG	Thickness of 0.94,1.22, 4.43 and 5.66 nm, size of 450, 25, 50 and 27 nm	Balb/c mice	4 mg/kg, intraperitoneal injection 1, 7 and 30 days	Accumulated in the reticuloendothelial (RES) system including liver and spleen over a long time	[31]
GO Graphene quantum dots (GQD)	Thickness of GO, GQD: 0.5–1 nm sizes of GO, GQD: 3–5 nm	Balb/c mice	20 mg/kg intravenous injection or intraperitoneal injection 14 days	GO appeared toxic and caused death GQD revealed no accumulation in organs and caused low cytotoxicity	[176]
Purified graphene oxide (pGO)	Thickness of 1–2 nm, lateral dimension of 100–500 nm	Female C57Bl/6 mice	50 μg/animal, intraperitoneal injection 24 h, 7 days,	Induced moderate inflammation and granuloma formation following	[99]
GO	Thickness of 3.9 and 4.05 nm, size of 350 nm and 2 μm	C57BL/6 male mice	Series concentrations, subcutaneous injection21 days	The micro-size of GO induced much stronger inflammation responses than the nanosized GO	[34]
GO	Size of 1110 to 16 200 nm	C57BL/6 J mice	2 or 20 mg/kg, subcutaneous and intraperitoneal injection	Both GO and a reduction of GO result in immune cell infiltration, uptake, and clearance.	[84]
RGO-iron oxide nanoparticles (rGO-IONP)	Thickness of ˂10 nm Size of 15.0 ± 2.0 nm	Female Balb/c mice	400 μg, subcutaneous injection,	RGO–IONP can effectively inactivate multiple-drug-resistant bacteria in subcutaneous abscesses	[236]

Table 1 Toxicity of GFNs in organs *(Continued)*

GO GO-PEG	Thickness of 0.94, 1.22, 4.43 and 5.66 nm, size of 450, 25, 50 and 27 nm	Female balb/c mice	100 mg/kg, Oral administration; 50 mg/kg, intraperitoneal injection, 1, 7 and 30 days	No obvious tissue uptake via oral administration, indicating the rather limited intestinal adsorption of those nanomaterials	[237]
RGO	sizes of small rGO: 87.97 ± 30.83, sizes of large rGO:472.08 ± 249.17 nm	Male C57black/6 mice	60 mg/kg, oral gavage, 5 days	RGO affected general locomotor activity, balance, and neuromuscular coordination, but showed little change in exploratory, anxiety-like, or learning and memory behaviors.	[31]

harmful effects on brain tissue development and the atypical ultrastructure was observed in the brain [101]. The recent researches of GFNs in the central nervous system are mostly involved in the application rather than the toxicity. The data of the toxic study on GFNs is underway.

Toxicity in reproduction and development system

Pristine graphene reduced the vascularization of the heart and the density of branched vessels after injection into fertilized chicken eggs followed by incubation for 19 d [101]. GO and rGO damage zebrafish embryos by influencing the embryo hatching rate and body length in a concentration-dependent manner. Although no obvious malformation or mortality was observed in exposed zebrafish embryos [102], GO adhered to and was wrapped in the chorion of the zebrafish embryos, causing remarkable hypoxia and hatching delay. GO aggregates were retained in many organelles, such as the eyes, heart, yolk sac, and tail of the embryos, and apoptosis and reactive oxygen species (ROS) generation were observed in these regions [103].

The GFNs exert different toxicological effects on male or female reproductive system. Data showed that GO exerted very low or nearly no toxic effects on male reproduction even at a high dose via intra-abdominal injection [66]. Additionally, rGO did not change the serum estrogen levels of non-pregnant female mice. The condition is different in the female mouse: mouse dams could give birth to healthy offspring after rGO injection before mating or during early gestation, and only a few abnormal foetuses were present among the rGO-injected dam litters. However, the pregnant mice had abortions at all dose, and most pregnant mice died when the high dose of rGO was injected during late gestation [44]. Notably, the development of offspring in the high dosage group was delayed during the lactation period. The high dose of GO decreased the maternal mice's water consumption by oral exposure, which reduced milk production and thus postponed the growth of offspring [53]. Though the findings indicate that GFNs are potentially harmful to development, but data on reproductive and developmental toxicity are still deficient. Studies of the influence of GFNs on male and female reproduction and development are still required to elucidate the underlying toxicity mechanism.

Influence of haemocompatibility

GO release into the blood is ineluctable. The haemocompatibility of GO was found to be dependent on the functional coating and the exposure conditions. GO with submicron size resulted in the greatest haemolytic activity, while aggregated graphene induced the lowest haemolytic reaction. Pristine graphene and GO demonstrated haemolytic effect up to 75 μg/mL [104]. GO-polyethylenimine (GO-PEI) exhibited notable toxicity by binding to HSA, even at 1.6 μg/mL [105]. Carboxylated graphene oxide (GO-COOH) showed significant cytotoxicity toward T lymphocytes at concentrations above 50 μg/mL and had good biocompatibility below 25 μg/mL, whereas GO-chitosan nearly inhibited haemolytic activity [106]. Until now, the corresponding risk of haemocompatibility has remained largely unknown.

In conclusion, the lung injury induced by GFNs has been studied in several studies, the results of which have demonstrated inflammatory cell infiltration, pulmonary edema and granuloma formation in the lungs. However, only a few specific studies have evaluated in other organs, such as the liver, spleen, and kidney, and the injury symptoms, damage index and level of damage to these internal organs were not fully investigated. Moreover, studies on the neurotoxicity of GFNs are quite rare; no data has revealed which nerves or brain areas experience damage, nor have the related behavioural manifestations been studied. The developmental toxicity of GFNs may induce structural abnormalities, growth retardation, behavioural and functional abnormalities, and even death. A study on the reproductive and developmental toxicity of GFNs will be extremely significant and gain extensive attention in the future. Almost all the GFNs toxicity studies were short-period experiments, and no studies have investigated long-term chronic toxic injury. However, based on studies of other nanomaterials toxicity, long-term GFNs exposure may be an important factor harming health [107–109]. Therefore, the long-term study of GFNs is necessary.

Toxicity of GFNs in cell models

The cytotoxicity of GFNs in vitro has been verified in various cells to change the cell viability and morphology, destroy the membrane integrity, and induce DNA damage [110–112]. GO or rGO decrease cell adhesion; induce cell apoptosis; and enter lysosomes, mitochondria, cell nuclei, and endoplasm [113]. GQDs entered cells and induced DNA damage by the increased expression of p53, Rad 51, and OGG1 proteins in NIH-3 T3 cells [87]. However, GQDs did not pose significant toxicity to human breast cancer cell lines (at a dose of 50 μg/mL) or human neural stem cells (at a dose of 250 μg/mL) [114, 115]. GO derivatives dramatically decreased the expression of differential genes that are responsible for the structure and function of the cell membrane, such as regulation of the actin cytoskeleton, focal adhesion and endocytosis [89]. In rat pheochromocytoma cells (PC12 cells), graphene and rGO caused cytotoxic effects and mitochondrial injury, such as the release of lactate dehydrogenase (LDH), an increase in

the activation of caspase-3, and the generation of ROS [82, 116].

Graphene can increase cell viability [117] or cause cell death [118] depending on the cell line, type of graphene material and the doseage. GO cytotoxicity was observed in human fibroblasts and lung epithelial cells at concentrations above 20 μg/mL after 24 h, but minimal toxicity was found in A549 cells at concentrations higher than 50 μg/mL [119]. The biological responses induced by GO such as ROS, malondialdehyde (MDA), and LDH increased, whereas superoxide dismutase (SOD) decreased dose-dependently in HeLa cells [120]. However, GO-molecular beacon (GO-MB) showed low cytotoxicity even at 20 μg/mL in HeLa cells [121]. GO decreased the viability of A549 cells, while the same concentration and time of exposure increased the cell viability of CaCo2 colorectal carcinoma cells [122]. Another study reported that GO dramatically enhanced the differentiation of SH-SY5Y, accompanied by increasing neurite length and the expression of neuronal marker MAP2 at low concentrations but that GO suppressed the viability of SH-SY5Y cells at high doses (≥80 mg/mL) [123]. Functionalized coatings on GO, such as GO-PEG [124] and GO-chitosan [125], can profoundly attenuate the particles' cytotoxicity by inhibiting the interactions between cells.

The toxicity of GFNs in vitro is summarized in Table 2. Data on the cytotoxicity of graphene nanomaterials are contrasting, and varying characteristics influence the results. The mechanisms and influencing factors of toxicity need to be elucidated in detail.

Origins of GFNs toxicity

Reportedly, the characteristics of graphene, including its concentration, lateral dimension, surface structure, functional groups, purity and protein corona, strongly influence its toxicity in biological systems [2, 7, 104, 126–129].

Concentration

Numerous results have shown that graphene materials cause dose-dependent toxicity in animals and cells, such as liver and kidney injury, lung granuloma formation, decreased cell viability and cell apoptosis [130–134]. In vivo studies, GO did not exhibit obvious toxicity in mice exposed to a low dose (0.1 mg) and middle dose (0.25 mg) but induced chronic toxicity at a high dose (0.4 mg). The high content of GO mainly deposited in the lungs, liver, spleen, and kidneys and was difficult to be cleaned by the kidneys via a single tail vein injection [135]. Intriguingly, increasing the dose resulted in a dramatic decrease in the hepatic uptake but an increase in the pulmonary uptake of s-GO by intravenous injection [31], because the high dose of GO potentially surpassed the uptake saturation or depleted the mass of plasma opsonins, which consequently suppressed the hepatic uptake. Moreover, an in vitro study reported that 20 μg/mL GO nanosheets exhibited no cytotoxicity in A549 within 2 h of incubation, but a higher concentration (85 μg/mL) decreased the cell viability to 50 % within 24 h [136, 137]. Lü et al. also demonstrated that GO had no obvious cytotoxicity at low concentrations for 96 h in a human neuroblastoma SH-SY5Y cell line, but the viability of cells sharply decreased to 20 % after treatment with 100 mg/mL GO for 96 h of incubation [123]. The results in HeLa cells, NIH-3 T3 cells, and breast cancer cells (SKBR3, MCF7) treated with graphene nanoribbons also showed a dose- (10–400 mg/ml) and time-dependent (12–48 h) decrease in cell viability [138]. Increasing concentrations of GO entered the lysosomes, mitochondria, endoplasm, and cell nucleus [119]. Several data indicated that rGO caused apoptosis-mediated cell death at a lower dose and early time point but that necrosis was prevalent with the increase in time/dose [110, 135].

Lateral dimension

Nanoparticles with sizes <100 nm can enter the cell, <40 nm can enter nucleus, and smaller than <35 nm can cross the blood brain barrier [85]. One study showed that GO (588, 556, 148 nm) did not enter A549 cells and had no obvious cytotoxicity [112]. When the diameter of graphene is between 100 ~ 500 nm, the smallest size may cause the most severe toxicity, and when the diameter is below 40 nm, the smallest sizes may be the safest. For instance, rGO with a diameter of 11 ± 4 nm could enter into the nucleus of the hMSCs and cause chromosomal aberrations and DNA fragmentation at very low concentrations of 0.1 and 1.0 mg/mL in 1 h. However, rGO sheets with diameters of 3.8 ± 0.4 nm exhibited no notable genotoxicity in hMSCs even at a high dose of 100 mg/mL after 24 h [118].

In an in vivo study, s-GO (100–500 nm) preferentially accumulated in the liver, whereas l-GO (1–5 μm) was mainly located in the lungs because l-GO formed larger GO-protein complexes that were filtered out by the pulmonary capillary vessels after intravenously injection [31]. Given the relative lateral sizes (205.8 nm, 146.8 nm and 33.78 nm) of the three GO nanosheets at the same concentration, smaller GO experiences much greater uptake than larger GO in Hela cells [139]. The high uptake of s-GO changed in the microenvironment of cells and consequently induced the greatest viability loss and most serious oxidative stress among three sizes of GO samples [119]. As a result, one study delineated that GO size-dependently induced the M1 polarization of macrophages and pro-inflammatory responses in vitro and in vivo. Larger GO showed stronger adsorption onto the plasma membrane with less phagocytosis, eliciting robust interactions with TLRs and activating NF-κB pathways, compared to smaller GO sheets, which were

Table 2 Toxicity of GFNs in cell models

Graphene family nanomaterias	Physiochemial properties and Functionalization	Cells	Dose and time incubation	Effects	Reference
Pristine graphene	Thickness of 2–3 nm, size of 500–1000 nm	Murine RAW 264.7 macrophages	5, 10, 20, 40, 80 and 100 mg/mL, 48 h	Depleted of the mitochondrial membrane potential, increased ROS, triggered apoptosis	[83]
Pristine graphene	Thickness of 3–5 nm, size of 100–110 nm	Rat pheochromocytoma cells PC12 cells	10–100 μg/mL 1–48 h	Increased LDH release, ROS levels and caspase3 activation, induced apoptosis	[82]
Graphene oxide(GO)	Four different diameters (342–765 nm)	Human Erythrocytes Human skin fibroblasts CRL-2522	3.125-200 μg/mL 24 h	Hemolytic activity, ROS generation, LDH release, decreased cell viability	[106]
GO	Thickness of 0.9 nm lateral size: s-GO, 160 ± 90 nm; m-GO, 430 ± 300 nm; l-GO, 780 ± 410 nm	Human lung epithelial A549 cells	10, 25, 50, 100 and 200 μg/mL 24 h	Dose-dependent oxidative stress, cell viability decreased at high concentration	[119]
GO	Thickness of 1 nm, lateral dimension of 200–500 nm	Human lung fibroblast cells HLF cells	10–500 μg/mL 2–24 h	Oxidative stress induced, concentration-dependent cytotoxicity and genotoxicity	[148]
GO	Size distribution: 592 ± 10.9 nm in PBS, 1272 ± 56.2 nm in FBS	HeLa cells	0–80 μg/mL 24 h	Released LDH, increased MDA and ROS generation, decreased SOD, reduction of cell viability,	[120]
GO	smaller-sized GO: 50–350 nm intermediate-sized GO: 350–750 nm larger-sized GO: 750–1,300 nm	Macrophage cell J774A.1 THP-1 cells HEK293 cells MEL cells HUT102 cells	20 μg/mL 1-24 h	Size-dependent M1 induction of macrophages, pro-inflammatory responses	[94]
GO	thickness: < 2 nm, lateral size: 450 nm	Mouse CT26 colon carcinoma cell	50–100 μg/mL 18 h	Triggered autophagy, enhances cell death	[206]
Reduced graphene oxide (rGO)	Thickness of 11 ± 4 nm lateral size of 3.8 ± 0.4 μm	Human mesenchymal stem cells (hMSCs)	0.01–100 μg/mL 1–24 h	Induced DNA fragmentations and chromosomal aberrations	[118]
RGO	Thickness of 7 nm lateral size of 40 nm	human liver carcinoma cells (HepG2 cells)	1–200 mg/L 4–72 h	Dose-dependent DNA damage, oxidative stress, cytotoxicity	[31]
RGO	Lateral size of 100–1500 nm	U87 and U118 glioma cell lines	0–100 μg/mL 24 h	Reduction of cell proliferation and cell viability, induced apoptosis	[238]
Bacterially reduced graphene oxide (B-rGO)	Thickness of 4.23 nm average size of 3833 nm	MCF-7 cells	20–100 μg/mL 24–72 h	Increased ROS generation, released LDH, dose-dependent toxicity	[181]
Reduced graphene oxide Nanoribbons(rGONR)	Thickness of 1 nm, length of 10 μm, width of 50–200 nm,	hMSCs	0.01, 0.1, 1.0, 10, 100 μg/mL 96 h	Caused DNA fragmentations and chromosomal aberrations	[239]
Reduced graphene oxide sheets (rGOSs)	Thicknesses of ~1.2 nm, lateral sizes of ~2 μm	hMSCs	0.01, 0.1, 1.0, 10, 100 μg/mL 96 h	Caused slight cell membrane damage and cytotoxicity	[239]
Graphene-dextran (GO-DEX)	Thickness of 2.8 nm size of 50–100 nm	HeLa cells	10, 50,200 mg/L 24, 48, 72 h	GO-DEX remarkably reduced cell toxicity	[91]
GNP-COOH GNP-NH2	Thickness of GNP-COOH: 735.9 nm thickness of GNP-NH2: 945.5 nm	Human bronchial epithelial cells (BEAS-2B cells)	10, 50 mg/L 24 h	Caused single stranded DNA damage, genotoxicity and hypomethylation	[240]

Table 2 Toxicity of GFNs in cell models *(Continued)*

PEG-DSPE (O-GNR-PEG-DSPE)	Width of 125–220 nm, lengths between of 500–2500 nm	HeLa cells NIH-3 T3 cells SKBR3 cells MCF7 cells	10–400 μg/mL 24–48 h	Dose-dependent and time-dependent decrease in cell viability	[138]
PEI-GO, PEG-GO, LA-PEG-GO	Thickness of 1–2 nm lateral width of 100–500 nm	Human lung fibroblast cells	1, 10, 50, 100 μg/ml 24 h	Caused concentration-dependent cytotoxicity and genotoxicity	[15]
PEG-GQD	Sizes of 3–5 nm	HeLa cells and A549 cells	10–160 μg/mL 24 h	No noticeable cytotoxicity	[176]
FBS-GO	Thickness of 4.0–18.0 nm	A549 cells	0–200 μg/mL 24 h	Cytotoxicity of GO was greatly mitigated at 10 % FBS	[166]

more likely taken up by cells [94]. To further uncover the detailed mechanism underlying these effects, more studies are needed to illustrate the vital mechanism of the lateral size of graphene materials.

Surface structure

GFNs possess widely varying surface chemistries. For example, the pristine graphene surface is hydrophobic, GO surface is partially hydrophobic with carboxylate groups [140–142], and rGO has intermediate hydrophilicity [143]. GFNs were observed to disrupt the function and structure of cell membranes and proteins probably by exceptionally strong molecular interactions with cells [2, 91]. For instance, rGO bonded to cell membranes, stimulated receptors and activated mitochondrial pathways, inducing apoptosis [110, 111, 144]. Limited evidence showed that GO is smaller and less toxic than rGO because of the high oxygen content, smoother edges, and hydrophilic properties of the former species [104, 145, 146]. Because of the different surface oxidation states of GO and rGO, GO possessing distinct hydrophilicity might be internalized and taken up by HepG2 cells easily. On the contrary, rGO with evident hydrophobicity, could be adsorbed and aggregated at cell surfaces without (or with lower) uptake [110]. Due to strong π-π stacking interactions, graphene is highly capability of breaking many residues of the protein, particularly the aromatic ones, such as the villin headpiece (HP), F10, W23, and F35. The protein's secondary and tertiary structures are largely lying on the graphene surface, disrupting the structure and function of the protein [41] (Fig. 2). In addition, GO can insert between the base pairs of double-stranded DNA and disturb the flow of genetic information at the molecular level, which might be one of the main causes of the mutagenic effect of GO [7, 112, 146, 147].

Charge

A number of studies have highlighted the importance of the GO surface charge because of its ability to affect the internalization and uptake mechanism of cells [148–150]. GO internalization was negligible in non-phagocytes, which was likely due to the strong electrostatic repulsion between the negatively charged GO and the cell surface [34]. However, others have suggested that negatively charged nanoparticles can be internalized into non-phagocytic cells by binding to available cationic sites on the cell surface and be taken up by scavenger receptors [110, 146, 150]. GO/GS particles reportedly cause morphological changes and significant lysis, leading to high haemolysis in red blood cells (RBCs). RBC membrane disruption is probably attributed to the strong electrostatic interactions between the negatively charged oxygen groups on the GO/GS surface and positively charged phosphatidylcholine lipids on the RBC outer membrane [106].

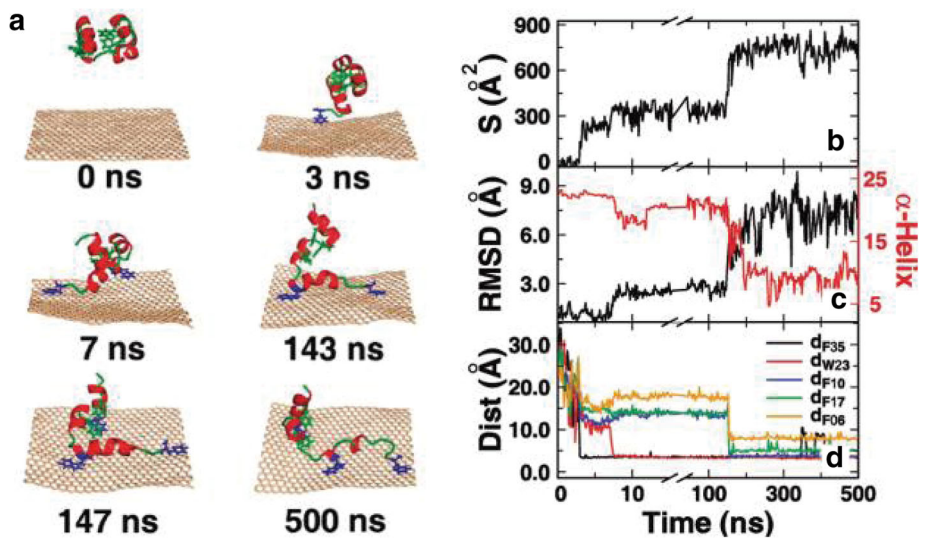

Fig. 2 A representative trajectory of HP35 adsorbing onto the graphene. (**a**) Representative snapshots at various time points. The proteins are shown in cartoons with red helix and green loop, and the graphene is shown in wheat. The aromatic residues that form the π-π stacking interactions are shown in blue, others are shown in green. (**b**) The contacting surface area of HP35 with the graphene. (**c**) The RMSD of HP35 from its native structure and the number of residues in the α-helix structure. Here, the secondary structures are determined by the DSSP program. (**d**) The distance between the graphene and the aromatic residues, including F35, W23, F10, F17, and F06. To show the adsorbing process clearer, the χ-axis had been truncated and rescaled. [41] Copyright (2011), with permission from Journal of Physical of Chemistry

Functionalization

Studies confirmed that functionalization with PEG [52], PEGylated poly-L-lysine (PLL) [151], poly(ε-caprolactone) [152], polyvinyl alcohol [3], Pluronic [153], amine [98], carboxyl, and dextran [79] groups largely decreases the toxicity and improves the biocompatibility of graphene. In vivo results revealed that only mild chronic inflammation emerged after the subcutaneous injection of GO-Pluronic hydrogel and no noticeable short-term toxicity was tested after the intravenous injection of GO-DEX [79, 154]. PEGylated GS did not induce appreciable toxicity in mice exposed to 20 mg/kg for 3 months, as evaluated by blood biochemistry and histological examinations, and showed relatively low retention in the RES [52, 155]. Coating GO with chitosan almost eliminated the haemolytic activity in blood [39]. Moreover, the PEG coating effectively alleviated GO-induced acute tissue injuries; decreased GO aggregation and retention in the liver, lungs, and spleen; and promoted the clearance of GO [81], GO-DEX [79], and fluorinated graphene oxide (FGO) [156].

In vitro, several cell function assays showed clear evidence that the surface functionalization of pristine graphene or GO was critical for reducing the strong toxicity effects [91]. PEG-GO, PEI-GO and LA-PEG-GO damaged human lung fibroblast cells less than GO [148]. PEG-GO exhibited no cytotoxicity toward several cell cultures, such as glioblastoma cells (U87MG), breast cancer cells (MCF-7), human ovarian carcinoma cells (OVCAR-3), colon cancer cells (HCT-116), and lymphoblastoid cells (RAJI), at concentrations up to 100 μg/mL [119, 157, 158]. GQDs-PEG exhibited very low or no toxicity against lung and cervical cancer cells even at very high concentrations (200 μg/mL) [159]. However, as a non-biodegradable material with great potential for cellular internalization, further investigation is needed to assess the possible long-term adverse effects of functionalized graphene.

Aggregations and sedimentation

Reportedly, nanomaterials have a propensity to form aggregates rather than individual units, particularly under physiological conditions. GS surfaces allowed fewer RBCs attach comparing to GO, and GS had the lower haemolytic activity for more aqueous aggregations formation. In contrast, the fast sedimentation and aggregate formation of GS greatly inhibited the nutrient availability of human skin fibroblast cells that were grown on the bottom of wells [106]. Therefore, the aggregations and sedimentation of graphene particles exert varying effects on different cells.

Impurities

Nanomaterial purity is an important consideration because residual, contaminating metals may be responsible for the observed toxicity, rather than the nanomaterial itself, which has resulted in conflicting data on GFNs cytotoxicity [35, 160]. Traditionally prepared GO often contains high levels of Mn^{2+} and Fe^{2+}, which are highly mutagenic to cells. The nonspecific release of these ions from traditionally prepared GO might lead to unusually high levels of cytotoxicity and DNA fracturing [39]. In particular, Peng et al. [161] produced high-purity GO containing only 0.025 ppm Mn^{2+} and 0.13 ppm Fe^{2+}, and Hanene et al. [162] invented a new method to prepare high-purity, single-layer GO sheets with good aqueous dispersibility and colloidal stability. GO produced by these new methods did not induce significant cytotoxic responses (at exposure doses up to 100 μg/mL) in vitro, and no obvious inflammatory response or granuloma formation (exposure doses up to 50 μg/animal) were observed in vivo. Therefore, the purity of GFNs deserves attention and is a vital step towards the determination of GFNs involved in bioapplications.

Protein corona effect

Because of the high free surface charge, nanomaterials can easily form “coronas” with proteins in biological systems [163, 164]. The protein corona is suggested to affect the circulation, distribution, clearance and toxicity of nanoparticles. Several papers reported that GO forms GO-protein coronas with adsorbed plasma proteins in serum and these GO-protein coronas play an important role in deciding the fate of the GO biokinetic behaviour in vivo. Such GO-protein coronas can regulate the adhesion of GO to endothelial and immune cells through both specific and nonspecific interactions [165]. Basically, immunoglobulin G and complement proteins in the protein corona help to reorganize nanoparticles in immune cells, causing the particles to be engulfed by the RES, and IgG-coated GO was taken up by either specific or nonspecific interactions with cell membrane receptors [31, 165]. However, another study found that GO could not adhere to mucosal epithelial cells directly in the intestinal tract after the filial mice drank an aqueous GO solution because abundant proteins in the milk had adsorbed on the surface of the GO and thus inhibited their direct interaction with the mucosal epithelial cells [53]. Protein corona mitigated the cytotoxicity of GO by limiting its physical interaction with the cell membrane and reducing the cellular morphological damage in HeLa, THP-1 and A549 cells [166–168]. The cytotoxic effect was largely reduced when GO was pre-coated with FBS and incubated with cells; nearly ~ 90 % survival was observed with 100 μg/mL FBS-coated GO and 100 % survival with 20 μg/mL FBS-coated GO. Similar trends were observed for GO covered by BSA [166, 169]. Consistently, additional serum could neutralize the toxicity of pristine GO in J774.A1 cells at a dose of 4 μg/mL, which

lead to a decrease in cell number of 52.5 % compared to untreated cells [89].

After reviewing many studies, it can be concluded that the toxicity of graphene is influenced by multiple factors. Those factors combined to largely change the toxicity of GFNs in many cases. Scientific studies often need the clear identification of cause and effect, which should keep only one factor different at a time, so that the effect of that single factor can be determined. But in some papers, several factors influencing GFNs toxicity were studied at the same time, which led to confused results.

Possible toxicity mechanisms of GFNs

Although some physicochemical properties and the toxicity of GFNs have been well studied by many scholars, the exact mechanisms underlying the toxicity of GFNs remain obscure. A schematic of the main mechanisms of GFNs cytotoxicity is illustrated in Fig. 3.

Physical destruction

Graphene is a unique nanomaterial compared with other spherical or one-dimensional nanoparticles due to its two-dimensional structure with sp2-carbons. The physical interaction of graphene nanoparticles with cell membranes is one of the major causes of graphene cytotoxicity [7, 170, 171]. Graphene has high capability to bind with the α-helical structures of peptides because of its favourable surface curvature [172]. At concentration above 75 μg/mL, pristine graphene largely adhered to the surfaces of RAW 264.7 cells and resulted in abnormal stretching of the cell membrane [104]. The strong hydrophobic interactions of GFNs with the cell membrane lead to the morphological extension of F-actin filopodial and cytoskeletal dysfunction. Furthermore, the sharpened edges of GNS may act as 'blades', inserting and cutting through bacterial cell membranes [173]. Moreover, GO also damaged the outer membrane of

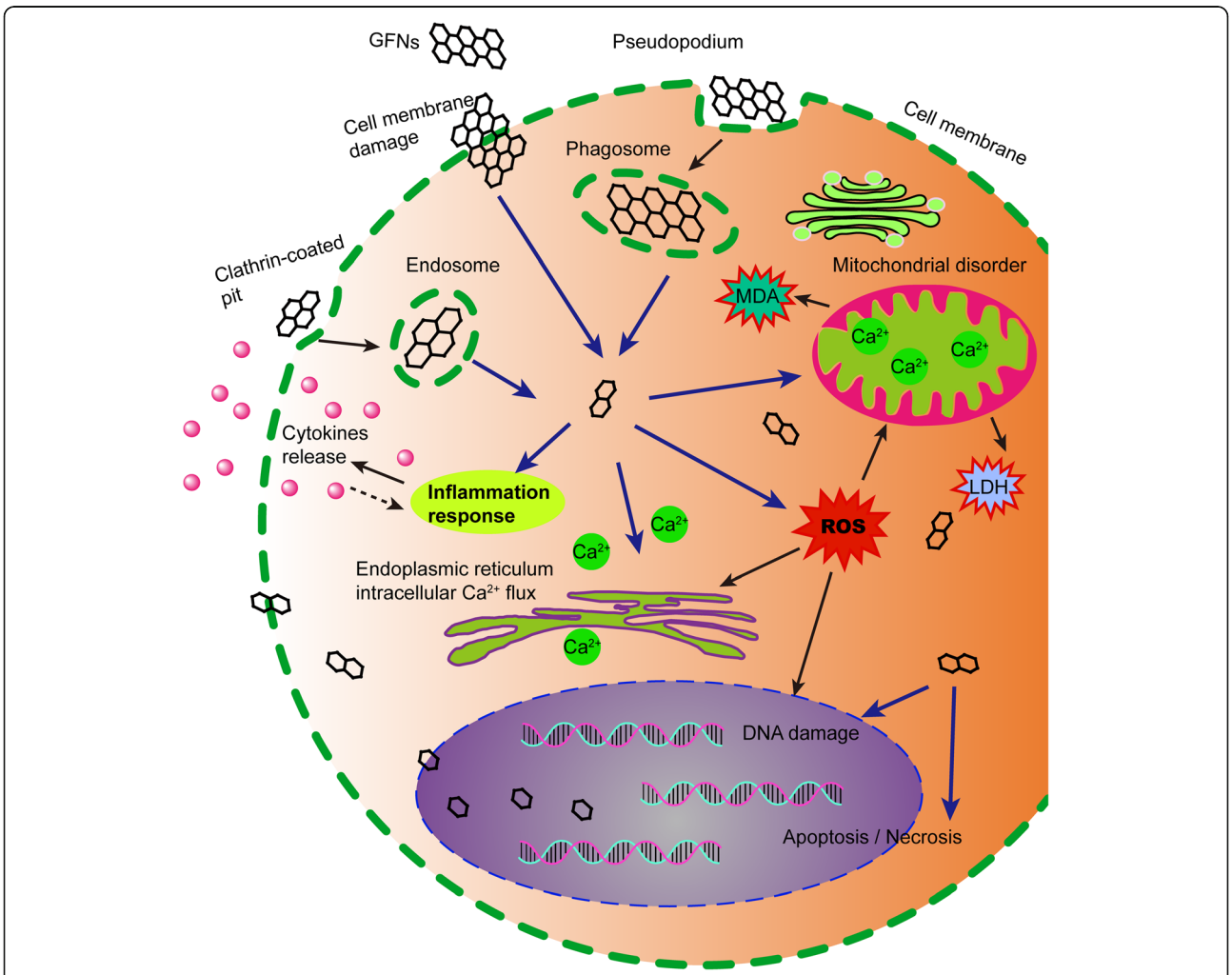

Fig. 3 Schematic diagram showed the possible mechanisms of GFNs cytotoxicity. GFNs get into cells through different ways, which induce in ROS generation, LDH and MDA increase, and Ca^{2+} release. Subsequently, GFNs cause kinds of cell injury, for instance, cell membrane damage, inflammation, DNA damage, mitochondrial disorders, apoptosis or necrosis

E. coli bacteria directly, resulting in the release of intracellular components [173]. However, TEM imaging revealed that pre-coating GO with FBS eliminated the destruction of cell membranes [166].

ROS production leading to oxidative stress

Oxidative stress arises when increasing levels of ROS overwhelm the activity of antioxidant enzymes, including catalase, SOD, or glutathione peroxidase (GSH-PX) [174]. ROS act as second messengers in many intracellular signalling cascades and lead to cellular macromolecular damage, such as membrane lipid breakdown, DNA fragmentation, protein denaturation and mitochondrial dysfunction, which greatly influence cell metabolism and signalling [175–177]. The interactions of GO with cells can lead to excessive ROS generation, which is the first step in the mechanisms of carcinogenesis, ageing, and mutagenesis [83, 122]. Oxidative stress had a significant role in GO-induced acute lung injury [30], and the inflammatory responses caused by oxidative stress often emerged upon exposure to GFNs [133, 177, 178]. The activity of SOD and GSH-PX decreased after exposed to GO in a time- and dosage-dependent manner [82, 106, 119]. Similarly, oxidative stress was the key cause of apoptosis and DNA damage after HLF cells were exposed to GO [148]. Both the mitogen-activated protein kinase (MAPK) (JNK, ERK and p38) and TGF-beta-related signalling pathways were triggered by ROS generation in pristine graphene-treated cells, accompanied by the activation of Bim and Bax, which are two pro-apoptotic members of the Bcl-2 protein family. As a result, caspase-3 and its downstream effector proteins such as PARP were activated, and apoptosis was initiated [83, 179]. Detailed information regarding the MAPK-, TGF-β- and TNF-α-related signalling pathways, which induce inflammation, apoptosis and necrosis, are summarized in Fig. 4.

Mitochondrial damage

Mitochondria are energy production centres involved in various signalling pathways in cells and are also a key point of apoptotic regulation [83]. After exposure to GO and carboxyl graphene (GXYG), the mitochondrial membrane was depolarized, and the amount of mitochondria decreased in HepG2 cells [180]. Exposure to GFNs resulted in significantly increased coupled and uncoupled mitochondrial oxygen consumption, dissipation of the mitochondrial membrane potential, and eventual triggering of apoptosis by activating the mitochondrial pathway [181]. For instance, GO increased the activity of mitochondrial electron transport complexes I/III and the supply of electrons to site I/II of the electron transport chain, accelerating the generation of ROS during mitochondrial respiration in MHS cells [99]. The formation of •OH mediated by GO and the cytochrome-c/H_2O_2 electron-transfer system could enhance oxidative and thermal stress to impair the mitochondrial respiration system and eventually result in dramatic toxicity [151]. Additionally, the oxygen moieties on GO might accept electrons from cellular redox proteins, supporting the redox cycling of cytochrome c and electron transport proteins, and cytochromes MtrA, MtrB, and MtrC/OmcA might be involved in transferring electrons to GO [182]. Therefore, except for the plasma membrane damage and oxidative stress induction, GFNs can cause apoptosis and/or cell necrosis by direct influencing cell mitochondrial activity [183, 184].

DNA damage

Due to its small size, high surface area and surface charge, GO may possess significant genotoxic properties and cause severe DNA damage, for example, chromosomal fragmentation, DNA strand breakages, point mutations, and oxidative DNA adducts and alterations [87, 122, 185, 186]. Mutagenesis was observed in mice after intravenous injection of GO at a dose of 20 mg/kg compared with cyclophosphamide (50 mg/kg), a classic mutagen [112]. Even if GO cannot enter into the nucleus of a cell, it may still interact with DNA during mitosis when the nuclear membrane breaks down, which increases the opportunity for DNA aberrations [87, 147, 187, 188]. The π stacking interaction between the graphene carbon rings and the hydrophobic DNA base pairs can make a DNA segment 'stand up' or 'lay on' the surface of graphene with its helical axis perpendicular or parallel, respectively. The intermolecular forces severely deform the end base pairs of DNA, which potentially increases the genotoxicity [189]. GO may also induce chromosomal fragmentation, DNA adducts and point mutations by promoting oxidative stress or triggering inflammation through the activation of intracellular signalling pathways such as MAPK, TGF-β and NF-κB [110, 112, 146]. Graphene and rGO can also elevate the expression of p53, Rad51, and MOGG1-1, which reflect chromosomal damage, and decrease the expression of CDK2 and CDK4 by arresting the cell cycle transition from the G1 to the S phase in various cell lines [112]. DNA damage can not only initiate cancer development but also possibly threaten the health of the next generation if the mutagenic potential of GO arises in reproductive cells, which impacts fertility and the health of offspring [112, 190].

Inflammatory response

GFNs can cause a significant inflammatory response including inflammatory cell infiltration, pulmonary edema and granuloma formation at high doses via intratracheally instillation or intravenous administration [30, 49]. Platelets are the important components in clot formation to

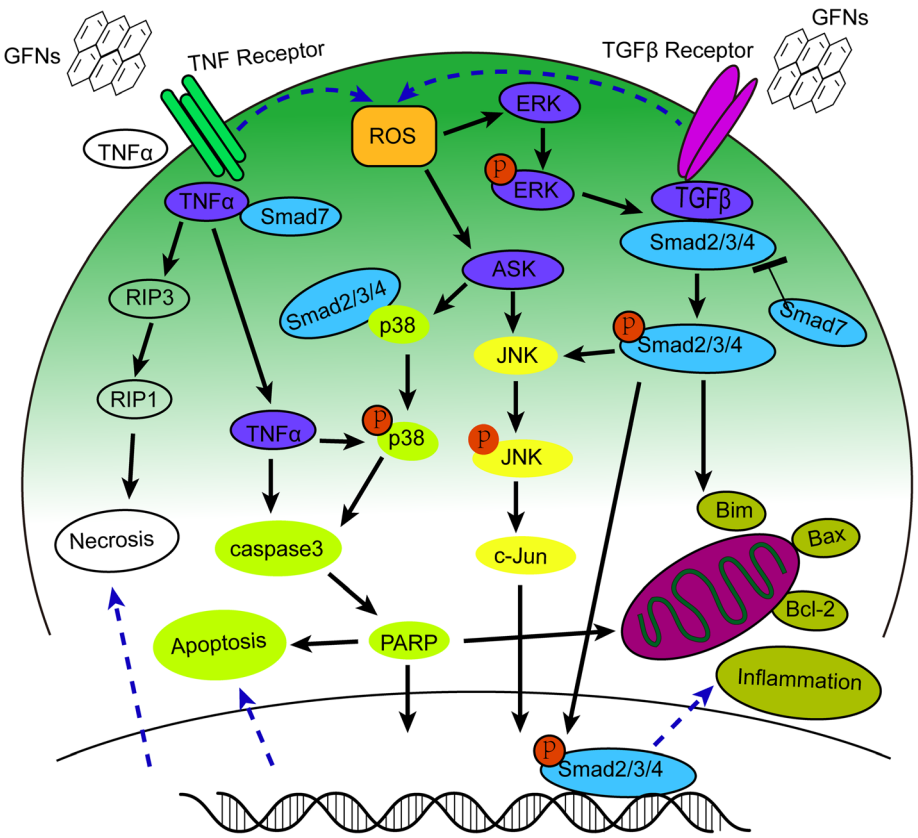

Fig. 4 Schematic diagram of MAPKs, TGF-beta and TNF-α dependent pathways involved in GFNs toxicity. ROS was the main factors activating the MAPKs and TGF-beta signaling pathways to lead to the activation of Bim and Bax, triggering the cascade of caspases and JNK pathway. The activation of caspase 3 and RIP1 resulted in apoptosis and necrosis finally

attack pathogens and particulate matter during the inflammatory response, and GO could directly activate platelet-rich thrombi formation to occlude lung vessels after intravenous injection [98, 191]. A strong inflammatory response was induced by subcutaneously injection with GO for 21 days, along with the secretion of key cytokines, including IL-6, IL-12, TNF-α, MCP-1, and IFN-g [34, 192]. GFNs can trigger an inflammatory response and tissue injury by releasing cytokines and chemokines that lead to the recruitment of circulating monocytes and stimulating the secretion of Th1/Th2 cytokines and chemokines [124, 193]. Additionally, pristine graphene [193] and rGO [110] evoke an inflammatory response by binding to toll-like receptors (TLRs) and activating the NF-κB signalling pathway in cells. The NF-κB signalling cascade is triggered by TLRs and pro-inflammatory cytokines such as IL-1 and TNF-α. Upon activation, NF-κB shifts from the cytoplasm to the nucleus, facilitating the binding of degrading IκB and acting as a transcription factor to synthesize numerous pro-inflammatory cytokines [194]. A schematic of the signalling pathway of TLR4 and TLR9 activated by GFNs is shown in Fig. 5.

Apoptosis

Apoptosis is defined as the self-destruction of a cell regulated by genes through complicated programmes [83, 195]. GO and rGO caused apoptosis and inflammation in mice lungs after inhalation [99], and GFNs also had pro-apoptotic effects in cells [111, 113, 124, 196]. Additionally, graphene and GO physically damaged cell membranes [166], increased the permeabilization of the outer mitochondrial membrane and changed the mitochondrial membrane potential; the increased ROS triggered the MAPK and TGF-β signalling pathways and activated caspase-3 via mitochondrial-dependent apoptotic cascades, prompting the execution of apoptosis [83, 99]. Similarly, rGO caused apoptosis at a low dose and an early time point, triggered by the death-receptor and canonical mitochondrial pathway [110]. Another study showed three different apoptosis pathways by GFNs: GO led to ROS-dependent apoptosis through direct interaction with protein receptors and subsequent activation of the B-cell lymphoma-2 (Bcl-2) pathway; GO-COOH transmitted a passive apoptosis signal to nuclear DNA by binding to protein receptors and activating a ROS-independent pathway; However,

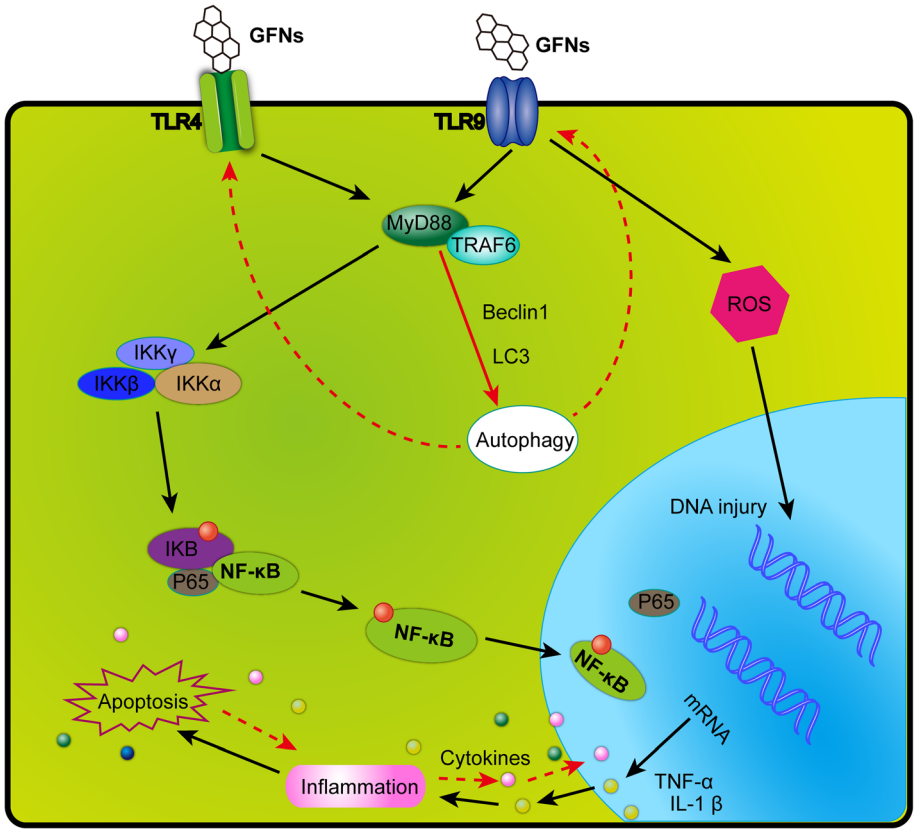

Fig. 5 A schematic diagram elucidating signalling pathway of TLR4 and TLR9 responsible for GFNs-induced cytotoxicity. GFNs can be recognized by TLRs, thus activate IKK and IκB by a MyD88-dependent mechanism, resulting in the release of NF-κB subunits and initiating the translocation into the nucleus. Thus, pro-inflammatory factors were transcribed and secreted out of nucleus, modulating the immune responses initiating programmed autophagy, apoptosis and necrosis

GO-PEI severely damaged the membranes of T lymphocytes to trigger apoptosis [105, 197].

Autophagy

Autophagy is the process of self-degradation of cellular components and recently recognized as non-apoptotic cell death [198–200]. Autophagy activation requires autophagosome formation containing Beclin 1, multiple autophagy-related proteins (ATG), microtubule-associated protein light chain 3 (LC3) and p62 [201]. Autophagosome accumulation is associated with exposure to various nanoparticles [202–205], and autophagy can remove extracellular organisms and destruct the organisms in the cytosol [206]. GO and GQDs was shown to induce autophagosome accumulation and the conversion of LC3-I to LC3-II; inhibit the degradation of the autophagic substrate p62 protein [207, 208]. Furthermore, GO can simultaneously trigger TLR4 and TLR9 responses in macrophages [34, 192] and colon cancer cells CT26 [206]. The autophagy pathway is linked to phagocytosis by TLR signalling in macrophages [206, 209].

Necrosis

Necrosis is an alternate form of cell death induced by inflammatory responses or cellular injury. The exposure of cells to pristine graphene causes apoptosis and necrosis at high doses (50 mg/mL) [83]. Reportedly, LDH leakage and the opening of the mitochondrial permeability transition pore, induced by elevated level of cytoplasmic Ca^{2+}, lead to apoptosis/necrosis [210]. GO treatment was revealed to induce macrophagic necrosis by activating TLR4 signalling and subsequently partly triggering autocrine TNF-α production [93]. GO combined with CDDP (GO/CDDP) triggered necrosis by decreasing RIP1 and increasing RIP3 proteins, accompanied with the release of high mobility group B1 (HMGB1) into the cytosol from the nucleus and out of CT26 cells [205, 211, 212].

Epigenetic changes

Epigenetics involve DNA methylation, genomic imprinting, maternal effects, gene silencing, and RNA editing [213–215]. DNA methylation, which is one of the best-studied epigenetic modifications, includes phosphorylation,

ubiquitination, and ATP-ribosylation and can lead to chromatin remodelling [197, 216, 217]. A recently paper reported that SL-GO/FL-GO exposure resulted in global DNA hypermethylation through upregulating DNMT3B and MBD1 genes; GNP treatment caused hypomethylation by decreasing the expression of DNMT3B and MBD1 genes [216]. GO could activate the miRNA-360 regulation pathway to suppress the DNA damage-apoptosis signalling cascade by affecting the component of CEP-1 [218]. Taken together, these data suggest that GFNs could cause subtle changes in gene expression programming by modulating epigenetic changes. However, studies of GFNs-induced epigenetic changes are few, and the epigenetic mechanism caused by GFNs exposure is not fully understood.

To conclude, many studies have discussed representative mechanisms of GFNs toxicity involving four signalling pathways: TLRs, TGF-β, TNF-α and MAPKs. These four signalling pathways are correlative and cross-modulatory, making the inflammatory response, autophagy, apoptosis and other mechanisms independent and yet connected to each other. Additionally, oxidative stress appears to play the most important role in activating these signalling pathways. It has been reported that there are intersections of apoptosis, autophagy and necrosis in the studies of other nanomaterials toxicity, they inhibit or promote mutually in some conditions. However, the signalling pathways of GFNs toxicity investigated in papers to date are only a small part of an intricate web, and the network of signalling pathways needs to be explored in detail in the future.

Data gaps and future studies

Currently, the literature is insufficient to draw conclusions about the potential hazards of GFNs. Two opposite opinions have begun to emerge: some researchers suggested that graphene materials are biocompatible in a number of studies focused on biomedical applications [119, 154, 162, 219], and other studies reported adverse biological responses and cytotoxicity [32, 118, 135, 138, 192]. These inconsistent results might have been caused by several factors, including the different research groups, various cellular or animal models, and varying physicochemical characterizations of GFNs. When GFNs are explored for in vivo applications in the human body or some other biomedical applications, biocompatibility must be considered, and more detailed and accurate studies of GFNs toxicity are needed.

First, detailed physicochemical characterization is imperative in all future studies of GFNs toxicity. In the experiments, feature descriptions of GFNs should include their size, morphology, surface area, charge, surface modifications, purity, and agglomeration [88, 141, 148, 162]. Because these physicochemical factors largely influence the toxicity and biocompatibility of GFNs, single-factor experimental designs and the exclusion of other interfering factors should be considered. Details of the fabrication process should also be provided because the formed oxidative debris could largely alter the surface structure of graphene and GO during functionalization [151]. Importantly, a single, universal method needs to be established in graphene technology, which will allow for better comparison of data from different studies or different laboratories.

Second, different observational criteria, parameters and selection of experimental methods might induce large inter-laboratory variations [220, 221]. For example, the MTT assay always fails to accurately predict graphene toxicity because the spontaneous reduction results in a false positive signal. Therefore, appropriate alternative assessments should be utilized, such as the water-soluble tetrazolium salt reagent (WST-8), ROS assay, and trypan blue exclusion test [106, 222]. Additionally, the comet assay often shows higher levels of DNA damage than the micronucleus assay because the former measures the repairable injury and the latter measures the gene damage that remains after cell division [159, 223]. Therefore, caution is required in choosing the most appropriate assay to evaluate the toxicity of graphene materials to avoid false-positive results.

Third, the selection of cell lines is of vital importance because cancer cell lines tend to be sensitive or resistant depending upon their genetic background. The same graphene nanoparticles can cause different reactions depending on their various cells origins. Suitable cell lines with good stability must be used to avoid false positive or negative results. Primary cells derived from humans or animals can better simulate the health conditions of humans. A large amount of primary cells have been utilized to test the toxicity of other nanomaterials [224–228], but the culturing of primary cells is extremely rare in the experiments with GFNs to date [210, 229]. Various cell experiments combined with primary cells should be performed to comprehensively evaluate the physicochemical properties and toxicity of GFNs.

Fourth, the administration route of GFNs plays a very important role in toxicity studies, and different delivery methods will result in different toxicological reactions [32, 53]. Thus, the route and period of exposure should be carefully chosen according to the aim of the study. Nasal drug delivery is often used to study the neurotoxicity of nanomaterials [230, 231], but this administration method has rarely been applied in the testing of GFNs toxicity. Toxicological studies of GFNs in the nervous system are rare, and the mechanism is unclear and needs to be studied further in the future. Recent toxicokinetic studies involving the absorption, distribution, metabolism, accumulation, and excretion of GFNs through different

exposure routes have yielded some results but are far from sufficient to clarify the internal complex mechanisms. For instance, further studies are needed to understand the specific molecular mechanisms of GFNs passing through the physiological barriers and the amount of accumulation or the excretion period of GFNs in tissues. In addition, given the increased exposure of humans to GFNs, the assessment of systemic toxicity in the human body is indispensable in future studies.

Fifth, another important issue requiring attention is the long-term fate of GFNs after entering the body or being taken up by cells. Most recent studies have consisted of short-term toxicity assessments [89, 232], and long-term toxic injury has not received much attention since the widespread application of GFNs in 2008. Moreover, a functionalized graphene surface can improve its biocompatibility, but the long-term stability of the surface coatings should be considered [233]. If the surface coatings eventually break down, their toxicity may be significantly different from the short-term exposure results. Extended studies are needed to determine if longer treatment times influence the nanotoxic potential of GFNs.

Sixth, more specific signalling pathways in the mechanism of GFNs toxicity need to be discovered and elucidated. Currently, several typical toxicity mechanisms of GFNs have been illustrated and widely accepted, such as oxidative stress, apoptosis, and autophagy. However, these mechanisms have only been described in general terms, and the specific signalling pathways within these mechanisms need to be investigated in detail. The signalling pathways involved in the toxicity of other nanomaterials may also be relevant to the study of GFNs. Therefore, more signalling pathways should be detected in future research. For instance, nano-epigenetics has been considered in numerous studies of nanomaterials, which is also helpful in assessing the limited toxicity and side effects of GFNs. Recent studies have shown that GFNs could cause epigenetic and genomic changes that might stimulate physical toxicity and carcinogenicity [234]. GFNs have high surface areas, smooth continuous surfaces and bio-persistence, similar to the properties of tumorigenic solid-state implants. It is unknown whether GFNs have the potential to induce foreign body sarcomas, and definitive studies of tumour potentialities or risks of graphene should therefore be conducted as soon as possible.

Conclusions

In the past few years, GFNs have been widely utilized in a wide range of technological and biomedical fields. Currently, most experiments have focused on the toxicity of GFNs in the lungs and livers. Therefore, studies of brain injury or neurotoxicity deserve more attention in the future. Many experiments have shown that GFNs have toxic side effects in many biological applications, but the in-depth study of toxicity mechanisms is urgently needed. In addition, contrasting results regarding the toxicity of GFNs need to be addressed by effective experimental methods and systematic studies. This review provides an overview of the toxicity of GFNs by summarizing the toxicokinetics, toxicity mechanisms and influencing factors and aimed to provide information to facilitate thorough research on the in vitro and in vivo haemo- and biocompatibility of GFNs in the future. This review will help address safety concerns before the clinical and therapeutic applications of GFNs, which will be important for further development of GFNs in biological applications.

Abbreviations

AMs: Alveolar macrophages; BBB: Blood-brain barrier; BEB: Blood-epididymis barriers; BTB: Blood-testis barrier; CR: Complement receptor; FcgR: Fcg receptor; FLG: Few-layer graphene; GFNs: Graphene family nanomaterials; GNS: Graphene nanosheets; GO: Graphene oxide; GO-COOH: Carboxylated graphene oxide; GO-DEX: GO-dextran; GO-MB: GO-molecular beacon; GO-NH2: Aminated GO; GO-PAA: Poly(acrylic acid)-functionalized GO; GO-PAM: Poly(acrylamide)-functionalized GO; GO-PEG: PEGylated GO derivatives; GO-PEI: GO-polyethylenimine; GQDs: Graphene quantum dots; GSH-PX: Glutathione peroxidase; GXVG: Carboxyl graphene; LDH: Lactate and dehydrogenase; MALDI: Matrix-assisted laser desorption/ionization; MAPKs: Mitogen-activated protein kinase; MDA: Malondialdehyde; MØ: Macrophage; MR: Mannose receptor; MSI: Mass spectrometry imaging; PC12 cells: Rat pheochromocytoma cells; PCGO: Protein-coated graphene oxide nanoparticles; PrGO: PEGylated reduced graphene oxide; RES: Reticuloendothelial system; rGO: Reduced graphene oxide; ROS: Reactive oxygen species; SOD: Superoxide dismutase; TLRs: Toll-like receptor

Acknowledgements

Not applicable.

Funding

This review was supported by the National Natural Science Foundation of China (81550011, 51172283, 81400557), Natural Science Foundation of Guangdong Province (2015A030313299) and Guangdong Provincial Medical Research Foundation (A2016360).

Availability of data and materials

Databases/repositories and materials is not applicable in this review.

Authors' contributions

All authors contributed to the design and concept of this article. LO drafted the manuscript. BS and JL critically revised the manuscript. All authors read and approved the final manuscript.

Competing interest

The authors declare that they have no competing interests.

Consent for publication

Not applicable.

Ethics approval and consent to participate

Not applicable.

Author details

[1]Nanfang Hospital, Southern Medical University, Guangzhou 510515, China. [2]The First Affiliated Hospital of Jinan University, Guangzhou, China. [3]The General Hospital of People's Liberation Army, Beijing, China.

Received: 13 June 2016 Accepted: 13 October 2016
Published online: 31 October 2016

References

1. Novoselov KS, Geim AK, Morozov SV, Jiang D, Zhang Y, Dubonos SV, et al. Electric field effect in atomically thin carbon films. Science. 2004; 306(5696):666–9.
2. Sanchez VC, Jachak A, Hurt RH, Kane AB. Biological interactions of graphene-family nanomaterials: an interdisciplinary review. Chem Res Toxicol. 2012;25(1):15–34.
3. Yang XY, Wang YS, Huang X, Ma YF, Huang Y, Yang RC, et al. Multi-functionalized graphene oxide based anticancer drug-carrier with dual-targeting function and pH-sensitivity. J Mat Chem. 2011;21(10):3448–54.
4. Park S, An J, Jung I, Piner RD, An SJ, Li X, et al. Colloidal suspensions of highly reduced graphene oxide in a wide variety of organic solvents. Nano Lett. 2009;9(4):1593–7.
5. Geim AK. Graphene: status and prospects. Science. 2009;324(5934):1530–4.
6. Guo X, Mei N. Assessment of the toxic potential of graphene family nanomaterials. J Food Drug Anal. 2014;22(1):105–15.
7. Seabra AB, Paula AJ, de Lima R, Alves OL, Duran N. Nanotoxicity of graphene and graphene oxide. Chem Res Toxicol. 2014;27(2):159–68.
8. Shen H, Zhang L, Liu M, Zhang Z. Biomedical applications of graphene. Theranostics. 2012;2(3):283–94.
9. Han U, Seo Y, Hong J. Effect of pH on the structure and drug release profiles of layer-by-layer assembled films containing polyelectrolyte, micelles, and graphene oxide. Sci Rep. 2016;6(2045–2322 (Electronic)):24158.
10. Wang H, Liang Y, Mirfakhrai T, Chen Z, Casalongue HS, Dai H. Advanced asymmetrical supercapacitors based on graphene hybrid materials. Nano Res. 2011;4(8):729–36.
11. Loh KP, Bao Q, Eda G, Chhowalla M. Graphene oxide as a chemically tunable platform for optical applications. Nat Chem. 2010;2(12):1015–24.
12. Wang D, Zhu L, Chen JF, Dai L. Mn3O4-graphene hybrid as a high-capacity anode material for lithium ion batteries. J Am Chem Soc. 2015;132(1520–5126 (Electronic)):13978–80.
13. Gurunathan S, Han JW, Dayem AA, Eppakayala V, Kim JH. Oxidative stress-mediated antibacterial activity of graphene oxide and reduced graphene oxide in Pseudomonas aeruginosa. Int J Nanomed. 2012;7(1178–2013 (Electronic)):e14.
14. Zhan S, Zhu D, Ma S, Yu W, Jia Y, Li Y, et al. Highly efficient removal of pathogenic bacteria with magnetic graphene composite. ACS Appl Mater Interf. 2015;7(1944–8252 (Electronic)):4290–8.
15. Yang HW, Hua MY, Chen SL, Tsai RY. Reusable sensor based on high magnetization carboxyl-modified graphene oxide with intrinsic hydrogen peroxide catalytic activity for hydrogen peroxide and glucose detection. Biosens Bioelectron. 2013;41:172–9.
16. Wang Y, Yuan R, Chai Y, Yuan Y, Bai L. In situ enzymatic silver enhancement based on functionalized graphene oxide and layer-by-layer assembled gold nanoparticles for ultrasensitive detection of thrombin. Biosens Bioelectron. 2012;38(1):50–4.
17. Huang J, Zhang L, Liang RP, Qiu JD. "On-off" switchable electrochemical affinity nanobiosensor based on graphene oxide for ultrasensitive glucose sensing. Biosens Bioelectron. 2013;41:430–5.
18. Gao L, Lian C, Zhou Y, Yan L, Li Q, Zhang C, et al. Graphene oxide-DNA based sensors. Biosens Bioelectron. 2014;60(1873–4235 (Electronic)):22–9.
19. Chen ML, Liu JW, Hu B, Chen ML, Wang JH. Conjugation of quantum dots with graphene for fluorescence imaging of live cells. Analyst. 2011;136(20): 4277–83.
20. Wang Y, Wang H, Liu D, Song S, Wang X, Zhang H. Graphene oxide covalently grafted upconversion nanoparticles for combined NIR mediated imaging and photothermal/photodynamic cancer therapy. Biomaterials. 2013;34(1878–5905 (Electronic)):7715–24.
21. Pan Y, Sahoo NG, Li L. The application of graphene oxide in drug delivery. Expert Opin Drug Deliv. 2012;9(11):1365–76.
22. Huiyun W, Chunyan D, Haiqing D, Aijun S, Wenjuan X, Xiaojun C, et al. Engineered redox-responsive PEG detachment mechanism in PEGylated nano-graphene oxide for intracellular drug delivery. Small. 2012;8(5):760–9.
23. Yang X, Qiu L, Cheng C, Wu Y, Ma ZF, Li D. Ordered gelation of chemically converted graphene for next-generation electroconductive hydrogel films. Angewandte Chem Int Ed Engl. 2011;50(32):7325–8.
24. Schinwald A, Murphy FA, Jones A, Macnee W, Donaldson K. Graphene-based nanoplatelets: a new risk to the respiratory system as a consequence of their unusual aerodynamic properties. ACS Nano. 2012;6(1):736–46.
25. Chaenyung C, Ryon SS, Xiguang G, Nasim A, Dokmeci MR, Xiaowu Shirley T, et al. Controlling mechanical properties of cell-laden hydrogels by covalent incorporation of graphene oxide. Small. 2014;10(3):514–23.
26. Arvidsson R, Molander S, Sandén BA. Review of potential environmental and health risks of the nanomaterial graphene. Hum Ecol Risk Assess. 2013;19(4): 873–87.
27. Lee JH, Han JH, Kim JH, Kim B, Bello D, Kim JK, et al. Exposure monitoring of graphene nanoplatelets manufacturing workplaces. Inhal Toxicol. 2016;28(6): 281–91.
28. Maynard RL. Nano-technology and nano-toxicology. Emerg Health Threats J. 2012;5.
29. Su WC, Ku BK, Kulkarni P, Cheng YS. Deposition of graphene nanomaterial aerosols in human upper airways. J Occup Environ Hyg. 2015;13(1):1–34.
30. Li B, Yang J, Huang Q, Zhang Y, Peng C, Zhang Y, et al. Biodistribution and pulmonary toxicity of intratracheally instilled graphene oxide in mice. NPG Asia Mater. 2013;5:E44.
31. Yang K, Gong H, Shi X, Wan J, Zhang Y, Liu Z. In vivo biodistribution and toxicology of functionalized nano-graphene oxide in mice after oral and intraperitoneal administration. Biomaterials. 2013;34(11):2787–95.
32. Wen KP, Chen YC, Chuang CH, Chang HY, Lee CY, Tai NH. Accumulation and toxicity of intravenously-injected functionalized graphene oxide in mice. J Appl Toxicol. 2015;35(10):1211–8.
33. Kurantowicz N, Strojny B, Sawosz E, Jaworski S, Kutwin M, Grodzik M, et al. Biodistribution of a high dose of diamond, graphite, and graphene oxide nanoparticles after multiple intraperitoneal injections in rats. Nanoscale Res Lett. 2015;10(1):398.
34. Yue H, Wei W, Yue Z, Wang B, Luo N, Gao Y, et al. The role of the lateral dimension of graphene oxide in the regulation of cellular responses. Biomaterials. 2012;33(16):4013–21.
35. Nezakati T, Cousins BG, Seifalian AM. Toxicology of chemically modified graphene-based materials for medical application. Arch Toxicol. 2014;88(11): 1987–2012.
36. Chng ELK, Pumera M. Toxicity of graphene related materials and transition metal dichalcogenides. Rsc Advances. 2015;5(4):3074–80.
37. Zheng XT, Ananthanarayanan A, Luo KQ, Chen P. Glowing graphene quantum dots and carbon dots: properties, syntheses, and biological applications. Small. 2015;11(1613–6829 (Electronic)):1620–36.
38. Caffo M, Merlo L, Marino D, Caruso G. Graphene in neurosurgery: the beginning of a new era. Nanomed. 2015;10:615–25.
39. Wu SY, An SS, Hulme J. Current applications of graphene oxide in nanomedicine. Int J Nanomed. 2015;10(Spec Iss):9–24.
40. Tonelli FMP, Goulart VAM, Gomes KN, Ladeira MS, Santos AK, Lorencon E, et al. Graphene-based nanomaterials: biological and medical applications and toxicity. Nanomedicine. 2015;10(15):2423–50.
41. Zhou R, Gao H. Cytotoxicity of graphene: recent advances and future perspective. Wiley Interdiscip Rev Nanomed Nanobiotechnol. 2014;6(5): 452–74.
42. Ema M, Hougaard KS, Kishimoto A, Honda K. Reproductive and developmental toxicity of carbon-based nanomaterials: A literature review. Nanotoxicology. 2015;10:391–412.
43. Jastrzebska AM, Olszyna AR. The ecotoxicity of graphene family materials: current status, knowledge gaps and future needs. J Nanopart Res. 2015; 17(1):1–21.
44. Xu S, Zhang Z, Chu M. Long-term toxicity of reduced graphene oxide nanosheets: Effects on female mouse reproductive ability and offspring development. Biomaterials. 2015;54:188–200.
45. Jennifer M, Maciej W. Nanoparticle technology as a double-edged sword: cytotoxic, genotoxic and epigenetic effects on living cells. J Biomater Nanobiotechnol. 2013;4:53–63.
46. Wu W, Yan L, Wu Q, Li Y, Li Q, Chen S, et al. Evaluation of the toxicity of graphene oxide exposure to the eye. Nanotoxicology. 2016;10(9):1329–40.
47. Lee K, Jeong Y, Bae J, Seok H, Yang Y, Roh S, et al. The role of surface functionalization on the pulmonary inflammogenicity and translocation into mediastinal lymph nodes of graphene nanoplatelets in rats. Arch Toxicol. 2016:1–10.
48. Schinwald A, Murphy F, Askounis A, Koutsos V, Sefiane K, Donaldson K, et al. Minimal oxidation and inflammogenicity of pristine graphene with residence in the lung. Nanotoxicology. 2013;8(8):824–32.
49. Zhang X, Yin J, Peng C, Hu W, Zhu Z, Li W, et al. Distribution and biocompatibility studies of graphene oxide in mice after intravenous administration. Carbon. 2011;49(3):986–95.
50. Singh SK, Singh MK, Nayak MK, Kumari S, Shrivastava S, Gracio JJ, et al. Thrombus inducing property of atomically thin graphene oxide sheets. ACS Nano. 2011;5(6):4987–96.

51. Gurunathan S, Han JW, Eppakayala V, Kim JH. Biocompatibility of microbially reduced graphene oxide in primary mouse embryonic fibroblast cells. Colloids Surf B Biointerf. 2013;105:58–66.
52. Yang K, Wan J, Zhang S, Zhang Y, Lee ST, Liu Z. In vivo pharmacokinetics, long-term biodistribution, and toxicology of PEGylated graphene in mice. ACS Nano. 2011;5(1):516–22.
53. Fu C, Liu T, Li L, Liu H, Liang Q, Meng X. Effects of graphene oxide on the development of offspring mice in lactation period. Biomaterials. 2015;40:23–31.
54. Hu Q, Jiao B, Shi X, Valle RP, Zuo YY, Hu G. Effects of graphene oxide nanosheets on the ultrastructure and biophysical properties of the pulmonary surfactant film. Nanoscale. 2015;7(43):18025–9.
55. Gosens I, Post JA, de la Fonteyne LJ, Jansen EH, Geus JW, Cassee FR, et al. Impact of agglomeration state of nano- and submicron sized gold particles on pulmonary inflammation. Part Fibre Toxicol. 2010;7(1743–8977 (Electronic)):1.
56. Geiser M, Kreyling WG. Deposition and biokinetics of inhaled nanoparticles. Part Fibre Toxicol. 2010;7:2.
57. Ruge CA, Schaefer UF, Herrmann J, Kirch J, Canadas O, Echaide M, et al. The interplay of lung surfactant proteins and lipids assimilates the macrophage clearance of nanoparticles. PLoS One. 2012;7(7):e40775.
58. Morfeld P, Treumann S, Ma-Hock L, Bruch J, Landsiedel R. Deposition behavior of inhaled nanostructured TiO2 in rats: fractions of particle diameter below 100 nm (nanoscale) and the slicing bias of transmission electron microscopy. Inhal Toxicol. 2012;24(1091–7691 (Electronic)):939–51.
59. Wiemann M, Vennemann A, Sauer UG, Wiench K, Ma-Hock L, Landsiedel R. An in vitro alveolar macrophage assay for predicting the short-term inhalation toxicity of nanomaterials. J Nanobiotechnol. 2016;14(1477–3155 (Electronic)):1.
60. Kreyling WG, Semmler-Behnke M, Takenaka S, Möller W. Differences in the biokinetics of inhaled nano- versus micrometer-sized particles. Accounts Chem Res. 2012;46(1520–4898 (Electronic)):714–22.
61. Liang M, Hu M, Pan B, Xie Y, Petersen EJ. Biodistribution and toxicity of radio-labeled few layer graphene in mice after intratracheal instillation. Part Fibre Toxicol. 2016;13(1):1–12.
62. Abbott NJ, Patabendige AA, Dolman DE, Yusof SR, Begley DJ. Structure and function of the blood–brain barrier. Neurobiol Dis. 2010;37(1):13–25.
63. Mendonca MC, Soares ES, de Jesus MB, Ceragioli HJ, Ferreira MS, Catharino RR, et al. Reduced graphene oxide induces transient blood–brain barrier opening: an in vivo study. J Nanobiotechnol. 2015;13:78.
64. Liu Y, Xu LP, Dai W, Dong H, Wen Y, Zhang X. Graphene quantum dots for the inhibition of beta amyloid aggregation. Nanoscale. 2015;7(45):19060–5.
65. Mital P, Hinton BT, Dufour JM. The blood-testis and blood-epididymis barriers are more than just their tight junctions. Biol Reprod. 2011;84(5):851–8.
66. Liang S, Xu S, Zhang D, He J, Chu M. Reproductive toxicity of nanoscale graphene oxide in male mice. Nanotoxicology. 2015;9(1):92–105.
67. Buerkithurnherr T, Von MU, Wick P. Knocking at the door of the unborn child: engineered nanoparticles at the human placental barrier. Swiss Med Wkly. 2012;142:w13559.
68. Yang H, Sun C, Fan Z, Tian X, Yan L, Du L, et al. Effects of gestational age and surface modification on materno-fetal transfer of nanoparticles in murine pregnancy. Sci Rep. 2012;2(46):847.
69. Huang X, Zhang F, Sun X, Choi KY, Niu G, Zhang G, et al. The genotype-dependent influence of functionalized multiwalled carbon nanotubes on fetal development. Biomaterials. 2014;35(2):856–65.
70. Qi W, Bi J, Zhang X, Wang J, Wang J, Liu P, et al. Damaging effects of multi-walled carbon nanotubes on pregnant mice with different pregnancy times. Sci Rep. 2014;4(3):doi: 10.1038/srep04352.
71. Du J, Wang S, You H, Jiang R, Zhuang C, Zhang X. Developmental toxicity and DNA damage to zebrafish induced by perfluorooctane sulfonate in the presence of ZnO nanoparticles. Environ Toxicol. 2014;31(1522–7278 (Electronic)):360–71.
72. Zhou Z, Son J, Harper B, Zhou Z, Harper S. Influence of surface chemical properties on the toxicity of engineered zinc oxide nanoparticles to embryonic zebrafish. Beilstein J Nanotechnol. 2015;6(2190–4286 (Electronic)):1568–79.
73. Rollerova E, Tulinska J, Liskova A, Kuricova M, Kovriznych J, Mlynarcikova A, et al. Titanium dioxide nanoparticles: some aspects of toxicity/focus on the development. Endocr Reg. 2014;49(1210–0668 (Print)):97–112.
74. Warheit DB, Boatman R, Brown SC. Developmental toxicity studies with 6 forms of titanium dioxide test materials (3 pigment-different grade & 3 nanoscale) demonstrate an absence of effects in orally-exposed rats. Reg Toxicol Pharmacol. 2015;73(1096–0295 (Electronic)):887–96.
75. Ema M, Gamo M, Honda K. Developmental toxicity of engineered nanomaterials in rodents. Toxicol Appl Pharmacol. 2015;299(1096–0333 (Electronic)):47–52.
76. Li Z, Geng Y, Zhang X, Qi W, Fan Q, Li Y, et al. Biodistribution of co-exposure to multi-walled carbon nanotubes and graphene oxide nanoplatelets radiotracers. J Nanopart Res. 2011;13(7):2939–47.
77. Wang Y, Li Z, Hu D, Lin CT, Li J, Lin Y. Aptamer/graphene oxide nanocomplex for in situ molecular probing in living cells. J Am Chem Soc. 2010;132(27):9274–6.
78. Liu JH, Yang ST, Wang H, Chang Y, Cao A, Liu Y. Effect of size and dose on the biodistribution of graphene oxide in mice. Nanomedicine. 2012;7(12):1801–12.
79. Zhang S, Yang K, Feng L, Liu Z. In vitro and in vivo behaviors of dextran functionalized graphene. Carbon. 2011;49(12):4040–9.
80. Hirn S, Semmler-Behnke M, Schleh C, Wenk A, Lipka J, Schaffler M, et al. Particle size-dependent and surface charge-dependent biodistribution of gold nanoparticles after intravenous administration. Eur J Pharm Biopharm. 2011;77(3):407–16.
81. Li B, Zhang XY, Yang JZ, Zhang YJ, Li WX, Fan CH, et al. Influence of polyethylene glycol coating on biodistribution and toxicity of nanoscale graphene oxide in mice after intravenous injection. Int J Nanomedicine. 2014;9:4697–707.
82. Zhang Y, Ali SF, Dervishi E, Xu Y, Li Z, Casciano D, et al. Cytotoxicity effects of graphene and single-wall carbon nanotubes in neural phaeochromocytoma-derived PC12 cells. ACS Nano. 2010;4(6):3181–6.
83. Li Y, Liu Y, Fu Y, Wei T, Le Guyader L, Gao G, et al. The triggering of apoptosis in macrophages by pristine graphene through the MAPK and TGF-beta signaling pathways. Biomaterials. 2012;33(2):402–11.
84. Sydlik SA, Jhunjhunwala S, Webber MJ, Anderson DG, Langer R. In vivo compatibility of graphene oxide with differing oxidation states. ACS Nano. 2015;9(4):3866–74.
85. Mytych J, Wnuk M. Nanoparticle technology as a double-edged sword: cytotoxic, genotoxic and epigenetic effects on living cells. J Biomater Nanobiotechnol. 2013;4:53–63.
86. Peng C, Hu W, Zhou Y, Fan C, Huang Q. Intracellular imaging with a graphene-based fluorescent probe. Small. 2010;6(15):1686–92.
87. Wang D, Zhu L, Chen JF, Dai L. Can graphene quantum dots cause DNA damage in cells? Nanoscale. 2015;7(21):9894–901.
88. Mu Q, Su G, Li L, Gilbertson BO, Yu LH, Zhang Q, et al. Size-dependent cell uptake of protein-coated graphene oxide nanosheets. ACS Appl Mater Interf. 2012;4(4):2259–66.
89. Xu M, Zhu J, Wang F, Xiong Y, Wu Y, Wang Q, et al. Improved in vitro and in vivo biocompatibility of graphene oxide through surface modification: poly(acrylic acid)-functionalization is superior to PEGylation. ACS Nano. 2016; 10:3267–81.
90. Kostarelos K, Novoselov KS. Materials science. Exploring the interface of graphene and biology. Science. 2014;344(6181):261–3.
91. Sasidharan A, Panchakarla LS, Chandran P, Menon D, Nair S, Rao CN, et al. Differential nano-bio interactions and toxicity effects of pristine versus functionalized graphene. Nanoscale. 2011;3(6):2461–4.
92. Li Y, Yuan H, von dem Bussche A, Creighton M, Hurt RH, Kane AB, et al. Graphene microsheets enter cells through spontaneous membrane penetration at edge asperities and corner site. Proc Natl Acad Sci U S A. 2013;110(1091–6490 (Electronic)):12295–300.
93. Qu G, Liu S, Zhang S, Wang L, Wang X, Sun B, et al. Graphene oxide induces toll-like receptor 4 (TLR4)-dependent necrosis in macrophages. ACS Nano. 2013;7(7):5732–45.
94. Ma J, Liu R, Wang X, Liu Q, Chen Y, Valle RP, et al. Crucial role of lateral size for graphene oxide in activating macrophages and stimulating Pro-inflammatory responses in cells and animals. ACS Nano. 2015;9(10):10498–515.
95. Mao L, Hu M, Pan B, Xie Y, Petersen EJ. Biodistribution and toxicity of radio-labeled few layer graphene in mice after intratracheal instillation. Part Fibre Toxicol. 2016;13(1743–8977 (Electronic)):1.
96. Park EJ, Lee SJ, Lee K, Choi YC, Lee BS, Lee GH, et al. Pulmonary persistence of graphene nanoplatelets may disturb physiological and immunological homeostasis. J Appl Toxicol. 2016.
97. Kim JK, Shin JH, Lee JS, Hwang JH, Lee JH, Baek JE, et al. 28-Day inhalation toxicity of graphene nanoplatelets in Sprague–Dawley rats. Nanotoxicology. 2016;10(7):891–901.
98. Singh SK, Singh MK, Kulkarni PP, Sonkar VK, Gracio JJ, Dash D. Amine-modified graphene: thrombo-protective safer alternative to graphene oxide for biomedical applications. ACS Nano. 2012;6(3):2731–40.

99. Duch MC, Budinger GR, Liang YT, Soberanes S, Urich D, Chiarella SE, et al. Minimizing oxidation and stable nanoscale dispersion improves the biocompatibility of graphene in the lung. Nano Lett. 2011;11(12):5201–7.
100. Wang X, Duch MC, Mansukhani N, Ji Z, Liao YP, Wang M, et al. Use of a profibrogenic mechanism-based predictive toxicological approach for tiered testing and decision analysis of carbonaceous nanomaterials. ACS Nano. 2015;9(1936-086X (Electronic)):3032–43.
101. Sawosz E, Jaworski S, Kutwin M, Hotowy A, Wierzbicki M, Grodzik M, et al. Toxicity of pristine graphene in experiments in a chicken embryo model. Int J Nanomed. 2014;9:3913–22.
102. Liu XT, Mu XY, Wu XL, Meng LX, Guan WB, Ma YQ, et al. Toxicity of multi-walled carbon nanotubes, graphene oxide, and reduced graphene oxide to zebrafish embryos. Biomed Environ Sci. 2014;27(9):676–83.
103. Chen Y, Hu X, Sun J, Zhou Q. Specific nanotoxicity of graphene oxide during zebrafish embryogenesis. Nanotoxicology. 2016;10(1):42–52.
104. Sasidharan A, Panchakarla LS, Sadanandan AR, Ashokan A, Chandran P, Girish CM, et al. Hemocompatibility and macrophage response of pristine and functionalized graphene. Smal. 2012;8(8):1251–63.
105. Ding Z, Zhang Z, Ma H, Chen Y. In vitro hemocompatibility and toxic mechanism of graphene oxide on human peripheral blood T lymphocytes and serum albumin. ACS Appl Mater Interf. 2014;6(22):19797–807.
106. Liao KH, Lin YS, Macosko CW, Haynes CL. Cytotoxicity of graphene oxide and graphene in human erythrocytes and skin fibroblasts. ACS Appl Mater Interfaces. 2011;3(7):2607–15.
107. Kouhi SMM, Lahouti M, Ganjeali A, Entezari MH. Long-term exposure of rapeseed (Brassica napus L.) to ZnO nanoparticles: anatomical and ultrastructural responses. Environ Sci Pollut Res. 2015;22(1614–7499 (Electronic)):10733–43.
108. Vales G, Rubio L, Marcos R. Long-term exposures to low doses of titanium dioxide nanoparticles induce cell transformation, but not genotoxic damage in BEAS-2B cells. Nanotoxicology. 2015;9(1743–5404 (Electronic)):568–78.
109. Sancey L, Kotb S, Truillet C, Appaix F, Marais A, Thomas E, et al. Long-term in vivo clearance of gadolinium-based AGulX nanoparticles and their biocompatibility after systemic injection. ACS Nano. 2015;9(1936-086X (Electronic)):2477–88.
110. Chatterjee N, Eom HJ, Choi J. A systems toxicology approach to the surface functionality control of graphene-cell interactions. Biomaterials. 2014;35:1109–27.
111. Jaworski S, Sawosz E, Grodzik M, Winnicka A, Prasek M, Wierzbicki M, et al. In vitro evaluation of the effects of graphene platelets on glioblastoma multiforme cells. Int J Nanomed. 2013;8:413–20.
112. Liu Y, Luo Y, Wu J, Wang Y, Yang X, Yang R, et al. Graphene oxide can induce in vitro and in vivo mutagenesis. Sci Rep. 2013;3:3469.
113. Vallabani NV, Mittal S, Shukla RK, Pandey AK, Dhakate SR, Pasricha R, et al. Toxicity of graphene in normal human lung cells (BEAS-2B). J Biomed Nanotechnol. 2011;7(1):106–7.
114. Peng J, Gao W, Gupta BK, Liu Z, Romero-Aburto R, Ge L, et al. Graphene quantum dots derived from carbon fibers. Nano Lett. 2012;12(1530–6992 (Electronic)):844–9.
115. Shang W, Zhang X, Zhang M, Fan Z, Sun Y, Han M, et al. The uptake mechanism and biocompatibility of graphene quantum dots with human neural stem cells. Nanoscale. 2014;6(2040–3372 (Electronic)):5799–806.
116. Zhang L, Xia J, Zhao Q, Liu L, Zhang Z. Functional graphene oxide as a nanocarrier for controlled loading and targeted delivery of mixed anticancer drugs. Small. 2010;6(4):537–44.
117. Ruiz ON, Fernando KA, Wang B, Brown NA, Luo PG, McNamara ND, et al. Graphene oxide: a nonspecific enhancer of cellular growth. ACS Nano. 2011;5(10):8100–7.
118. Akhavan O, Ghaderi E, Akhavan A. Size-dependent genotoxicity of graphene nanoplatelets in human stem cells. Biomaterials. 2012;33(32):8017–25.
119. Chang Y, Yang ST, Liu JH, Dong E, Wang Y, Cao A, et al. In vitro toxicity evaluation of graphene oxide on A549 cells. Toxicol Lett. 2011;200(3):201–10.
120. Zhang X, Hu W, Li J, Tao L, Wei Y. A comparative study of cellular uptake and cytotoxicity of multi-walled carbon nanotubes, graphene oxide, and nanodiamond. Toxicol Res. 2012;1(1):62–8.
121. Lu CH, Zhu CL, Li J, Liu JJ, Chen X, Yang HH. Using graphene to protect DNA from cleavage during cellular delivery. Chem Commun. 2010;46(1364-548X (Electronic)):3116–8.
122. De Marzi L, Ottaviano L, Perrozzi F, Nardone M, Santucci S, De Lapuente J, et al. Flake size-dependent cyto and genotoxic evaluation of graphene oxide on in vitro A549, CaCo2 and vero cell lines. J Biol Regul Homeost Agents. 2014;28(2):281–9.
123. Lv M, Zhang Y, Liang L, Wei M, Hu W, Li X, et al. Effect of graphene oxide on undifferentiated and retinoic acid-differentiated SH-SY5Y cells line. Nanoscale. 2012;4(13):3861–6.
124. Reshma SC, Syama S, Mohanan PV. Nano-biointeractions of PEGylated and bare reduced graphene oxide on lung alveolar epithelial cells: A comparative in vitro study. Colloids Surf B Biointerf. 2016;140(1873–4367 (Electronic)):104–16.
125. Rana VK, Choi MC, Kong JY, Kim GY, Mi JK, Kim SH, et al. Synthesis and drug-delivery behavior of chitosan-functionalized graphene oxide hybrid nanosheets. Macromol Mater Eng. 2011;296(2):131–40.
126. Yang K, Li Y, Tan X, Peng R, Liu Z. Behavior and toxicity of graphene and its functionalized derivatives in biological systems. Small. 2013;9(9–10):1492–503.
127. Yoon OJ, Kim I, Sohn IY, Kieu TT, Lee NE. Toxicity of graphene nanoflakes evaluated by cell-based electrochemical impedance biosensing. J Biomed Mater Res A. 2014;102(7):2288–94.
128. Jastrzebska AM, Kurtycz P, Olszyna AR. Recent advances in graphene family materials toxicity investigations. J Nanopart Res. 2012;14(12):1320.
129. Misra SK, Kondaiah P, Bhattacharya S, Rao CN. Graphene as a nanocarrier for tamoxifen induces apoptosis in transformed cancer cell lines of different origins. Small. 2012;8(1):131–43.
130. Singh Z. Applications and toxicity of graphene family nanomaterials and their composites. Nanotechnol Sci Appl. 2016;9(1177–8903 (Electronic)):15.
131. Combarros RG, Collado S, Diaz M. Toxicity of graphene oxide on growth and metabolism of Pseudomonas putida. J Hazard Mater. 2016;310(1873–3336 (Electronic)):246–52.
132. Lee JK, Jeong AY, Bae J, Seok JH, Yang JY, Roh HS, et al. The role of surface functionalization on the pulmonary inflammogenicity and translocation into mediastinal lymph nodes of graphene nanoplatelets in rats. Arch Toxicol. 2016(1432–0738 (Electronic)):1–10. DOI: .1007/s00204-016-1706-y
133. Patlolla AK, Randolph J, Kumari SA, Tchounwou PB. Toxicity evaluation of graphene oxidein kidneys of Sprague–Dawley rats. Int J Environ Res Public Health. 2016;13(1660–4601 (Electronic)):380.
134. Wang ZG, Zhou R, Jiang D, Song JE, Xu Q, Si J, et al. Toxicity of graphene quantum dots in zebrafish embryo. Biomed Environ Sci. 2015;28(0895–3988 (Print)):341–51.
135. Wang K, Jing R, Song H, Zhang J, Yan W, Guo S, et al. Biocompatibility of graphene oxide. Nanoscale Res Lett. 2010;6(1):1–8.
136. Hu W, Peng C, Luo W, Lv M, Li X, Li D, et al. Graphene-based antibacterial paper. ACS Nano. 2010;4(7):4317–23.
137. Dreyer DR, Park S, Bielawski CW, Ruoff RS. The chemistry of graphene oxide. Chem Soc Rev. 2010;39(1):228–40.
138. Mullick Chowdhury S, Lalwani G, Zhang K, Yang JY, Neville K, Sitharaman B. Cell specific cytotoxicity and uptake of graphene nanoribbons. Biomaterials. 2013;34(1):283–93.
139. Zhang H, Peng C, Yang J, Lv M, Liu R, He D, et al. Uniform ultrasmall graphene oxide nanosheets with low cytotoxicity and high cellular uptake. ACS Appl Mater Interf. 2013;5(5):1761–7.
140. Hasan SA, Rigueur JL, Harl RR, Krejci AJ, Isabel GJ, Rogers BR, et al. Transferable graphene oxide films with tunable microstructures. ACS Nano. 2010;4(12):7367–72.
141. Hsieh CT, Chen WY. Water/oil repellency and work of adhesion of liquid droplets on graphene oxide and graphene surfaces. Surf Coat Technol. 2011;205(19):4554–61.
142. Yang ST, Chang Y, Wang H, Liu G, Sheng C, Wang Y, et al. Folding/aggregation of graphene oxide and its application in Cu 2+ removal. J Colloid Interf Sci. 2010;351(1):122–7.
143. Bagri A, Mattevi C, Acik M, Chabal YJ, Chhowalla M, Shenoy VB. Structural evolution during the reduction of chemically derived graphene oxide. Nat Chem. 2010;2(7):581–7.
144. Hinzmann M, Jaworski S, Kutwin M, Jagiello J, Kozinski R, Wierzbicki M, et al. Nanoparticles containing allotropes of carbon have genotoxic effects on glioblastoma multiforme cells. Int J Nanomed. 2014;9:2409–17.
145. Jin C, Wang F, Tang Y, Zhang X, Wang J, Yang Y. Distribution of graphene oxide and TiO2-graphene oxide composite in A549 cells. Biol Trace Elem Res. 2014;159(1–3):393–8.
146. Jarosz A, Skoda M, Dudek I, Szukiewicz D. Oxidative stress and mitochondrial activation as the main mechanisms underlying graphene toxicity against human cancer cells. Oxid Med Cell Longev. 2016;2016:5851035.
147. Ren H, Wang C, Zhang J, Zhou X, Xu D, Zheng J, et al. DNA cleavage system of nanosized graphene oxide sheets and copper ions. ACS Nano. 2010;4(12):7169–74.

148. Wang A, Pu K, Dong B, Liu Y, Zhang L, Zhang Z, et al. Role of surface charge and oxidative stress in cytotoxicity and genotoxicity of graphene oxide towards human lung fibroblast cells. J Appl Toxicol. 2013;33(10):1156–64.
149. Jiang X, Dausend J, Hafner M, Musyanovych A, Rocker C, Landfester K, et al. Specific effects of surface amines on polystyrene nanoparticles in their interactions with mesenchymal stem cells. Biomacromolecules. 2010;11(3):748–53.
150. Yue ZG, Wei W, Lv PP, Yue H, Wang LY, Su ZG, et al. Surface charge affects cellular uptake and intracellular trafficking of chitosan-based nanoparticles. Biomacromolecules. 2011;12(7):2440–6.
151. Zhang W, Wang C, Li Z, Lu Z, Li Y, Yin JJ, et al. Unraveling stress-induced toxicity properties of graphene oxide and the underlying mechanism. Adv Mater. 2012;24(39):5391–7.
152. Wojtoniszak M, Chen X, Kalenczuk RJ, Wajda A, Łapczuk J, Kurzewski M, et al. Synthesis, dispersion, and cytocompatibility of graphene oxide and reduced graphene oxide. Colloids Surf B Biointerf. 2011;89(1):79–85.
153. Hu H, Yu J, Li Y, Zhao J, Dong H. Engineering of a novel pluronic F127/graphene nanohybrid for pH responsive drug delivery. J Biomed Mater Res A. 2012;100(1):141–8.
154. Sahu A, Choi WI, Tae G. A stimuli-sensitive injectable graphene oxide composite hydrogel. Chem Commun (Camb). 2012;48(47):5820–2.
155. Yang K, Zhang S, Zhang G, Sun X, Lee ST, Liu Z. Graphene in mice: ultrahigh in vivo tumor uptake and efficient photothermal therapy. Nano Lett. 2010;10(9):3318–23.
156. Romero-Aburto R, Narayanan TN, Nagaoka Y, Hasumura T, Mitcham TM, Fukuda T, et al. Fluorinated graphene oxide; a new multimodal material for biological applications. Adv Mater. 2013;25(39):5632–7.
157. Feng L, Liu Z. Graphene in biomedicine: opportunities and challenges. Nanomed (Lond). 2011;6(2):317–24.
158. Robinson JT, Tabakman SM, Liang Y, Wang H, Casalongue HS, Vinh D, et al. Ultrasmall reduced graphene oxide with high near-infrared absorbance for photothermal therapy. J Am Chem Soc. 2011;133(17):6825–31.
159. Singh N, Manshian B, Jenkins GJS, Griffiths SM, Williams PM, Maffeis TGG, et al. NanoGenotoxicology: The DNA damaging potential of engineered nanomaterials. Biomaterials. 2009;30(s 23–24):3891–914.
160. Yin PT, Shah S, Chhowalla M, Lee KB. Design, synthesis, and characterization of graphene-nanoparticle hybrid materials for bioapplications. Chem Rev. 2015;115(7):2483–531.
161. Peng L, Xu Z, Liu Z, Wei Y, Sun H, Li Z, et al. An iron-based green approach to 1-h production of single-layer graphene oxide. Nat Commun. 2015;6:5716.
162. Ali-Boucetta H, Bitounis D, Raveendran-Nair R, Servant A, Van den Bossche J, Kostarelos K. Purified graphene oxide dispersions lack in vitro cytotoxicity and in vivo pathogenicity. Adv Healthc Mater. 2013;2(3):433–41.
163. Dell'Orco D, Lundqvist M, Oslakovic C, Cedervall T, Linse S. Modeling the time evolution of the nanoparticle-protein corona in a body fluid. PLoS One. 2010;5(6):e10949-e.
164. Eudald C, Tobias P, Albert D, Gertie Janneke O, Victor P. Time evolution of the nanoparticle protein corona. ACS Nano. 2010;4(7):3623–32.
165. Aggarwal P, Hall JB, McLeland CB, Dobrovolskaia MA, McNeil SE. Nanoparticle interaction with plasma proteins as it relates to particle biodistribution, biocompatibility and therapeutic efficacy. Adv Drug Deliv Rev. 2009;61(6):428–37.
166. Hu W, Peng C, Lv M, Li X, Zhang Y, Chen N, et al. Protein corona-mediated mitigation of cytotoxicity of graphene oxide. ACS Nano. 2011;5(5):3693–700.
167. Duan G, Kang SG, Tian X, Garate JA, Zhao L, Ge C, et al. Protein corona mitigates the cytotoxicity of graphene oxide by reducing its physical interaction with cell membrane. Nanoscale. 2015;7:15214–24.
168. Cuicui G, Jiangfeng D, Lina Z, Liming W, Ying L, Denghua L, et al. Binding of blood proteins to carbon nanotubes reduces cytotoxicity. Proc Natl Acad Sci U S A. 2011;108(41):16968–73.
169. Li Y, Feng L, Shi X, Wang X, Yang Y, Yang K, et al. Surface coating-dependent cytotoxicity and degradation of graphene derivatives: towards the design of non-toxic, degradable nano-graphene. Small. 2014;10(8):1544–54.
170. Gurunathan S, Han J, Park JH, Kim JH. An in vitro evaluation of graphene oxide reduced by Ganoderma spp. in human breast cancer cells (MDA-MB-231). Int J Nanomed. 2014;9:1783–97.
171. Yuan J, Gao H, Ching CB. Comparative protein profile of human hepatoma HepG2 cells treated with graphene and single-walled carbon nanotubes: an iTRAQ-coupled 2D LC-MS/MS proteome analysis. Toxicol Lett. 2011;207(3):213–21.
172. Tomasio SM, Walsh TR. Modeling the binding affinity of peptides for graphitic surfaces. Influences of aromatic content and interfacial shape. J Phys Chem C. 2009;113(20):8778–85.
173. Akhavan O, Ghaderi E. Toxicity of graphene and graphene oxide nanowalls against bacteria. ACS Nano. 2010;4(10):5731–6.
174. Burton GJ, Jauniaux E. Oxidative stress. Best Pract Res Clin Obstet Gynaecol. 2011;25:287–99.
175. Waiwijit U, Kandhavivorn W, Oonkhanond B, Lomas T, Phokaratkul D, Wisitsoraat A, et al. Cytotoxicity assessment of MDA-MB-231 breast cancer cells on screen-printed graphene-carbon paste substrate. Colloids Surf B Biointerf. 2014;113:190–7.
176. Chong Y, Ma Y, Shen H, Tu X, Zhou X, Xu J, et al. The in vitro and in vivo toxicity of graphene quantum dots. Biomaterials. 2014;35(19):5041–8.
177. Chen M, Yin J, Liang Y, Yuan S, Wang F, Song M, et al. Oxidative stress and immunotoxicity induced by graphene oxide in zebrafish. Aqua Toxicol. 2016;174(1879–1514 (Electronic)):54–60.
178. Meng C, Zhi X, Li C, Li C, Chen Z, Qiu X, et al. Graphene oxides decorated with carnosine as an adjuvant to modulate innate immune and improve adaptive immunity in vivo. ACS Nano. 2016;10(1936-086X (Electronic)):2203–13.
179. Ravichandran P, Baluchamy S, Sadanandan B, Gopikrishnan R, Biradar S, Ramesh V, et al. Multiwalled carbon nanotubes activate NF-κB and AP-1 signaling pathways to induce apoptosis in rat lung epithelial cells. Apoptosis. 2010;15(12):1507–16.
180. Lammel T, Boisseaux P, Fernandez-Cruz ML, Navas JM. Internalization and cytotoxicity of graphene oxide and carboxyl graphene nanoplatelets in the human hepatocellular carcinoma cell line Hep G2. Part Fibre Toxicol. 2013;10:27.
181. Gurunathan S, Han JW, Eppakayala V, Kim JH. Green synthesis of graphene and its cytotoxic effects in human breast cancer cells. Int J Nanomedicine. 2013;8:1015–27.
182. Salas EC, Sun Z, Luttge A, Tour JM. Reduction of graphene oxide via bacterial respiration. ACS Nano. 2010;4(8):4852–6.
183. Shekaramiz E. Immobilization of mitochondria on graphene. Dissert Theses Gradworks. 2012;217(1):120–31.
184. Park EJ, Lee GH, Han BS, Lee BS, Lee S, Cho MH, et al. Toxic response of graphene nanoplatelets in vivo and in vitro. Arch Toxicol. 2015;89(9):1557–68.
185. Chatterjee N, Yang J, Choi J. Differential genotoxic and epigenotoxic effects of graphene family nanomaterials (GFNs) in human bronchial epithelial cells. Mutat Res Gen Tox En. 2016;798(1879–3592 (Electronic)):1–10.
186. Ivask A, Voelcker NH, Seabrook SA, Hor M, Kirby JK, Fenech M, et al. DNA melting and genotoxicity induced by silver nanoparticles and graphene. Chem Res Toxicol. 2015;28(1520–5010 (Electronic)):1023–35.
187. Magdolenova Z, Collins A, Kumar A, Dhawan A, Stone V, Dusinska M. Mechanisms of genotoxicity. A review of in vitro and in vivo studies with engineered nanoparticles. Nanotoxicology. 2014;8(3):233–78.
188. Golbamaki N, Rasulev B, Cassano A, Marchese Robinson RL, Benfenati E, Leszczynski J, et al. Genotoxicity of metal oxide nanomaterials: review of recent data and discussion of possible mechanisms. Nanoscale. 2015;7(6):2154–98.
189. Zhao X. Self-assembly of DNA segments on graphene and carbon nanotube arrays in aqueous solution: A molecular simulation study. J Phys Chem C. 2011;115(14):6181–9.
190. Ciccia A, Elledge SJ. The DNA damage response: making it safe to play with knives. Mol Cell. 2010;40(2):179–204.
191. Satoshi F, Macconmara MP, Maung AA, Yan Z, Mannick JA, Lederer JA, et al. Platelet depletion in mice increases mortality after thermal injury. Blood. 2006;107(11):4399–406.
192. Chen GY, Yang HJ, Lu CH, Chao YC, Hwang SM, Chen CL, et al. Simultaneous induction of autophagy and toll-like receptor signaling pathways by graphene oxide. Biomaterials. 2012;33(27):6559–69.
193. Zhou H, Zhao K, Li W, Yang N, Liu Y, Chen C, et al. The interactions between pristine graphene and macrophages and the production of cytokines/chemokines via TLR- and NF-kappaB-related signaling pathways. Biomaterials. 2012;33(29):6933–42.
194. Lawrence T. The nuclear factor NF-kappaB pathway in inflammation. Cold Spring Harb Perspect Biol. 2009;1(1943–0264 (Electronic)):a001651.
195. Hengartner MO. The biochemistry of apoptosis. Nature. 2000;407(6805):770–6.
196. Matesanz MC, Vila M, Feito MJ, Linares J, Goncalves G, Vallet-Regi M, et al. The effects of graphene oxide nanosheets localized on F-actin filaments on cell-cycle alterations. Biomaterials. 2013;34(5):1562–9.
197. Yao Y, Costa M. Genetic and epigenetic effects of nanoparticles. J Mol Genet Med. 2013;7:86.
198. Stern ST, Adiseshaiah PP, Crist RM. Autophagy and lysosomal dysfunction as emerging mechanisms of nanomaterial toxicity. Part Fibre Toxicol. 2012;9(1743–8977 (Electronic)):1.

199. Mizushima N, Yoshimori T, Levine B. Methods in mammalian autophagy research. Cel. 2010;140(1097–4172 (Electronic)):313–26.
200. Patel AS, Lin L, Geyer A, Haspel JA, An CH, Cao J, et al. Autophagy in idiopathic pulmonary fibrosis. PLoS One. 2012;7(1932–6203 (Electronic)):e41394.
201. Levine B, Mizushima N, Virgin HW. Autophagy in immunity and inflammation. Nature. 2011;469(7330):323–35.
202. Kenzaoui BH, Bernasconi CC, Guney-Ayra S, Juillerat-Jeanneret L. Induction of oxidative stress, lysosome activation and autophagy by nanoparticles in human brain-derived endothelial cells. Biochem J. 2012;441(1470–8728 (Electronic)):813–21.
203. Hussain S, Garantziotis S. Interplay between apoptotic and autophagy pathways after exposure to cerium dioxide nanoparticles in human monocytes. Autophagy. 2013;9(1554–8635 (Electronic)):101–3.
204. Sun T, Yan Y, Zhao Y, Guo F, Jiang C. Copper oxide nanoparticles induce autophagic cell death in A549 cells. PLoS One. 2012;7(1932–6203 (Electronic)):e43442.
205. Chen GY, Meng CL, Lin KC, Tuan HY, Yang HJ, Chen CL, et al. Graphene oxide as a chemosensitizer: Diverted autophagic flux, enhanced nuclear import, elevated necrosis and improved antitumor effects. Biomaterials. 2015;40:12–22.
206. Chen GY, Chen CL, Tuan HY, Yuan PX, Li KC, Yang HJ, et al. Graphene oxide triggers toll-like receptors/autophagy responses in vitro and inhibits tumor growth in vivo. Adv Healthc Mater. 2014;3(9):1486–95.
207. Wan B, Wang ZX, Lv QY, Dong PX, Zhao LX, Yang Y, et al. Single-walled carbon nanotubes and graphene oxides induce autophagosome accumulation and lysosome impairment in primarily cultured murine peritoneal macrophages. Toxicol Lett. 2013;221(1879–3169 (Electronic)):118–27.
208. Markovic ZM, Ristic BZ, Arsikin KM, Klisic DG, Harhaji-Trajkovic LM, Todorovic-Markovic BM, et al. Graphene quantum dots as autophagy-inducing photodynamic agents. Biomaterials. 2012;33(29):7084–92.
209. Sanjuan MA, Dillon CP, Tait SW, Moshiach S, Dorsey F, Connell S, et al. Toll-like receptor signalling in macrophages links the autophagy pathway to phagocytosis. Nature. 2007;450(7173):1253–7.
210. Sasidharan A, Swaroop S, Chandran P, Nair S, Koyakutty M. Cellular and molecular mechanistic insight into the DNA-damaging potential of few-layer graphene in human primary endothelial cells. Nanomed. 2016; 12(1549–9642 (Electronic)):1347–55.
211. Yang H, Rivera Z, Jube S, Nasu M, Bertino P, Goparaju C, et al. Programmed necrosis induced by asbestos in human mesothelial cells causes high-mobility group box 1 protein release and resultant inflammation. Proc Natl Acad Sci U S A. 2010;107(1091–6490 (Electronic)):12611–6.
212. Raucci A, Palumbo R, Bianchi ME. HMGB1: a signal of necrosis. Autoimmunity. 2007;40(4):285–9.
213. Smith ZD, Meissner A. DNA methylation: roles in mammalian development. Nat Rev Genet. 2013;14(3):204–20.
214. Fabian MR, Sonenberg N. The mechanics of miRNA-mediated gene silencing: a look under the hood of miRISC. Nat Struct Mol Biol. 2012;19(6): 586–93.
215. Nishikura K. Functions and regulation of RNA editing by ADAR deaminases. Annu Rev Biochem. 2010;79(79):321–49.
216. Dubey P, Matai I, Kumar SU, Sachdev A, Bhushan B, Gopinath P. Perturbation of cellular mechanistic system by silver nanoparticle toxicity: Cytotoxic, genotoxic and epigenetic potentials. Adv Colloid Interf Sci. 2015; 221:4–21.
217. Collins AR, Ferguson LR. DNA repair as a biomarker. Mutat Res. 2012;736(1–2):2–4.
218. Zhao Y, Wu Q, Wang D. An epigenetic signal encoded protection mechanism is activated by graphene oxide to inhibit its induced reproductive toxicity in Caenorhabditis elegans. Biomaterials. 2016;79(1878–5905 (Electronic)):15–24.
219. Liu C, Yu W, Chen Z, Zhang J, Zhang N. Enhanced gene transfection efficiency in CD13-positive vascular endothelial cells with targeted poly(lactic acid)-poly(ethylene glycol) nanoparticles through caveolae-mediated endocytosis. J Contr Rel. 2011;151(1873–4995 (Electronic)):162–75.
220. Ema M, Aoyama H, Arima A, Asano Y, Chihara K, Endoh K, et al. Historical control data on prenatal developmental toxicity studies in rabbits. Congenit Anom. 2012;52(3):155–61.
221. Ema M, Endoh K, Fukushima R, Fujii S, Hara H, Hirata-Koizumi M, et al. Historical control data on developmental toxicity studies in rodents. Congenit Anom. 2014;54(3):150–61.
222. Bitounis D, Ali-Boucetta H, Hong BH, Min DH, Kostarelos K. Prospects and challenges of graphene in biomedical applications. Adv Mater. 2013;25(16): 2258–68.
223. Van Goethem F, Lison D, Kirsch-Volders M. Comparative evaluation of the in vitro micronucleus test and the alkaline single cell gel electrophoresis assay for the detection of DNA damaging agents: genotoxic effects of cobalt powder, tungsten carbide and cobalt-tungsten carbide. Mutat Res. 1997; 392(1–2):31–43.
224. Natarajan V, Wilson CL, Hayward SL, Kidambi S. Titanium dioxide nanoparticles trigger loss of function and perturbation of mitochondrial dynamics in primary hepatocytes. PLoS One. 2015;10(1932–6203 (Electronic)):e0134541.
225. Hong F, Zhao X, Chen M, Zhou Y, Ze Y, Wang L, et al. TiO2 nanoparticles-induced apoptosis of primary cultured Sertoli cells of mice. J Biochem Mater Res A. 2016;104(1552–4965 (Electronic)):124–35.
226. Yang WE, Lan MY, Lee SW, Chang JK, Huang HH. Primary human nasal epithelial cell response to titanium surface with a nanonetwork structure in nasal implant applications. Nanoscale Res Lett. 2015;10(1931–7573 (Print)):1–10.
227. Wang J, Deng X, Zhang F, Chen D, Ding W. ZnO nanoparticle-induced oxidative stress triggers apoptosis by activating JNK signaling pathway in cultured primary astrocytes. Nanoscale Res Lett. 2014;9(1931–7573 (Print)):1–12.
228. Osmond-McLeod MJ, Osmond RI, Oytam Y, McCall MJ, Feltis B, Mackay-Sim A, et al. Surface coatings of ZnO nanoparticles mitigate differentially a host of transcriptional, protein and signalling responses in primary human olfactory cells. Part Fibre Toxicol. 2013;10(1743–8977 (Electronic)):1.
229. Meng S, Peng R. Growth and follow-up of primary cortical neuron cells on nonfunctionalized graphene nanosheet film. J Appl Biomater Funct Mater. 2016;14(2280–8000 (Electronic)):e26–34.
230. Kwon JT, Seo GB, Jo, Lee M, Kim HM, Shim I, et al. Aluminum nanoparticles induce ERK and p38MAPK activation in rat brain. Toxicol Res. 2013;29(1976–8257 (Print)):181–5.
231. Radcliffe PM, Olabisi AO, Wagner DJ, Leavens T, Wong BA, Struve MF, et al. Acute sodium tungstate inhalation is associated with minimal olfactory transport of tungsten (188W) to the rat brain. Neurotoxicology. 2009; 30(1872–9711 (Electronic)):445–50.
232. Zhang H, Li ZF, Snyder A, Xie J, Stanciu LA. Functionalized graphene oxide for the fabrication of paraoxon biosensors. Anal Chim Acta. 2014;827:86–94.
233. Schriver M, Regan W, Gannett WJ, Zaniewski AM, Crommie MF, Zettl A. Graphene as a long-term metal oxidation barrier: worse than nothing. ACS Nano. 2013;7(1936-086X (Electronic)):5763–8.
234. Soldano C, Mahmood A, Dujardin E. Production, properties and potential of graphene. Carbon. 2010;48(8):2127–50.
235. Han SG, Kim JK, Shin JH, Hwang JH, Lee JS, Kim TG, et al. Pulmonary Responses of Sprague–Dawley Rats in Single Inhalation Exposure to Graphene Oxide Nanomaterials. Biomed Res Int. 2015;2015:376756.
236. Pan WY, Huang CC, Lin TT, Hu HY, Lin WC, Li MJ, et al. Synergistic antibacterial effects of localized heat and oxidative stress caused by hydroxyl radicals mediated by graphene/iron oxide-based nanocomposites. Nanomedicine. 2016;12(2):431–8.
237. Yang K, Gong H, Shi X, Wan J, Zhang Y, Liu Z. Invivo biodistribution and toxicology of functionalized nano-graphene oxide in mice after oral and intraperitoneal administration. Biomaterials. 2013;34(11):2787–95.
238. Jaworski S, Sawosz E, Kutwin M, Wierzbicki M, Hinzmann M, Grodzik M, et al. In vitro and in vivo effects of graphene oxide and reduced graphene oxide on glioblastoma. Int J Nanomedicine. 2015;10:1585–96.
239. Akhavan O, Ghaderi E, Emamy H, Akhavan F. Genotoxicity of graphene nanoribbons in human mesenchymal stem cells. Carbon. 2013;54(2):419–31.
240. Chatterjee N, Yang J, Choi J. Differential genotoxic and epigenotoxic effects of graphene family nanomaterials (GFNs) in human bronchial epithelial cells. Mut Res Gen Tox Environ Mutagenesis. 2016;798–799:1–10.

A summary of the article ‘Toxicity of graphene-family nanoparticles: a general review of the origins and mechanisms’.

Graphene was discovered in 2004. Isolated from graphite crystals, it is made up of flat sheets, each an atom thick. Graphene oxide is one of several derivatives of graphene and its unique properties have so far seen it used in a variety of fields, including biomedical applications such as drug delivery.

Data on its toxicity are based on a limited mix of animal and in vitro studies, where various derivatives of graphene have been administered in different ways. This is important to note as the type of graphene and the way it enters the body – e.g. through inhalation or via subcutaneous injection – affects where it ends up in the body and its degree of toxicity. More research is needed to understand the impact of graphene oxide administered subcutaneously, as with the Covid-19 mRNA vaccines.

What makes graphene toxic?
The extent of its toxicity depends on its characteristics, from the size of the material, to its concentration, surface structure and charge.

- Dosage: higher concentrations of GO tend to cause more damage: in one study, a high dose caused chronic toxicity, with GO deposits found in the lungs, liver, spleen and kidneys.
- Size: where graphene nanoparticles end up in the body and the impact they have depends on their size. More research on this is needed.
- Surface structure: GFNs in general can disrupt the function and structure of cell membranes and proteins. GO can insert between the base pairs of double-stranded DNA and disturb the flow of genetic information.
- Charge: the surface charge of GO can cause it to be taken in by cells. It can reportedly alter cell structure and cause extensive destruction of red blood cells.
- Surface modification: studies confirm that altering the surface of GFNs using substances such as PEG (a process called functionalisation) largely decreases toxicity. However, given its high potential to be taken in by cells, further studies are needed to assess the possible long-term effects.
- Impurities: traditionally prepared GO often contains high levels of Mn^{2+} and Fe^{2+}, which could lead to unusually high levels of cell toxicity and DNA fracturing.
- Protein corona effect: graphene’s high free surface charge can cause it to form ‘coronas’ with proteins in the body. Several papers report that GO forms such coronas and these may regulate the adhesion of GO to certain cells and even mitigate its toxicity to cells.

What does it do to the body?
Again, studies here are lacking but here is what data have shown so far:

Graphene nanomaterials (GFNs) can penetrate the body's natural barriers
Their small size means graphene nanomaterials – including graphene oxide (GO) – can penetrate the body's existing protective barriers and infiltrate the brain, placenta and potentially the testes. In terms of the placenta, some studies have found that the placenta does not prevent nanoparticles from transferring to foetuses; this has a significant impact on foetal development.

Graphene oxide can damage internal organs
GO can cause acute inflammation and injury to vital organs. In the lungs, it was found to cause inflammation, pulmonary oedema and the formation of granulomas. There has been very little research into the toxicity of GFNs to other organs such as the liver, spleen and kidneys.

GFNs can damage the central nervous system
Graphene nanomaterials are increasingly used in neurosurgery, and studies have mainly focused on its applications rather than its toxicity. However, studies do show that these materials can decrease the level of ribonucleic acid and its rate of synthesis, which harms brain tissue development. More studies on its toxicity are underway.

GO damages the reproduction and development system
Animal studies show that GO and reduced GO (rGO) damage embryos. One study on mice found that all pregnant females injected with rGO had abortions, regardless of dose. Most of the mice given a high dose died, and their offspring suffered delayed development.

GO destroys blood health
It is impossible to prevent GO from entering the blood. Its impact on the blood depends on its coating, size and dosage but it has been found to damage red blood cells and T lymphocytes.

GO damages and destroys cells
Graphene nanomaterials in general alter the viability, shape, size and structure of cells. GO specifically decreases cell adhesion, which can disrupt important processes and lead to disease. It also causes apoptosis – a form of programmed cell death – and enters into the lysosomes, mitochondria, nucleus and endoplasm of cells. GO derivatives dramatically decrease the expression of differential genes that are responsible for the structure and function of the cell membrane.

GO can trigger cancer and accelerate ageing
GO's interaction with cells causes extensive oxidative stress which can trigger the generation of cancer cells, cause cells to mutate, and accelerates ageing. GO-induced oxidative stress has been implicated in acute lung damage, cell death and DNA damage.

GO damages mitochondria
Mitochondria are the vital energy centres within cells. Studies have found that exposure to GO can both reduce the number of mitochondria in particular cells, and impair mitochondrial activity in such a way that it generates oxidative stress and causes cell death.

GO damages DNA
GO's small size, high surface area and surface charge could potentially cause severe DNA damage. Even if GO is unable to enter a cell's nucleus, it can still interact with DNA at the point in the cell's cycle when the nuclear membrane breaks down (mitosis). This increases the potential for DNA aberrations. Interaction between graphene and the DNA base pairs can severely deform the end base pairs of DNA. GO may also cause mutations that could lead to the development of cancer – and if those mutations happen in reproductive cells, they could impact fertility and threaten the health of the next generation.

GO triggers an inflammatory response and three different kinds of cell death
GFNs (including GO) can cause significant inflammatory responses and tissue injury. GO has been found to trigger apoptosis and autophagy – both forms of programmed cell death – as well as necrosis, a form of cell death that occurs as a result of infection or injury.

GO causes epigenetic changes
Data suggests that GFNs including GO could modulate epigenetic changes that cause subtle changes in gene expression programming. However, this is not fully understood.

A lack of data
There simply isn't sufficient data with which to fully understand the toxicity of GFNs to the body. Recent studies have focused on short-term impact but little is known about long-term effects. For example, while functionalised graphene does seem to have lower toxicity, what happens if the surface coatings that lower the toxicity break down over time? Also, it is unknown as to whether GFNs could induce foreign body sarcomas, so more studies on this are urgently needed.